

STANFORD ROCKPHYSICS & BOREHOLE GEOPHYSICS PROJECT

VOLUME 39

February, 1990

**ACOUSTICAL, MECHANICAL, AND TRANSPORT PROPERTIES
OF SEDIMENTS AND GRANULAR MATERIALS**



**A DISSERTATION
SUBMITTED TO THE DEPARTMENT OF GEOPHYSICS
AND THE COMMITTEE ON GRADUATE STUDIES
OF STANFORD UNIVERSITY
IN PARTIAL FULFILLMENT OF THE REQUIREMENTS
FOR THE DEGREE OF
DOCTOR OF PHILOSOPHY**

By


Dominique Paul Marion

January 1990

©Copyright by Dominique Marion 1990

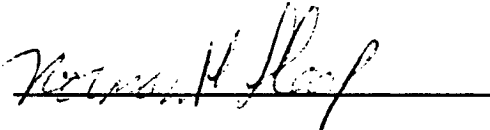
All Rights Reserved

I certify that I have read this dissertation and that in my opinion it is fully adequate, in scope and quality, as a dissertation for the degree of Doctor of Philosophy.

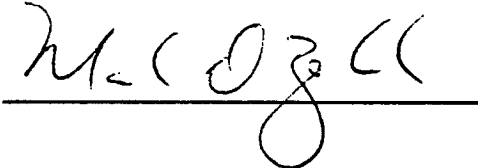


(Principal Advisor)

I certify that I have read this dissertation and that in my opinion it is fully adequate, in scope and quality, as a dissertation for the degree of Doctor of Philosophy.



I certify that I have read this dissertation and that in my opinion it is fully adequate, in scope and quality, as a dissertation for the degree of Doctor of Philosophy.



Approved for the University Committee
on Graduate Studies:

Dean of Graduate studies

Abstract

Unconsolidated materials such as marine sediments, soils and alluvium have a marked imprint on seismic and acoustic wave propagation characteristics. Because of their ubiquitous nature and economical importance as gas, oil, or water reservoir, there is great need to understand relationships between seismic and physical properties of sediments. This thesis contains new results, models, and theory of acoustic velocity in unconsolidated materials and the influence of porosity, compaction, packing parameters, lithology and fluid type on velocity measurements.

A series of laboratory experiments on artificial sediments reveals that the functional dependence of velocity on porosity must be divided into three regimes depending on the mechanical interactions between the solid particles: In suspension, particles barely interact mechanically. Consequently velocity varies only slightly with the amount and the type of suspended particles. At the transition from a suspension to grain-supported sediments, the first mechanical contacts between grains occur and velocity exhibits a sharp increase from the suspension behavior. Upon compaction, elastic moduli of grain-supported sediments are found to depend primarily on the applied stress and the number of grain contacts. Furthermore, experiments reveal that dynamic elastic moduli (derived from velocity) are less sensitive to pressure than static compressibility. Model results show that this differing sensitivity is due to number of grain contacts.

Velocity-porosity relationship is influenced also by lithology specifically by clay content. A geometrical model for sand and shale is used to estimate the systematic effect of clay content on velocity, porosity and permeability in sediments. The model provides an explanation for the scatter in velocity-porosity and porosity-permeability relationships observed in actual sediments. This scatter is directly caused by clay content and compaction.

Finally, a method was developed to relate P and S velocity in sediments and rocks to the elastic moduli of the pore-filling material, including materials with non zero shear stiffness such as infilling clay, ice, or heavy hydrocarbons. Potential applications of the method include the prediction of temperature dependence of velocity in permafrost sediments at the ice-water phase transition, and prediction of velocity in tar-reservoirs at the hydrocarbon solid-liquid phase transition.

Acknowledgements

I would like to thank all the friends, professors, and students that made my stay at Stanford a most unique and enjoyable experience.

I wish to express my sincere thanks to Amos Nur. This dissertation profited greatly from his advice, and I am indebted to Amos for his continuous support throughout my stay at Stanford.

Also beneficial were the useful discussions with the members of my dissertation committee: Mark Zoback, Norm Sleep, and Gary Mavko.

I am grateful to Richard Nolen-Hoeksema for a detailed and critical review of my dissertation, for teaching me some subtleties of the English language, and for his continued encouragement. I also enjoyed working with Dan Moos who pointed out possible applications of my work.

Over my many years at Stanford, it has been a great experience to be part of the Stanford Rock Physics group. I really wish to thank all former and present students of SRB for the stimulating research environment they created and for their friendship. Thanks go especially to Margaret Muir for her kindness and support from my Day One at Stanford.

I also thank Patricia Arditty and Jean Pierre Panziera at Elf Aquitaine for making my stay at Stanford possible and for supporting me financially during my first 16 months.

Finally, my special thanks go to Diane Jizba. If I enjoyed these years at Stanford, it is due to her encouragement, advice and her communicative enthusiasm at work and outside. Many thanks also to my parents, my grandfather, and my brother for their moral support and their continued believe in me.

Contents

1 Introduction	1
2 Compaction of sediments and its effect on acoustic properties	6
2.1 Introduction	7
2.2 Suspensions	8
2.2.1 Ultrasonic measurements vs. Wood's relation	9
2.2.2 Experimental procedure	13
2.2.3 Comparison between experimental data and Wood's relation ...	14
2.2.4 Departure from Wood's relation in sediments: possible causes ..	18
2.3 Transition from suspension to compacted sediment	24
2.3.1 Experimental set-up	29
2.3.2 Experimental results	31
2.3.3 Comparison with marine data	33
2.3.4 Relationships between velocity, density and impedance	37
2.4 Conclusion	40
3 Velocity, porosity, and permeability, in sand, shale, and shaley sand.	44
3.1 Introduction	45
3.2 The sand-clay model	46
3.2.1 Topology of the model	46
3.2.2 Porosity-clay content relationship	46
3.2.3 Velocity-clay content relationship	49
3.2.4 Departure from ideal model for porosity and velocity	55
3.2.5 Permeability-clay content relationship	58
3.3 Influence of clay content on velocity-porosity relationships	61
3.3.1 Unconsolidated sand-clay mixtures	63
3.3.2 Unconsolidated marine sediments	64

3.3.3 Gulf Coast sandstones	69
3.3.4 Consolidated sediments	70
3.4 Influence of clay content on porosity-permeability transform	73
3.6 Summary	75
3.7 Appendix	77
4 Elastic properties of granular materials	84
4.1 Introduction	85
4.2 Contact models for granular materials	86
4.2.1 Hertz' contact theory	87
4.2.2 Mindlin's contact theory	89
4.2.3 Walton's contact model	91
4.2.4 Moduli of a packing of spheres under hydrostatic pressure	91
4.3 Percolation Theory and Granular Materials	94
4.3.1 Percolation and electrical conductivity	94
4.3.2 Percolation and elasticity	96
4.4 Dependence of Elastic Moduli on Number of Contacts	99
4.4.1 Experimental Procedure	100
4.4.2 Number of deforming contacts versus pressure	101
4.4.3 Dependence of elastic moduli on number of contacts	105
4.5 Ratio of Static to Dynamic Moduli	106
4.6 Conclusion	112
5 Effect of pore-filling material on velocity in rocks	117
5.1 Introduction	118
5.2 The Bound Averaging Method	119
5.3 From dry to saturated rock	124
5.4 Velocity in water saturated rocks at permafrost temperatures	129

5.5 Velocity vs. temperature in Hydrocarbon saturated rocks	133
5.6 Conclusion	135

List of Tables

Table 2.1: Properties of silver-coated glass beads and sodiumpolytungstate ...	16
Table 2.2: Critical frequency in sand, silt, and clay	23
Table 2.3: Velocity, Porosity, and density in sediments at the transition "suspension-unconsolidated"	34
Table 3.1: Specific surface-area in clays and sandstones	60
Table 3.2: Input parameters for calculation of velocity, porosity, and permeability of Gulf-Coast Sandstones	61
Table 3.3: Input parameters for calculation of velocity, and density in shale and sandstones (Figure 3.13)	73
Table 4.1: Contact stiffnesses for various contact models	92
Table 5.1: Mineral Properties used in BAM calculations	135

List of Figures

Figure 1.1: Velocity vs. porosity in sediments and rocks	3
Figure 2.1: Velocity vs. porosity in ocean bottom sediments.	10
Figure 2.2: Experimental set-up for velocity measurements in suspensions. ...	15
Figure 2.3: P-velocity vs. porosity for artificial suspensions.	17
Figure 2.4: Effect of pressure and temperature on P-velocity in suspensions. .	20
Figure 2.5: Effect of skeleton rigidity and bulk stiffness on P-velocity.	22
Figure 2.6: Permeability vs. porosity for sand, silt, and clay.	25
Figure 2.7: Velocity versus frequency for sand, silt, and clay.	26
Figure 2.8: Effect of frequency on velocity-porosity relationship.	27
Figure 2.9: Calculated vs. measured velocity in ocean bottom sediments.	28
Figure 2.10: Transition from liquid to grain supported sediment: experimental set-up.	30
Figure 2.11: Transition from liquid to grain supported sediment: experimental results	32
Figure 2.12: Velocity vs. porosity in sediments at the transition from suspension to load-bearing sediment.	35
Figure 2.13: Velocity and density vs. depth profiles for sediments from DSDP site 206.	36
Figure 2.14: Impedance vs. density and velocity relationship in suspension and load-bearing sediments.	38
Figure 2.15: Impedance vs. density and velocity relationship for DSDP data, site 574.	39
Figure 3.1: Model of porosity vs. clay content for sand-clay mixtures.	48
Figure 3.2: Porosity vs. clay weight fraction vs. confining pressure. Calculated vs. measured.	50

Figure 3.3: Model of velocity vs. clay content for sand-clay mixtures	53
Figure 3.4: Velocity vs. clay weight fraction vs. confining pressure. Calculated vs. measured.	54
Figure 3.5: Influence of packing on porosity and velocity of sand-clay mixtures.	57
Figure 3.6: Permeability vs. clay content: model results vs. Gulf Coast sandstone data.	62
Figure 3.7: Velocity vs. porosity in sand-clay mixtures.	65
Figure 3.8: Influence of clay content on velocity-porosity relationship at a constant confining pressure.	66
Figure 3.9: Calculated velocity and porosity vs. pressure	67
Figure 3.10: Velocity and porosity data in marine shaley environment.	68
Figure 3.11: Sand-Clay model for porosity an velocity vs. Gulf Coast sandstones data.	71
Figure 3.12: Effect of clay content on the velocity-porosity relationship in Gulf Coast sandstones.	72
Figure 3.13: Density vs. P-velocity well-log data in shales and sandstones. ...	74
Figure 3.14: Permeability vs. porosity data in Gulf-Coast sandstones	76
Figure 4.1: Hertzian contact.	90
Figure 4.2: Mindlin contact.	90
Figure 4.3: Analogy between resistor networks and granular materials	98
Figure 4.4: Percolation relation in granular materials	98

Figure 4.5: Conductivity vs. pressure for mixtures of conducting and non conducting particles	103
Figure 4.6: Variations of number of contacts with pressure	104
Figure 4.7: Dependence of elastic moduli on number of contacts during unloading.	107
Figure 4.8: Static and dynamic moduli during loading and unloading.	109
Figure 4.9: Ratio of static to dynamic moduli versus pressure during loading and unloading.	110
Figure 4.10: Ratio of static to dynamic moduli vs. number of contacts during unloading.	111
Figure 5.1: Veugt-Reuss and Hashin-Shtrikman bounds for a Quartz-Water composite.	121
Figure 5.2: Bound Averaging Method	122
Figure 5.3: Sensitivity of BAM to type of bounds.	125
Figure 5.4: BAM vs. Gassmann's relations	126
Figure 5.5: P-Velocity versus Pressure in Westerley granite.	128
Figure 5.6: Bulk and Shear moduli in water saturated Boise Sandstone versus temperature.	130
Figure 5.7: Bulk and Shear moduli in water saturated Spergen Limestone versus temperature.	131
Figure 5.8: Bulk and Shear moduli of diabase versus pressure and temperature.	132
Figure 5.9: Compressional velocity in Massillon Light sandstone saturated with parawax versus temperature.	134

Chapter 1

Introduction

Naval surveillance, reflection seismology, civil engineering, oil reservoir geophysics are among the many different disciplines that are greatly concerned with physical properties of unconsolidated materials and their lateral and vertical variability.

In reflection seismology and naval surveillance, interaction of seismic and acoustic waves with unconsolidated materials is almost inevitable due to wide coverage of ocean floor with sediments. Significant amount of seismic or acoustic energy is dissipated at the water-sediment interface and within sediments. Hence understanding wave propagation phenomena in unconsolidated materials and their relationships with sediment properties is becoming essential for adequate signal processing.

Inversely, the detailed description of sediments properties from wave propagation characteristics has major applications in civil engineering and reservoir geophysics for problems including prediction of slope stability, detection of gas pockets, and description of oil fields heterogeneities.

Recent improvements in the resolution and sophistication of seismic and sonic measurements have increased our capability to image more complicated and finer scale geological structures. In addition, the continuing development of shear wave exploration, Vertical Seismic Profiling, well-to-well tomography, and amplitude versus offset techniques will provide a considerable amount of "potential" information on rock properties. To convert such information into rock properties, there is a first

order need to evaluate in a quantitative manner how physical properties of sediments such as porosity and pore geometry, lithology, clay content, fluid type, saturation, and state parameters such as temperature, state of stress, and pore pressure influence seismic and sonic velocities.

In this thesis, I restricted my study to the dependence of velocity on the following parameters: (1) porosity and compaction, (2) clay content , (3) packing properties and coordination number, and (4) fluid type. With this objective in mind, my dissertation has been divided in four chapters that describe the influence of each of these parameters on velocity in unconsolidated materials. However, because many of these parameters are not independent of each other, a complete understanding of the influence of one given property on velocity is a complex problem that requires knowledge of the relationships between dependent properties. To illustrate this point, Figure 1.1 shows the relationship between velocity and porosity in clastic sediments and rocks. It will be shown in this thesis that the apparent complexity of this relationship may be attributed to the effect of compaction (Chapter 2), the effect of clay content and location of clay in the pore space (Chapter 3), the influence of packing parameters on elastic properties (Chapter 4), and the type of fluid filling the rock pore space (Chapter 5).

In chapter 2, the dependence of velocity on porosity is investigated experimentally on an artificial sediment. The state of consolidation of sediments is found to dictate the behavior of the velocity-porosity relationship. In suspended sediments, velocity varies negligibly with porosity and is in good agreement with Wood's equation for suspensions (Wood, 1941). When porosity of the suspended sediment attains porosity of a loose random packing, a significant departure of velocity from Wood's equation is observed in experimental and in-situ data. This change of behavior of velocity corresponds to the transition from a fluid-supported to grain-supported sediment.

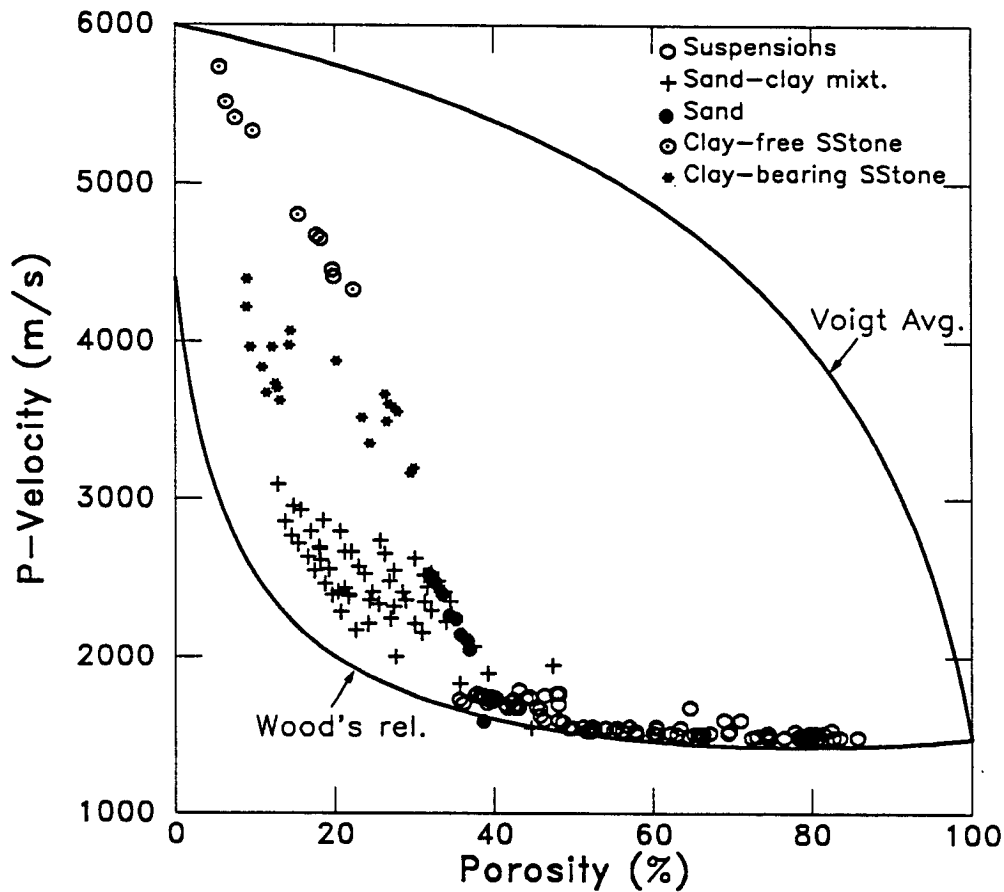


Figure 1.1: Velocity-porosity relationship in clastic sediments and rocks.

The apparent complexity of relationship between velocity and porosity is primarily due to the influence of compaction (Chapter 2) and clay content (Chapter 3) on both velocity and porosity. For suspended materials (○, data from Hamilton, 1956) velocity increases very slowly with decreasing porosity. In grain supported sediments such as unconsolidated sand (●, data from Yin et al., 1988) and consolidated clay free sandstones (⊙, data from Han et al., 1986), velocity departs significantly from the suspension behavior. The effect of clay content is to create apparent scatter in the velocity-porosity relationship as data in unconsolidated sand-clay mixtures (+, data from Yin et al., 1988) and clay-bearing sandstones (*, data from Han et al., 1986) suggest.

In chapter 3 a geometrical model is proposed which accounts for the influence of dispersed clay on velocity, porosity, and permeability of sediment mixtures. The model predicts a minimum in porosity and permeability vs. clay content and a maximum in velocity vs. clay content. Model results compare reasonably well with experimental data on unconsolidated sand-clay mixtures (Yin et al., 1988) and clay bearing sandstones (Han et al., 1986). The model also predicts that existence of scatter in velocity-porosity and porosity-permeability relationships in sediments has a deterministic cause and may be related to clay content.

Chapter 4 deals with elastic properties of granular materials and more specifically with the influence of coordination number on elastic moduli. An experiment was designed to determine indirectly the average number of contacts of a granular material. Variations in the number of deforming contacts with pressure that were observed experimentally illustrate the need to consider the average number of deforming contacts as an additional varying parameter in theoretical modeling of elastic moduli of granular materials. Results of this study also show a differing sensitivity of static and dynamic moduli to coordination number. This may account partially for the scaling factors between static and dynamic moduli in granular materials.

Chapter 5 illustrates a method to estimate the dependence of elastic properties of porous rocks and sediments on the elastic properties of the pore-filling material. This method differs from Gassmann's relations in the sense that it can account for pore filling materials that exhibit finite shear stiffness such as heavy oil, tar, ice. The method closely approximates Gassmann's predictions (1951) for data on dry vs. water saturated rocks. It is then applied to predict the temperature dependence of velocity in rocks saturated with water at the ice-water phase transition, and in hydrocarbon saturated rocks at the hydrocarbon solid-liquid phase transition.

References

- Gassmann, F., 1951, Elastic waves through a packing of spheres: *Geophysics*, v. 16, 673-685.
- Hamilton, E.L., 1956, Low sound velocities in high porosity sediments: *J. Acoust. Soc. Am.* , 28, 16-19.
- Han, D., Nur, A., and Morgan, D., 1986, Effect of porosity and clay content on wave velocity in sandstones: *Geophysics*, v. 51, 2093-2107.
- Voigt W. 1928, *Lehrbuch der Kristallphysik*, Teubner, Leipzig. Macmillan, New York.
- Wood, A.B., 1941, *A Textbook of Sound*. Macmillan, New York.
- Yin, H., Han D. H. and Nur A., 1988, Study of velocity and compaction on sand-clay mixtures, *Stanford Rock and Borehole Project*, Vol 33.

Chapter 2

Compaction of sediments and its effect on acoustic properties

Abstract

The dependence of compressional velocity on the state of compaction of sediments was investigated experimentally on suspensions and unconsolidated materials. Measurements of compressional velocity and electrical conductivity were made on conductive spheres immersed in a fluid of the same density, for grain volume fraction ranging from 0 to 64 percent. For grain fractions less than 60 percent, grains were in suspension: the system was not electrically conductive and compressional velocities were consistent with Wood's relation. At a critical grain fraction of 61 percent, mechanical interactions between grains and the existence of a solid skeleton became evident as pressure was required to expel additional fluid out of the sample cell, electrical conductivity departed abruptly from zero, and there was significant departure of the compressional velocity from its Wood's prediction. This experiment reveals that 1) compressional velocity is sensitive to the rheological transition between suspended and load-bearing unconsolidated materials and 2) that this transition occurs when porosity of the system attains porosity of loose packing. These observations were confirmed from marine in-situ velocity and density data.

2.1 Introduction

Two stages of consolidation for marine sediments are commonly observed in the first hundred meters of the sedimentary column: a *suspended state* where mechanical interactions between particles are negligible, and a *load-bearing state* where contacts between particles govern rigidity and stiffness of the material. As will be shown in this paper, state of consolidation strongly determines the range of variability of seismic properties of sediments. In suspensions, it is observed that velocity is quasi independent of sediment type, and impedance contrasts are primarily due to density variations caused by lithology contrasts. In unconsolidated sediments velocity is found to increase rapidly with depth with velocity gradients that depend on sediment types such that impedance contrasts can be attributed to both velocity and density variations.

In unconsolidated sediments, the effect of compaction on velocity has been investigated experimentally in numerous studies in geophysics and civil engineering (Laughton, 1957; Domenico, 1977; Hardin and Richard, 1963 ; Hamdi and Smith, 1982). Their main objective was to evaluate the pressure dependence of rigidity and bulk modulus in sediments and soils and identify their relationships with physical parameters such as porosity, mineralogy, sorting, angularity, etc. Results of these studies were combined with in situ seismic reflection and refraction surveys to build geoacoustical models, a concept developed by Hamilton (1980) that describes the velocity (or other physical properties) vs. depth profiles in sediments of various environments. The development of such models was aimed at predicting wave propagation in the ocean floor to gain a better understanding of the structure of the crust. However, a main limitation in the accuracy of the model is the limited amount of well log and core data that are used to calibrate the seismic measurements in suspension and unconsolidated sediment.

In this study , our objective is to evaluate experimentally how changes of physical

properties of sediments during consolidation affect the compressional wave velocity in the first hundred meters of the sedimentary column. In particular, attention will be focused on the transition between suspension and unconsolidated load-bearing sediments that delineates materials with different seismic and mechanical characteristics. With this objective in mind, we have simulated experimentally a sedimentation process measuring acoustic and electrical properties during the continuous transition from a suspension to a compacted material. The first part of this study is related to understanding compressional wave propagation in suspended sediments and identify the causes for variations of P-velocity in such suspensions. The second part, is an experimental study of the transition from a suspension to a compacted material in which the sensitivity of compressional waves and electrical conductivity to this transition is investigated. Experimental data are then qualitatively compared with available marine in-situ data.

2.2 Suspensions

Materials in suspension are widely encountered at the surface of ocean floors and lake bottoms with thicknesses reaching a few hundreds of meters. Because in any seismic survey, waves travel at least twice in suspended sediments, it is important to determine how wave propagation is affected by the physical properties of sediments. Many studies have been concerned with laboratory and in-situ measurements of wave propagation in ocean bottom sediment at sonic and ultrasonic frequencies (Ament, 1953; Hamilton, 1956; Hamilton et al., 1956; Sutton et al., 1957; Shumway, 1960; Tucholke and Shirley, 1979; Initial Report of the Deep Sea Drilling Project.). The objective of these measurements was to evaluate which physical properties and geological factors may affect velocity and attenuation in suspensions. These measurements have been used to establish relationships between compressional velocity and other physical properties such as porosity, bulk density, mean grain size. In particular, the

relationship between compressional velocity and porosity has been the object of special interest (Nafe and Drake, 1957; Shumway, 1960; Hamilton, 1978; Akal, 1972). The results of these studies show that the trend of the relationship between porosity and velocity in suspended sediments can be matched as a first order approximation by Wood's relation (Wood, 1941) an extension of the Reuss average (Reuss, 1929) or isostress model. In Wood's relation (see equation 2.14), effective compliance of the suspension is a volume fraction weighted sum of the compliances of liquid and solid particles. However, because Wood's equation tends to underestimate values of velocity, many semi-empirical and regression relations have been proposed to better fit velocity-porosity data in sediments. In figure 2.1, a compilation of velocity and porosity data for ocean bottom sediments (Hamilton et al., 1956; Shumway, 1960; DSDP data from site 574, leg 85) illustrates the difference between measured and predicted velocity which can be as high as 5-10 % in highly porous sediments (60 to 85 % porosity). This discrepancy between Wood's velocity prediction for suspension and measured velocities can have two possible causes: 1) highly porous sediments do not behave as suspended sediments or 2) the Wood-isostress relation does not correctly describe dependence of velocity on porosity in suspensions.

In this section, our objective is to test experimentally the validity of the Wood-isostress relation on artificial suspensions in order to determine the nature of the discrepancy between measured and predicted velocities in ocean bottom sediments.

2.2.1 Ultrasonic measurements vs. "zero frequency" Wood-isostress relation

Because most laboratory velocity measurements are performed at ultrasonic frequencies (100 kHz and greater), the use of high frequency measurements may not be appropriate to validate Wood's relation, a zero frequency approximation for velocity. Using theoretical considerations based on Biot's theory, we show here how ultrasonic velocity measurements may coincide with "zero frequency" measurements in a few

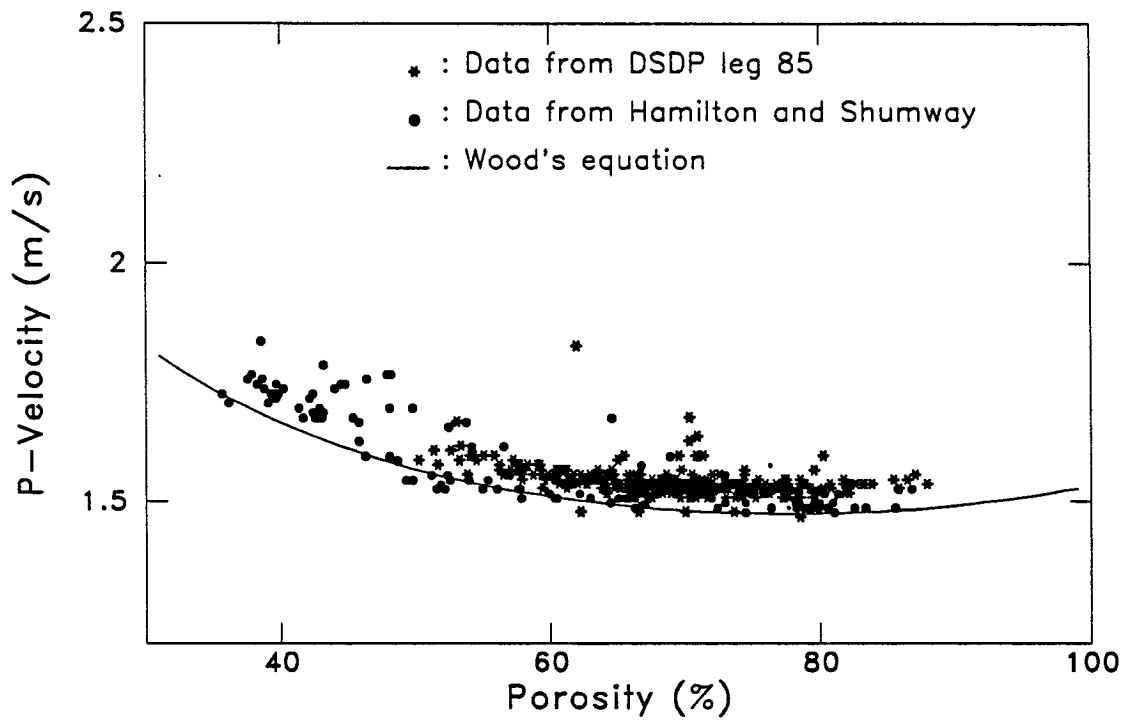


Figure 2.1: Velocity vs. porosity in ocean bottom sediments. Velocity data from Hamilton et al. (1956) and Shumway (1960) (●) are core measurements from shallow water sediments off San Diego. Data from Deep Sea Drilling Project (*) are core measurements from site 574, leg 85. Data are compared with Wood's equation for suspension of quartz particles in sea water at 20 deg C, 35 ‰ salinity and 0.1MPa.

particular cases. Biot (1956) derived a theory for wave propagation in a porous elastic solid saturated with a viscous fluid. In his derivation, Biot considers that when waves propagate through a porous solid saturated with a viscous fluid, relative motion between fluid and solid phases may occur. At low frequencies, the relative motion of the fluid in the pore is assumed to be of the Poiseuille type (steady laminar flow in circular cylinder) whereas at high frequency assumption of laminar flow may not be valid.

In the high frequency regime, shear and compressional velocities, V_s and V_p , can be computed using the following relations:

$$V_s^2 = \frac{G_{fr}}{(1 - \phi)\rho_s + \phi(1 - \alpha^{-1})\rho_{fl}} \quad (2.1)$$

$$V_p^2 = \frac{\Delta + (\Delta^2 - 4(\rho_1\rho_2 - \rho_{12}^2)(PR - Q^2))^{1/2}}{2(\rho_1\rho_2 - \rho_{12}^2)} \quad (2.2)$$

where

$$\Delta = P\rho_2 + R\rho_1 - 2Q\rho_{12} \quad (2.3)$$

$$P = \frac{4G_{fr}}{3} + \frac{((1 - \phi)(1 - \phi \frac{K_{fr}}{K_s})K_s + \phi K_{fr} \frac{K_s}{K_{fl}})}{(1 - \phi - \frac{K_{fr}}{K_s} + \phi \frac{K_s}{K_{fl}})} \quad (2.4)$$

$$Q = \frac{(1 - \phi - \frac{K_{fr}}{K_s})\phi K_s}{(1 - \phi - \frac{K_{fr}}{K_s} + \phi \frac{K_s}{K_{fl}})} \quad (2.5)$$

$$R = \frac{\phi^2 K_s}{(1 - \phi - \frac{K_{fr}}{K_s} + \phi \frac{K_s}{K_{fl}})} \quad (2.6)$$

$$\rho_1 + \rho_{12} = (1 - \phi)\rho_s \quad (2.7)$$

$$\rho_2 + \rho_{12} = \phi \rho_{fl} \quad (2.8)$$

$$\rho_{12} = \phi(\alpha - 1)\rho_{fl} \quad (2.9)$$

where K_s , K_{fl} , K_{fr} , G_{fr} are the bulk modulus of the solid, the fluid, the dry frame, and the shear modulus of the dry frame respectively. ϕ , ρ_s , and ρ_{fl} are the porosity, mineral density and fluid density respectively and α , the inertial drag parameter, is a geometrical parameter which in the case of solid spheres immersed in a fluid is given by Berryman (1980) as

$$\alpha = \frac{1}{2}(\phi^{-1} + 1) \quad (2.10)$$

For non spherical particles in suspension the expression for α vs. porosity, ϕ , may be slightly different from equation (2.10) such that α has to be determined experimentally.

In the particular case of grains suspended in a liquid, bulk and shear moduli of the skeletal frame, K_{fr} , and G_{fr} , are equal to zero and

$$PR - Q^2 = 0 \quad (2.11)$$

In the high frequency limit equations (2.1) and (2.2) for suspended materials become:

$$V_s^2 = 0 \quad (2.12)$$

$$V_p^2 = \left(\frac{1-\phi}{K_s} + \frac{\phi}{K_{fl}} \right)^{-1} \left(\frac{\phi(1-\phi)\rho_s + (\alpha - 2\phi + \phi^2)\rho_{fl}}{\alpha\rho_{fl}[(1-\phi)\rho_s + (1-\alpha^{-1})\phi\rho_{fl}]} \right) \quad (2.13)$$

Finally, the low frequency limit ("zero frequency") for compressional velocity can be extrapolated from the high frequency limit by considering that the inertial drag parameter α is infinite. This physically corresponds to the case where fluid and solid particles are perfectly coupled and locked together by viscous forces. With analogy to a viscous dashpot in a viscoelastic solid, this corresponds to complete relaxation of the dashpot. P-velocity then finally reduces to Wood's equations:

$$V_p^2 = \frac{\left(\frac{1-\phi}{K_s} + \frac{\phi}{K_f}\right)^{-1}}{\rho_s(1-\phi) + \rho_{fl}\phi} \quad (2.14)$$

where the effective bulk modulus of the suspension (numerator on the right hand side of the equation (2.14)) is given by the Reuss or isostress average.

In the particular case where liquid and solid have the same density ($\rho_s = \rho_{fl}$), we notice that equation 2.13 simplifies greatly and the high frequency limit for P-velocity reduces to the Wood-isostress relation (eqn. 2.14). In summary, we have shown that, according to Biot's theory, ultrasonic measurements reduce to the simple Wood-Isostress relation (1) for materials in suspension, (2) when densities of fluid and solid phases are identical.

2.2.2 Experimental procedure

A homogeneous suspension was achieved by immersing grains in a liquid of the same density. The solid particles were silver coated glass spheres manufactured by Potters Industry (product 2429-S). Average particle diameter was 75 microns and particle size distribution was ranging from 53 to 105 microns. Silver coating was 4 % by weight and density of the particles was equal to 2.42 g/cm³. The liquid used was sodiumpolytungstate, a heavy liquid manufactured by Tungstene Compounds. The heavy liquid solution was obtained by diluting dry sodiumpolytungstate crystal pow-

der in deionized water to the desired density (2.42 g/cc).

Measurements were conducted in a transparent container to ensure visual control of the state of the suspension. Compressional velocity was measured using the pulse transmission technique (Birch, 1960). Both travel time and amplitude of the first peak were recorded in this experiment. Two piezoelectric transducers operating at a central frequency of 1.2 MHz were positioned on two parallel sides of the container (see Figure 2.2 for experimental set-up). The wave length was of the order of 1-2 mm and 15-20 times greater than the average grain diameter. The distance between the transducers was fixed at $2.54 \text{ cm} \pm 0.01$. The signal was generated by a high power pulse generator (Velonex 345), amplified after propagation through the sample and recorded on a digital oscilloscope (Nicolet 204) with reading accuracy of ± 0.05 microseconds.

A complete coverage of grain volume fraction between 0 and 56 percent (100 to 44 percent porosity) was achieved stepwise by introducing grains to the mixture by increments of 1 to 4 percent.

2.2.3 Comparison between experimental data and the Wood-isostress relation

Comparison between experimental data and the Wood-isostress relation first necessitates an estimate of elastic moduli of silver coated spheres and sodiumpolytungstate. Bulk modulus of the heavy solution of sodiumpolytungstate was calculated directly from velocity and density measurements in pure sodiumpolytungstate. The value for the bulk modulus of sodiumpolytungstate is listed in table I. Elastic moduli of the silver coated spheres were calculated using the arithmetic average between Voigt (1928) and Reuss (1929) bounds for a silver-glass composite. Voigt and Reuss bounds were calculated for a 1% silver coated glass beads using the values of elastic moduli of pure silver and pure glass listed in table 1.1. Note that because of the small amount of silver (1% by volume) Voigt and Reuss moduli are not significantly different from

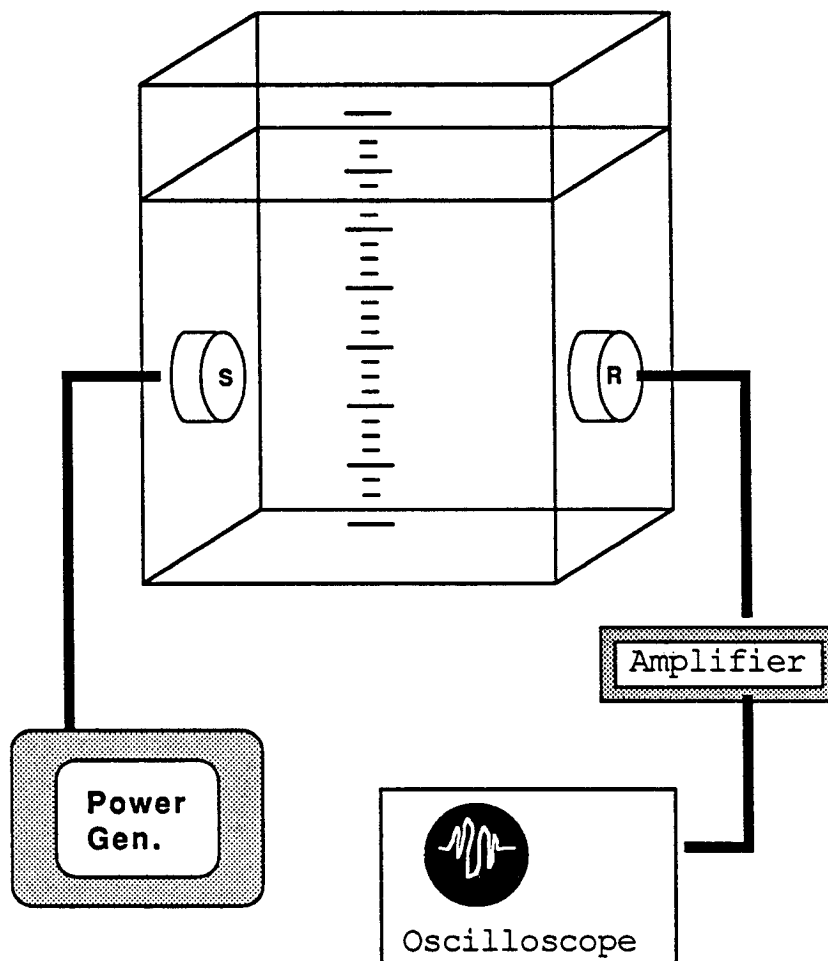


Figure 2.2 : Experimental set-up for velocity measurements in suspensions. Two piezoelectric transducers (S for source and R for receiver) operating at a central frequency of 1.2 MHz are located on two parallel sides of a plexiglass container. Grain volume concentration is varied by adding particles to the mixture.

their arithmetic average and the error due to the choice of one formula rather than another is less than 0.5 %.

Table 2.1

	Bulk Mod. (MPa)	Shear Mod. (MPa)	Dens. (g/cm ³)
Silver *	102610	26957	10.4
Glass *	40519	24959	2.32
Voigt (Calc.)	41140	24979	—
Reuss (Calc.)	40765	24978	—
Silver coated glass beads	40952	24979	2.42
Sodiumtung.	4595	0	2.42

* *CRC Handbook on Rock properties, Carmichael, 1981*

Using the Wood-isostress model, effective bulk and shear moduli of the "silver coated glass bead-sodiumpolytungstate" suspension, K^* , and G^* , are computed using the following relations:

$$\frac{1}{K^*} = \frac{1-\phi}{K_s} + \frac{\phi}{K_{fl}} \quad (2.15)$$

$$\frac{1}{G^*} = \frac{1-\phi}{G_s} + \frac{\phi}{G_{fl}} \quad (2.16)$$

where K_s , K_{fl} , G_s , G_{fl} , and ϕ are the bulk modulus of the solid, bulk modulus of the fluid, shear modulus of the solid, shear modulus of the fluid (from C.R.C. handbook on physical properties of rocks, Carmichael,1981), and porosity of the solid-fluid mixture respectively. Because G_{fl} in equation (2.16) is assumed to be equal to zero, the effective shear modulus of the suspension is also equal to zero and the effective compressional velocity, V_p^* , of the mixture reduces to Wood's equation (eqn. 2.14) with

$$(1-\phi)\rho_s + \phi\rho_{fl} = \rho_s = \rho_{fl} \quad (2.17)$$

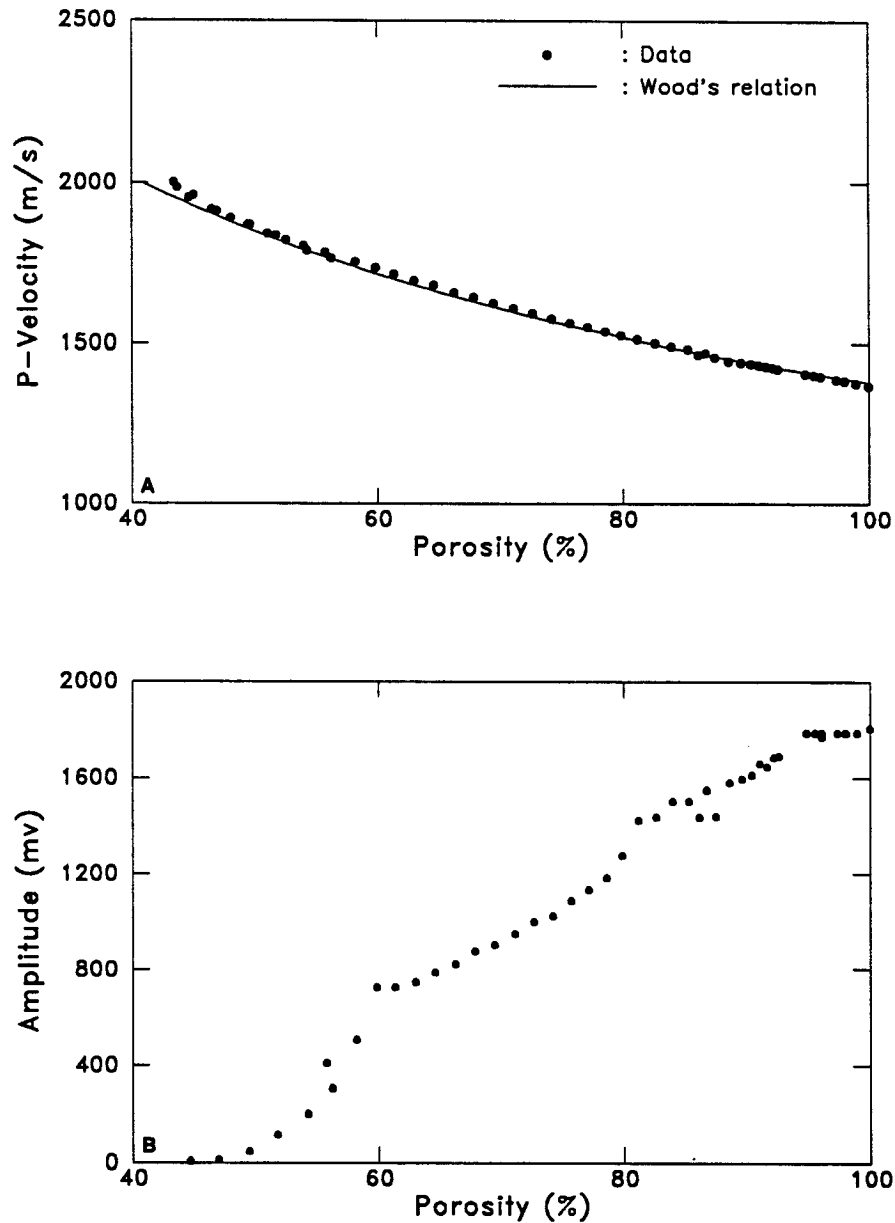


Figure 2.3: Compressional velocity versus porosity for a suspension of silver coated glass spheres immersed in sodiumpolytungstate. Experimental data (•) are compared with the Wood-isostress relation (solid line) in figure 2.3a. Measurements of first peak amplitude (figure 2.3b) show that quality and accuracy of the signal decreases with increasing volume fraction due to scattering effect of suspended spheres.

The comparison between velocity data and the Wood-isostress is shown in Figure 2.3a. The Wood-isostress relation was calculated for three values of the silver coated glass beads bulk modulus (Voigt, Reuss and the arithmetic average of Reuss and Voigt average shown in table I). The difference between the three curves is not resolvable in this figure scale and generally is less than 0.1%. Velocity data are in close agreement (within 1.5 %) with the Wood-isostress relation for solid volume fraction ranging from zero to 50 percent (50 percent porosity). For grain fraction greater than 50 % (porosity less than 50 %) velocity measurements exhibit a slight positive departure from Wood's relation. Note however from figure 2.3b that the amplitude of the first peak in the signal decreases with increasing grain fraction rendering the accuracy of measurements questionable for grain fractions greater than 50 %.

This experiment demonstrates that the Wood-isostress relationship can adequately describe (within 1.5 %) the velocity-porosity relationship of suspended sediments at low frequencies.

2.2.4 Departure from Wood's relation in sediments: possible causes

We have shown in Figure 2.1 that in sediments in suspension compressional velocity is generally higher than the Wood-isostress prediction. This section is a discussion of physical parameters that may affect velocity measurements in sediments and their departure from the Wood-Isostress relation.

Velocity vs. temperature, salinity, and pressure in sea water.

Variations of sea water velocity with temperature, salinity and pressure are important parameters to be considered when calculating the Wood-isostress relation and comparing it with in situ data. Studies of the effect of temperature on velocity in sediments (Shumway, 1958; Bell and Shirley, 1980) have shown that variations of

compressional velocity in sediments with temperature are primarily related to the variation of sea-water velocity with temperature. Such behavior is not surprising for suspensions considering that the Wood-isostress relation is very sensitive to variations of elastic moduli of the fluid phase and is less affected by variations of the elastic moduli of the mineral phase. The velocity of sea-water is also strongly dependent on pressure and salinity. Consequently, velocity in suspended sediments is also expected to be affected by pressure (or identically depth below sea level) and sea-water salinity. In Figure 2.4, P-velocity was calculated as a function of temperature and pressure for suspended sediment (porosity of 65 %). Variations of water velocity with temperature and pressure are from CRC Handbook of physical properties of rocks (Volume II, p134; Carmichael, 1981). An increase of temperature from 0 to 22 °C is expected to cause velocity of the sediment to increase by 5 %. Identically, pressure or equivalently depth below sea level can affect velocity by few percent.

Skeleton frame

The existence of weak skeleton frame with finite rigidity and bulk stiffness have been proposed as a possible mechanism responsible for the discrepancy between velocity measured in sediments and Wood's prediction (Shumway, 1960; Hamilton, 1971). Existence of rigidity for materials in suspension has been observed experimentally on laboratory sediments made of kaolinite in suspension in water (Shirley and Hampton, 1978). In their study, Shirley and Hampton measured shear velocities ranging from 2 m/s for a 25% kaolinite 75% water suspension to 20 m/s for a 35 % kaolinite 65 % water suspension. Shear velocity measurements on weakly flocculated suspensions (Goodwin et al, 1986) also exhibit rigidity (10^{-2} MPa) for porosities as high as 75 %. Rigidity in flocculated suspensions is shown to be heavily dominated by the particles pair distribution function and the particle pair potential (Van der Waals' attraction forces and steric and electrostatic repulsion forces). Finally in-situ shear

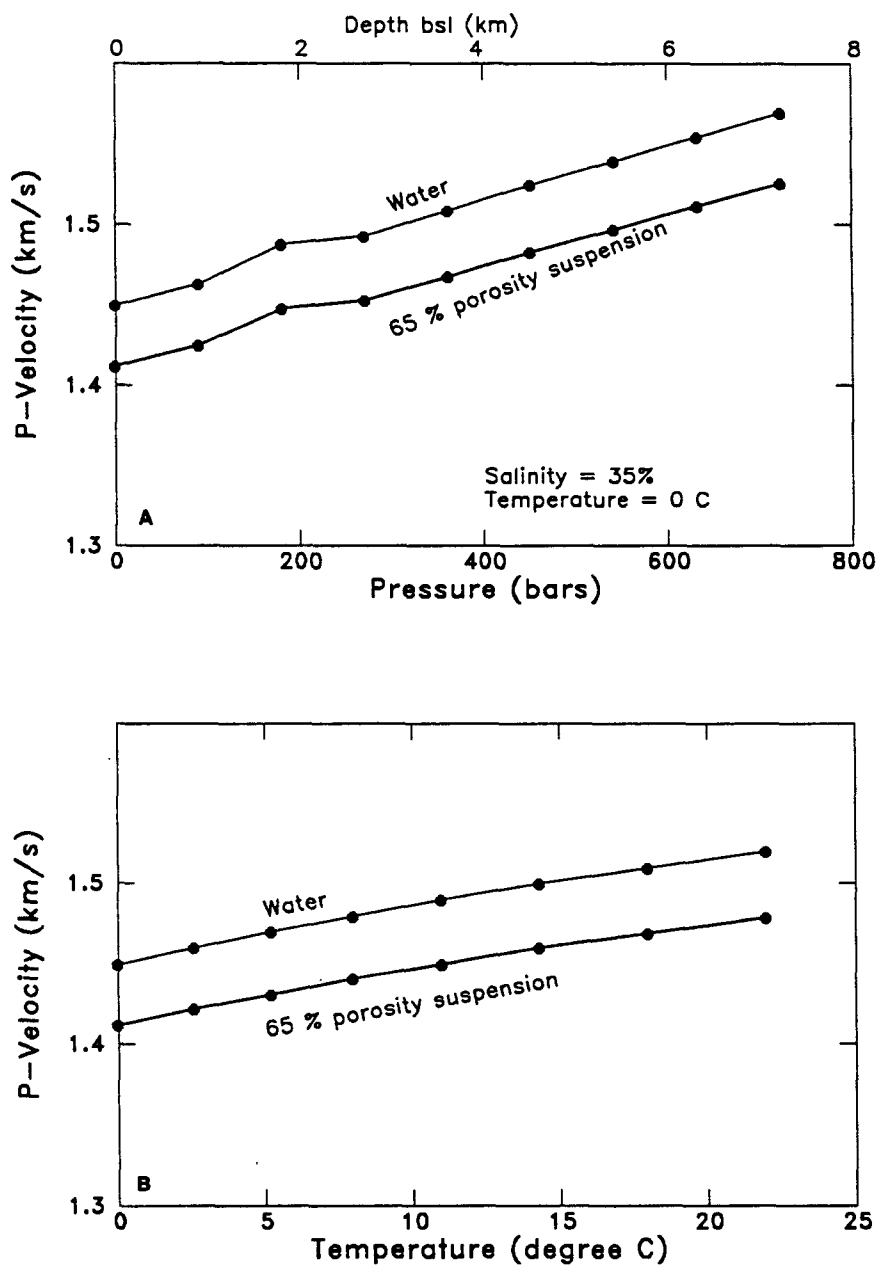


Figure 2.4: Influence of pressure (Figure 2.4a) and temperature (Figure 2.4b) on sea water velocity and its effect on compressional velocity in suspended sediment. Sea water velocity data vs. temperature and pressure are from CRC handbook of physical properties of rocks (Carmichael, 1981). Velocity in sediment is calculated for a 65 % porosity sediment composed of quartz particles using the Wood-Isostress relation.

wave seismic surveys in clay rich sediments (Stoll et al., 1988; Hamilton, 1971) or shear velocity measurements derived from Rayleigh wave measurements (Gabriels et al., 1987) reveal values of shear velocity of the order of 100 m/s, corresponding to rigidity of the order of tens of MPa within the first meters of the ocean floor. We estimate here the influence of skeleton frame rigidity and bulk stiffness on compressional velocity using Biot's low frequency relations. Using a constant value of rigidity of 15 MPa (corresponding to shear velocity of 100 m/s) for a sediment of 60 % porosity, we calculate the low frequency limit compressional velocity for various values of the skeleton bulk modulus. Results in figure 2.5 show that rigidity similar to that measured in sediments and reasonable values of the skeleton bulk modulus (ratio of compressional to shear velocity of the order of 2 (Stoll, 1977)) can account for departure of compressional velocity from Wood's equation of the order of 1 % but can not explain discrepancy of the order of a few percent.

Frequency.

As equations (2.13) and (2.14) suggest, the discrepancy between velocity measured ultrasonically and velocity calculated using Wood's equation may be partially attributed to frequency. To evaluate the effect of frequency on velocity of suspended materials, we use the approximate solution derived by Geertsma and Smit (1961) where velocity is related to frequency, ω , and Biot's low and high frequency velocities, V_0 and V_∞

$$V(\omega) = \left(\frac{V_\infty^4 + V_0^4 \left(\frac{\omega_c}{A\omega} \right)^2}{V_\infty^2 + V_0^2 \left(\frac{\omega_c}{A\omega} \right)^2} \right)^{1/2} \quad (2.18)$$

with

$$A = \frac{2\rho_{12} + \rho_1 + \rho_2 + \frac{\rho_2}{\phi^2} - \frac{\rho_{12} + \rho_2}{\phi}}{(2\rho_{12} + \rho_1 + \rho_2)^2} \quad (2.19)$$

where, ω_c , the critical frequency between high and low frequencies, is related to the density of the system, the viscosity of the liquid phase, μ , and the permeability of

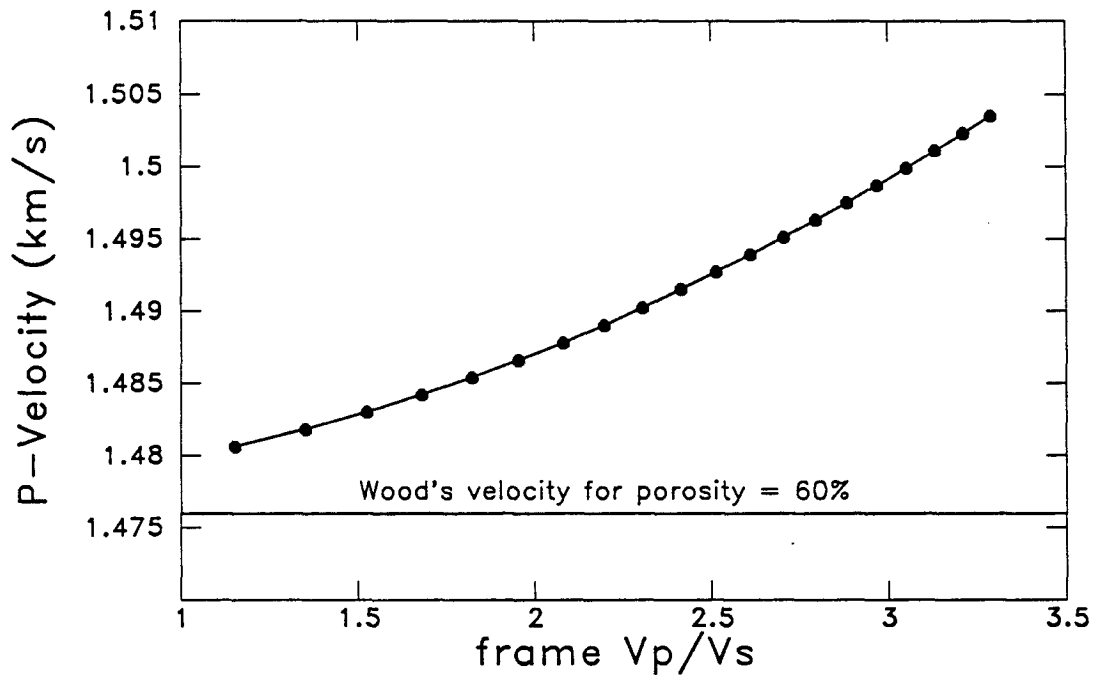


Figure 2.5: Influence of rigidity and bulk stiffness of sediment skeleton frame on compressional velocity. Compressional velocity is calculated using Biot's low frequency relationship for the dependence of compressional velocity on skeleton frame properties. Rigidity is fixed to 15 MPa (Shear velocity of 100 m/s) and calculations are carried out for various values of frame bulk stiffness and plotted as a function of the skeleton frame V_p/V_s ratio. For reasonable values of V_p/V_s ratio (between 1.5 and 2.5), rigidity of 15 MPa can not account for departures from Wood's equation of more than 1.5 %.

the system, k , following the relation:

$$\omega_c = \frac{\mu}{k(2\rho_{12} + \rho_1 + \rho_2)} \quad (2.20)$$

where ρ_1 , ρ_2 , and ρ_{12} are defined in equations (2.7) to (2.9) (see Biot's high frequency velocity).

Calculations of ω_c were carried out for various sediment types using a relationship between permeability and porosity (solid line in Figure 2.6) derived from soil mechanics literature (Lambe and Whitman, 1969). Figure 2.6 shows the permeability-porosity data for sand, silts, and clay and a regression curve. Values of critical frequency for typical sand, silt and clay are shown in table 2.2.

Table 2.2

	Porosity (%)	Permeability (mD)	Critical frequency MHz
Sand	40	10000	0.02
Silt	60	30	10
Clay	80	1	1000

Using the values of critical frequencies listed in table 2.2 we calculated the velocity dispersion curve for sand, silts, and clay using equation (2.18). Results in figure 2.7 show that in the typical frequency range of ultrasonic measurements (100 KHz-MHz), velocity measurements in sands are high frequency measurements whereas in silts and clay they are low frequency measurements.

Similar results are shown in Figure 2.8 on a velocity-porosity plot. In figure 2.8 velocity was calculated at various frequencies (1 KHz, 100KHz, and 10MHz) as a function of porosity. We find that in the range of frequency used in in-situ sonic well-log measurements (10-20 KHz) and laboratory ultrasonic measurements on cores (100kHz-MHz), velocity dispersion may influence the porosity-velocity relationship. For high porosity and low permeability sediments such as silts and clay, sonic and ultrasonic velocity measurements can be considered as low frequency measurements. In low porosity and high permeability materials such as sands, velocity measurements

are in the low frequency limit at sonic frequencies. Velocity data in shallow ocean floor sediments (Hamilton et al., 1956; Shumway, 1960) measured at frequencies of 20-35 KHz tend to confirm our observations. Data shown in Figure 2.9 suggest that fine sediments such as silts and clay are generally closely matched by the Wood-isostress relation for suspension whereas coarser materials such as sands slightly depart from Wood's low frequency approximation. We suggest that this type of behavior for the porosity-velocity relationship may be related to frequency at which measurements were conducted. In low permeability silts and shale, 30 KHz is a low frequency measurement as shown in Figure 2.7. In contrast for sands with porosity of the order of 40-50 % and permeability of 1-100 Darcy (Figure 2.6), measurements made at 30 KHz are in the range of sand critical frequency. Hence, velocity in sand (* in figure 2.9) is expected to depart from Wood's low frequency relation and lie in between low and high frequency behavior depending on sand permeability.

2.3 Transition from suspension to compacted sediment

The previous section has shown that the relationship between compressional velocity and porosity in materials in suspensions could be matched within a few percent by the Wood-isostress relation for porosity as low as 50 % and velocity measurements made at frequencies lower than 100 KHz range. The relatively close agreement between Wood's equation and high porosity data was found to be essentially due to 1) the absence of significant mechanical interactions between particles in suspension and 2) the absence of velocity dispersion in these low permeability sediments. Upon compaction, however, contacts between grains may form at the transition from suspension to unconsolidated material. A load bearing frame is then expected to form and velocity should depart rather significantly from the Wood-isostress model. The objective of this section is to (1) determine whether the transition between suspen-

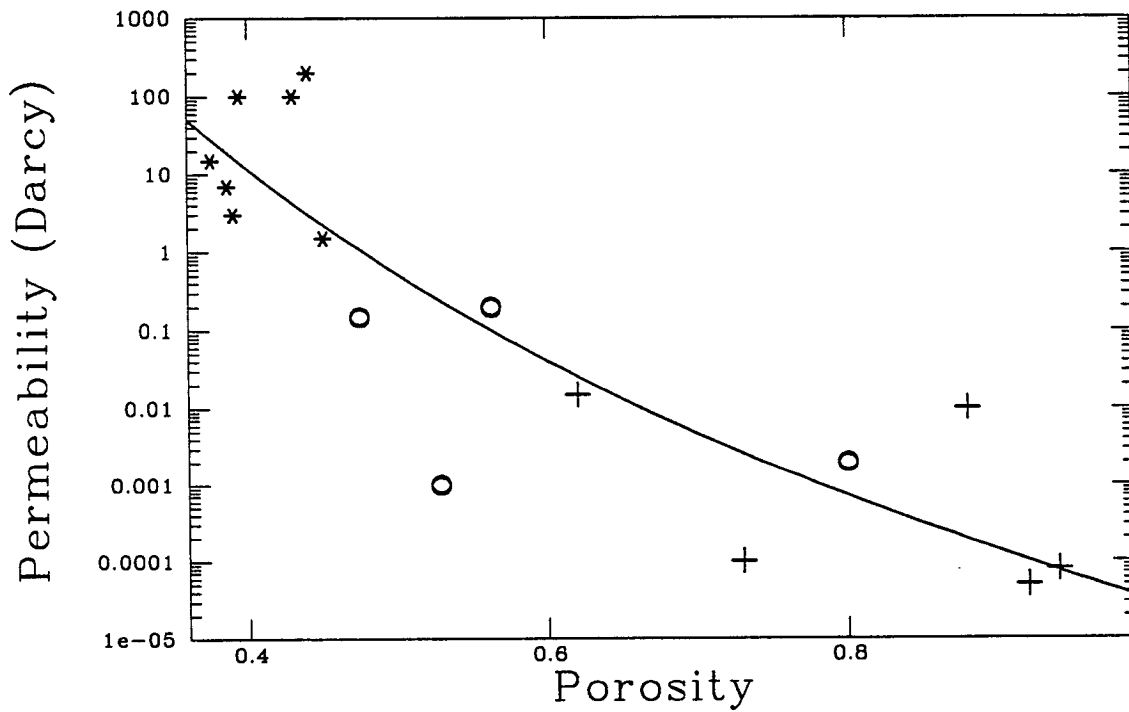


Figure 2.6: Permeability vs. porosity for sand (*), silt (o) and clay (+). Data are from Lambe and Whitman (1969). A regression equation (solid line) of the form $k = 10^{a-b\text{LOG}_{10}(\phi)}$ has been used to relate permeability (in Darcy) to porosity with $a = -4.5$ and $b = -13.8$.

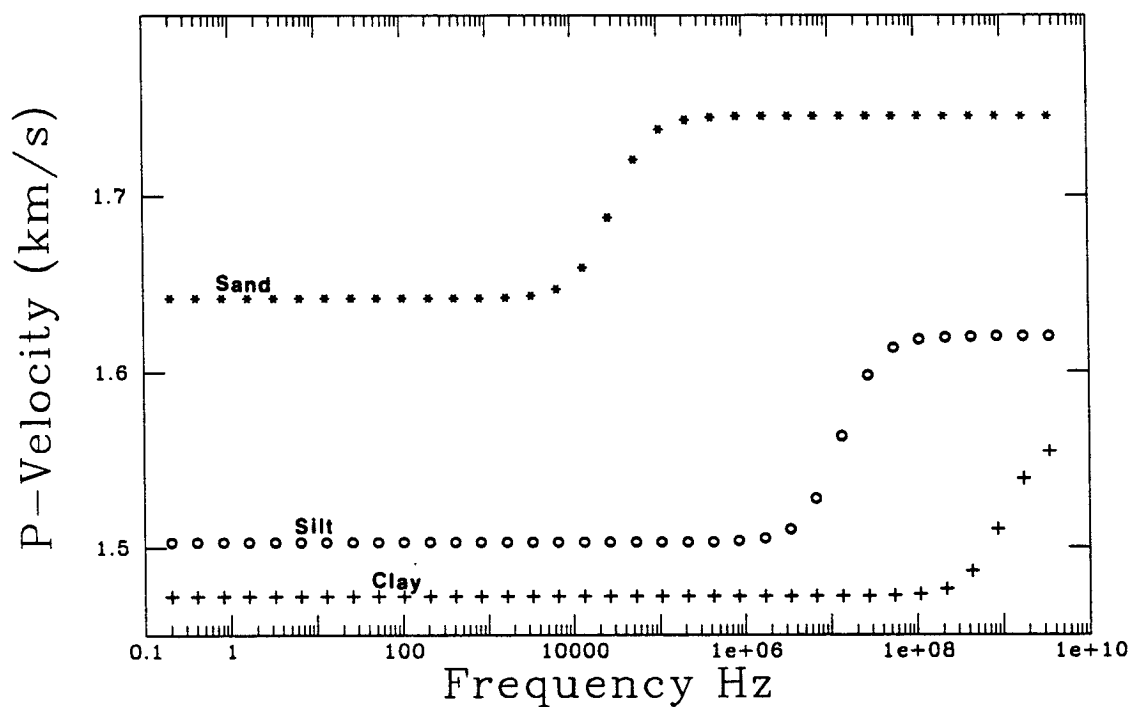


Figure 2.7: Calculated velocity versus frequency for sand (*), silt (o), and clay (+). For a sand of 40 % porosity and 10 Darcy permeability, critical frequency is in the sonic-ultrasonic range (10-100 kHz). For a silt of 60 % porosity and 10 mD permeability, critical frequency is in the high ultrasonic frequency range (10 MHz). In clay with 80 % porosity and permeability of the order of 0.5 mD, critical frequency is in the GHz range.

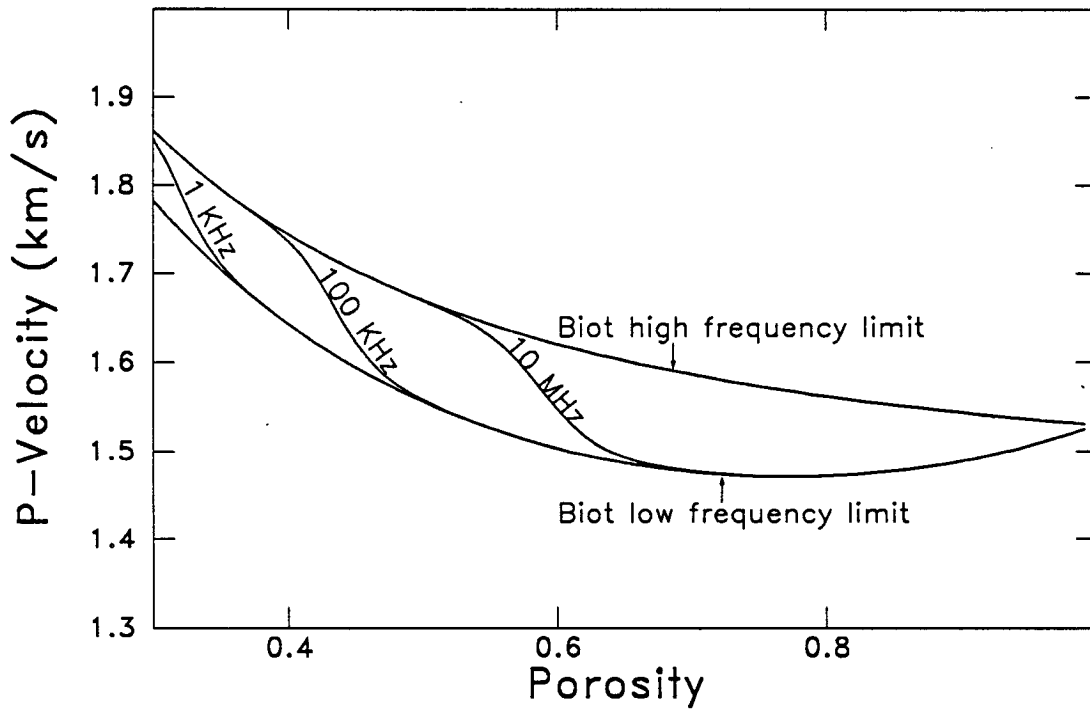


Figure 2.8: Influence of frequency on velocity- porosity relationship. Biot high and low frequency velocity-porosity behavior are shown for comparison. In the sonic frequency range (10-20 KHz) velocity measurements follow the low frequency behavior (Wood's equation) for porosities as low as 45 % and then depart from Wood's equation to reach the Biot high frequency limit for velocity. In the ultrasonic range transition between low and high frequency measurements occurs for porosities ranging between 50 and 60 %.

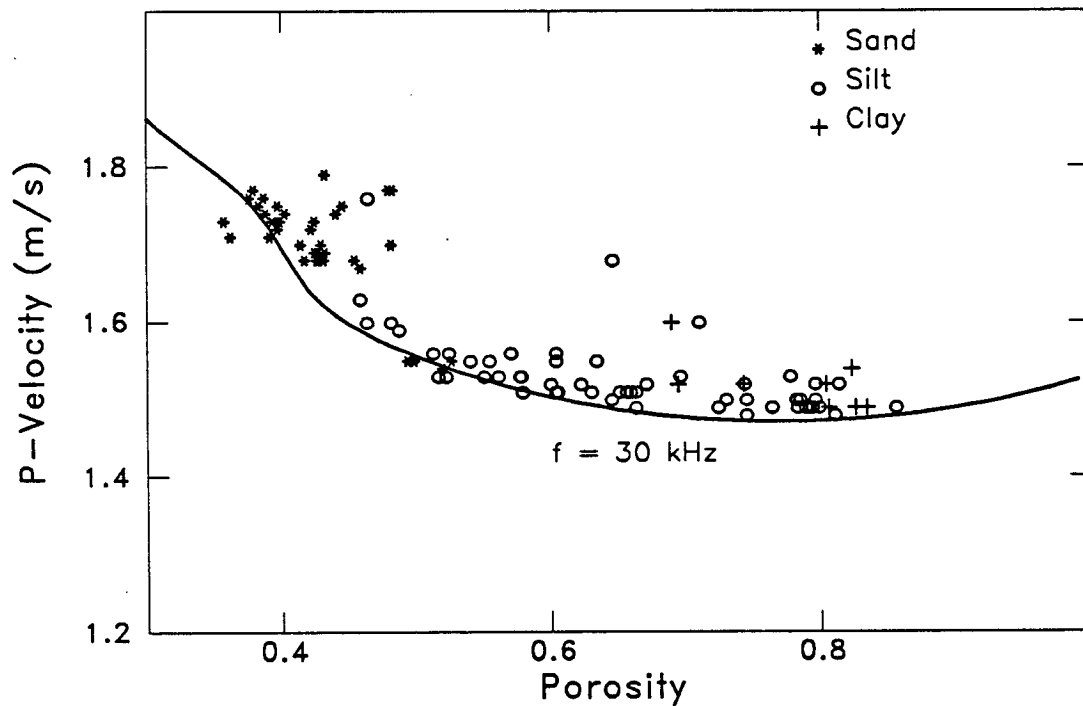


Figure 2.9: Compressional velocity measurements on ocean bottom sediment cores (Data from Shumway, 1960) recorded at frequencies ranging between 22-35 KHz. The slight increase in velocity that occurs for porosity ranging between 35 and 45 % may be attributed to frequency as the computed velocity-positivity relationship (solid line) suggests. In sands (porosity of 35-45 %), 30 KHz may correspond to a low or high frequency measurement depending on the sand permeability (.1-100 Darcy) whereas in silts and clay (porosity from 50 to 85), 30 KHz is a low frequency measurement and data follow Wood's relation.

sions and compacted materials is instantaneous and can be detected using acoustic measurements and (2) define at which porosity mechanical interaction between grains in contacts appear upon compaction.

2.3.1 Experimental set-up

In order to determine whether velocity measurements are sensitive or not to the rheological transition from a suspension to a load bearing material, a test measurement was necessary. Electrical conductivity measurements were chosen as a test measurement based on the sensitivity of electrical conductivity of granular materials to grain contacts and grain interactions (Batchelor and O'Brien, 1977). The sample was achieved by immersing conducting silver coated glass beads with sodiumpolytungstate (the same material was used in the experiment described in the previous section).

In this experiment, the sample was jacketed in a plexiglass cylinder and fluid was allowed to flow out of the cell through a fiber glass paper filter (see Figure 2.10 for experimental set-up). Grain volume fraction was increased from five percent to 65 percent by expelling some liquid out of the cell using two end-plug pistons connected to a uniaxial hydraulic press. Grain volume fraction was calculated using the proportionality between grain volume fraction and the inverse of the sample length. Change of length of the sample was measured using three micrometers positioned at 120 degrees of each other around the sample. Compressional velocity was measured at a center frequency of .9 MHz using two piezoelectric transducers located on both ends of the sample. Travel time was recorded with an accuracy of $\pm 0.05 \mu\text{s}$. Resistance of the sample was measured simultaneously using a digital Ohmmeter (HP 3478A) with reading accuracy of 10^{-4} ohms.

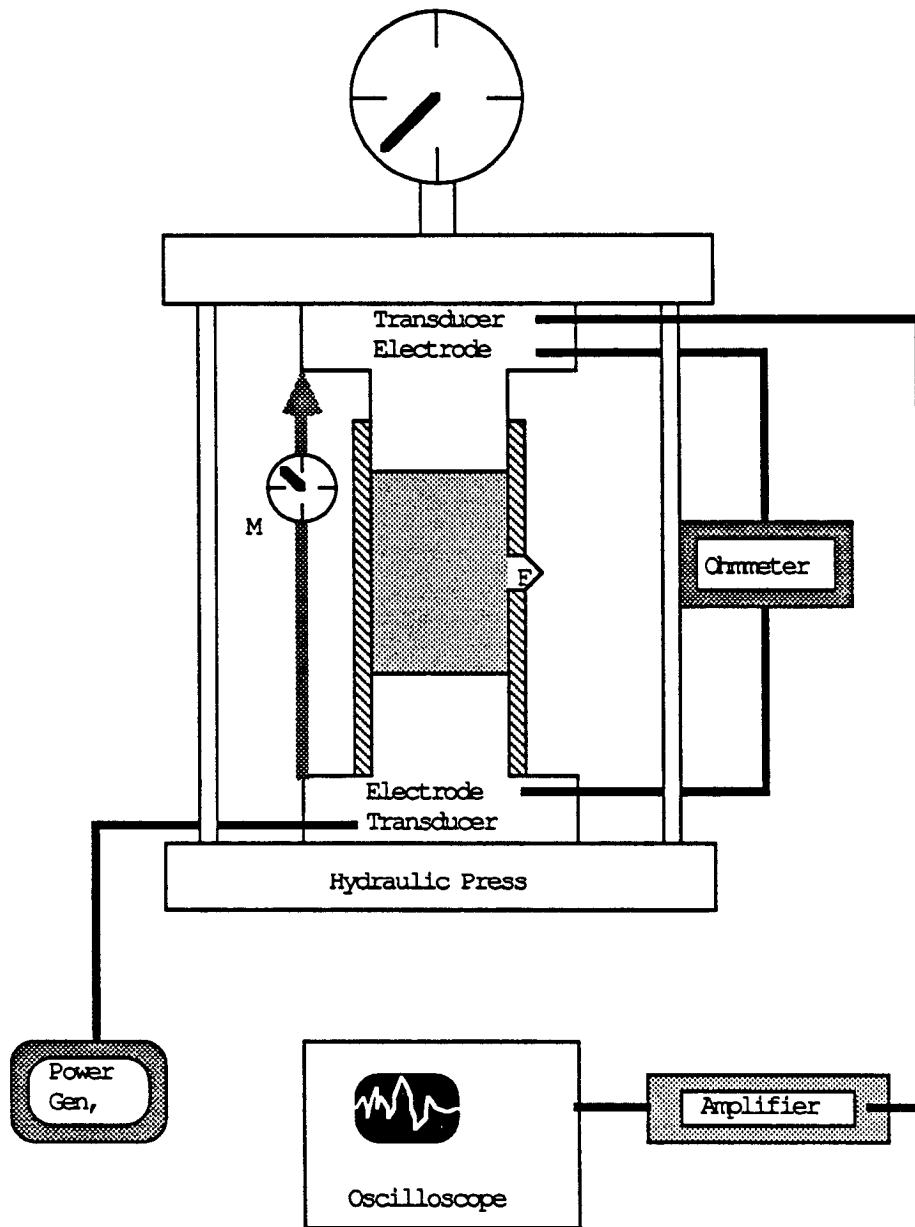


Figure 2.10: Experimental set-up for velocity and electrical conductivity measurements versus grain volume fraction. Grain volume fraction is increased by expelling liquid out of the cell through a fiberglass paper filter (F). Two piezoelectric transducers and two electrodes are located on both ends of the sample. Sample length is measured using three micrometers (M).

2.3.2 Experimental results

For grain volume fraction less than 60 percent (porosity greater than 40 percent), resistance of the sample remains constant and equal to 32 KOhms suggesting that no significant grain interactions occur in this porosity range (100-40 percent). This observation is supported by velocity measurements which follow the Wood-isostress relation. Note also that because the sample is drained, there is no pressure build-up in the sample when pistons are displaced.

At a critical grain volume fraction of 61 percent (39 percent porosity), the system percolates for electrical and elastic properties (Figure 2.11). At this critical threshold, pressure is required to expel more liquid out of the cell.

This suggests that grains begin to touch and that a solid skeleton that withstands applied pressure forms. Simultaneously, the system becomes electrically conductive confirming the existence of mechanical interaction between grains in contact. Finally, velocity measurements exhibit a significant departure from the Wood-isostress relation that is recognized as being due to the presence of rigid skeleton.

These experimental results suggest three comments:

- 1) Transition occurs at porosity of 39 % (61 % grain volume fraction), within the range of porosity of a loose random packing of spheres (Gray, 1968; Cumberland and Crawford, 1987). Note however that because loose random packings are metastable, the system has little rigidity and increase of conductivity, pressure build up and velocity from the suspension state are almost imperceptible. In contrast, when the system reaches the porosity of a close packing of spheres at 36 % porosity (Scott and Kilgour, 1969; Finney, 1970) the rigidity of the system is drastically increased and departure from the suspension state is clearly seen.
- 2) Noticeable changes of velocity can be recorded at the transition from a suspension to a load-bearing system suggesting that such transition may be recorded in real sediments.

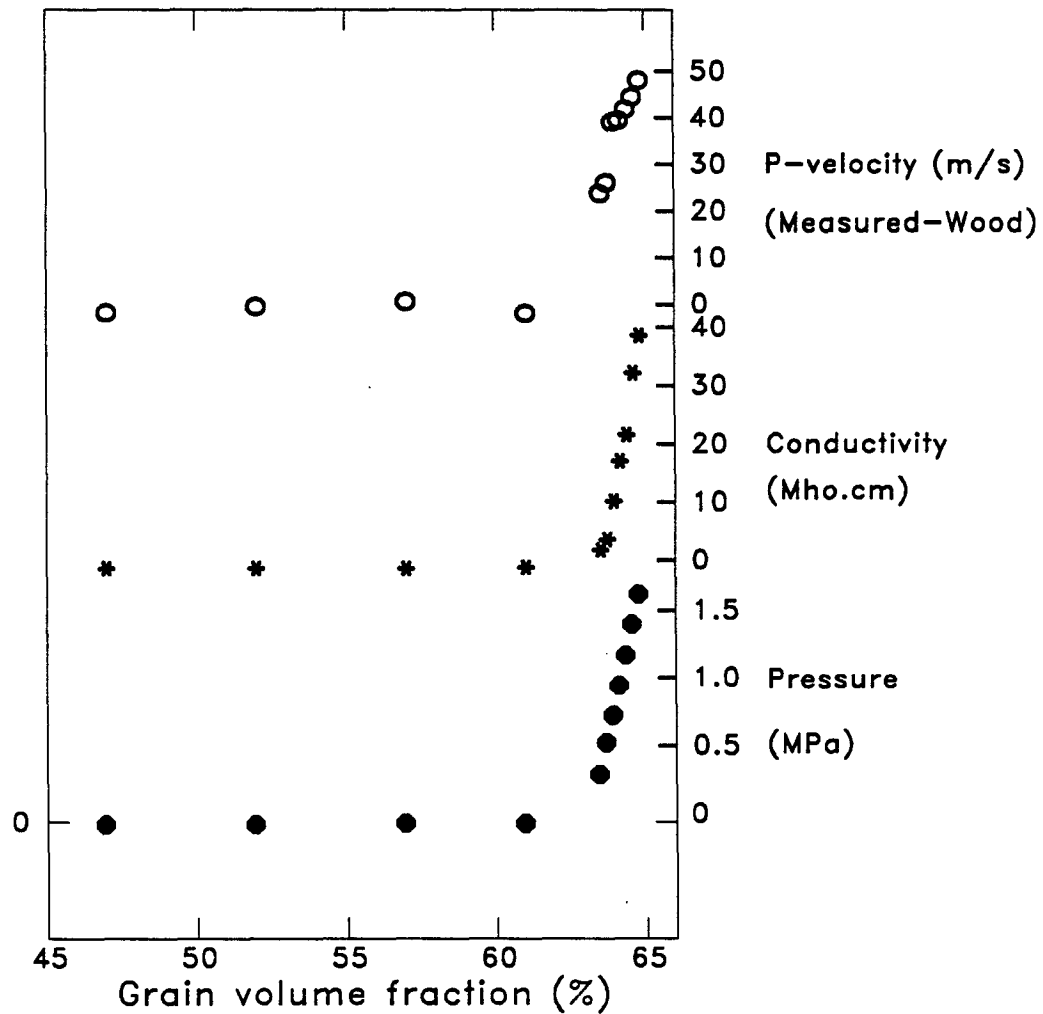


Figure 2.11: Transition from liquid-supported to grain-supported sediment. From 0 to 60 % grain fraction, no significant force (or pressure) is required to expel liquid out of the cell, the system is not electrically conductive and velocity measurements are in close agreement with the Wood-Isostress model. At a critical grain fraction of 61 %, pressure is required to further decrease grain fraction, the system become electrically conductive and velocity depart abruptly from the Wood-Isostress relation. These observations suggest that at a critical threshold for porosity of 39 % for a sphere pack, mechanical interactions appear at grain contact.

3) Electrical and elastic properties exhibit simultaneously a critical behavior at the transition from a suspension to a load bearing material. Such behavior for electrical properties may be recognized as a bond percolation mechanism. From bond percolation theory, the system of conducting spheres is expected to become electrically conductive when the average number of deforming contacts per sphere exceeds a critical threshold of 1.5 (see Chapter 4 for a more detailed description of percolation theory results applied to granular materials). Experimental results would therefore suggest that the system becomes rigid at the same time it becomes conductive, i.e., when the average number of deforming contact exceeds 1.5.

2.3.3 Comparison with marine data

From this experiment, we find that the transition from a suspension to an unconsolidated sphere pack occurs when porosity of the system approaches the porosity of a loose random packing of spheres. Using this result, we anticipate that the porosity at which transition from a suspension to a compacted sediment occurs will depend upon packing of the material in unstressed conditions. The influence of texture on packing of unconsolidated sand has been investigated experimentally (Beard and Weyl, 1973). In their study, Beard and Weyl measured porosity on various sands as a function of sorting and size 1) in dry condition unstressed and 2) in saturated condition under slight compaction. Dry measurements are likely to be representative of the loose packing for the sediment whereas saturated measurement may represent the close packing state. Using Beard and Weyl's data for porosity of dry-loose sands, we anticipate that porosity at the transition from a suspension to a load-bearing granular material may range from 30 % when coarse poorly sorted to 60 % when fine poorly sorted. Applying Wood's relation (eqn. 2.14) to quartz particles and water (input parameters listed in table 1.3) we determine the possible range of compressional velocity at the transition. We find that velocity may vary from 1.5 km/s for a fine poorly sorted sediment to 1.8 km/s for a coarse poorly sorted material.

Table 2.3

Sand grain density (g/cc)	2.65
Fluid density (g/cc)	1
Sand grain bulk modulus (GPa)	38
Fluid bulk modulus (GPa)	2.2
Porosity at the transition (%)	30 - 60
Density at the transition (g/cc)	2.15 - 1.66
Velocity at the transition (km/s)	1.8 - 1.5

In the following section, we present examples of in situ marine data where significant departure from the Wood-isostress relation is observed and may be interpreted as the rheological transition from a suspension to a compacted sediment.

The first example taken from DSDP data, leg 85, site 574 in carbonate sediments (Figure 2.12) shows that sediments are in a quasi suspension state (velocity close to Wood's equation) for porosity ranging from 85 to 55 % and depth from 0 to 350 m. At porosity of 55 % and depth greater than 350 m, significant departure from Wood's equation can be observed. Such departure could be attributed to frequency as mentioned in the previous section and shown in Figure 2.9. However, a plot of the high frequency limit for velocity shows that for sediments that are deeper than 350 meters, velocity is higher than both high and low frequencies predictions for suspensions. This suggests that sediments have undergone compaction to reach an unconsolidated load-bearing state.

In figure 2.13, data from DSDP site 208 show a rapid increase of velocity at 250 m below sea floor. Density however remains fairly constant (1.7 g/cc). The increase in velocity does not correspond to any major changes of lithology. From core appearance, the increase of velocity coincides with a transition from a "soupy or creamy" sediment to a "semilithified" material that may correspond to our transition from suspension to compacted sediment. Note also that in this example, the change of velocity at the transition zone is large enough to give rise to a seismic reflector. Velocity at the transition zone is found to be close to 1.55 km/s and within our

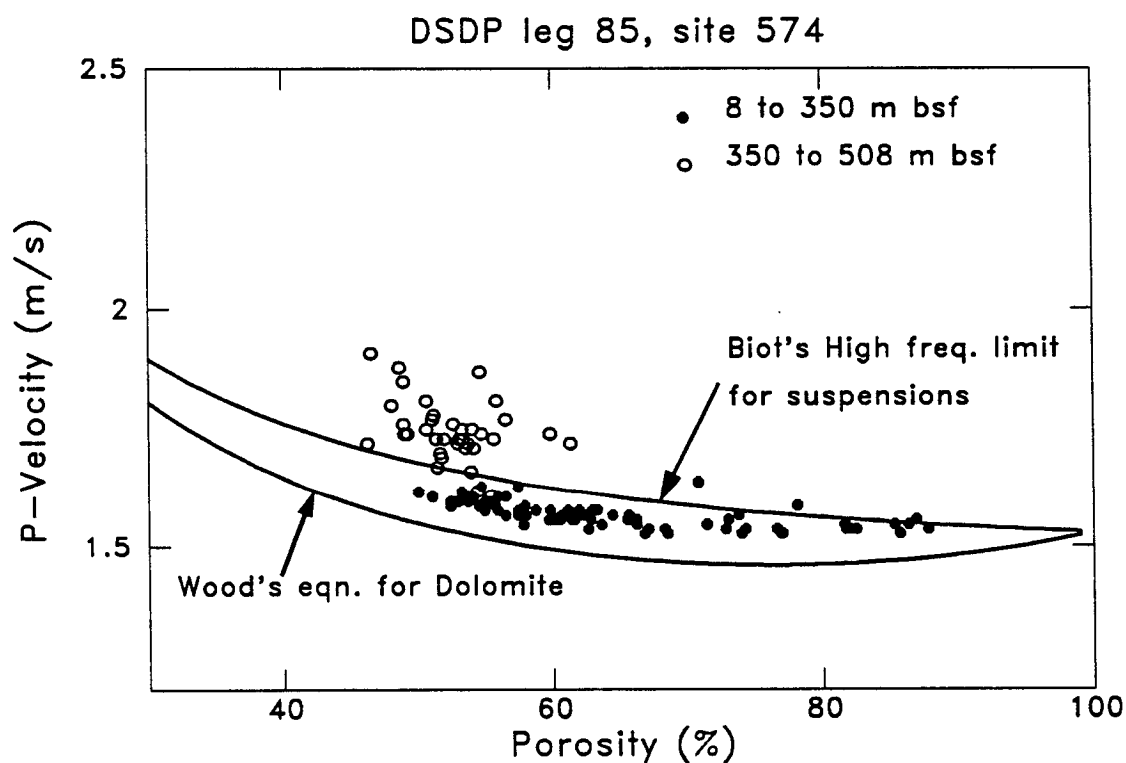


Figure 2.12: Velocity-porosity relationship in sediments at the rheological transition from suspension to load-bearing sediment. Data are from DSDP site 574 in carbonated sediments. Significant departure from Wood's equation is observed at a depth of 350 m below sea floor for porosity ranging from 60 to 45 %. Velocity data at depth greater than 350 m lie above Biot's high frequency limit for suspension suggesting that departure from Wood's relation is not due to frequency, as in the case of Figure 2.9, but to compaction.

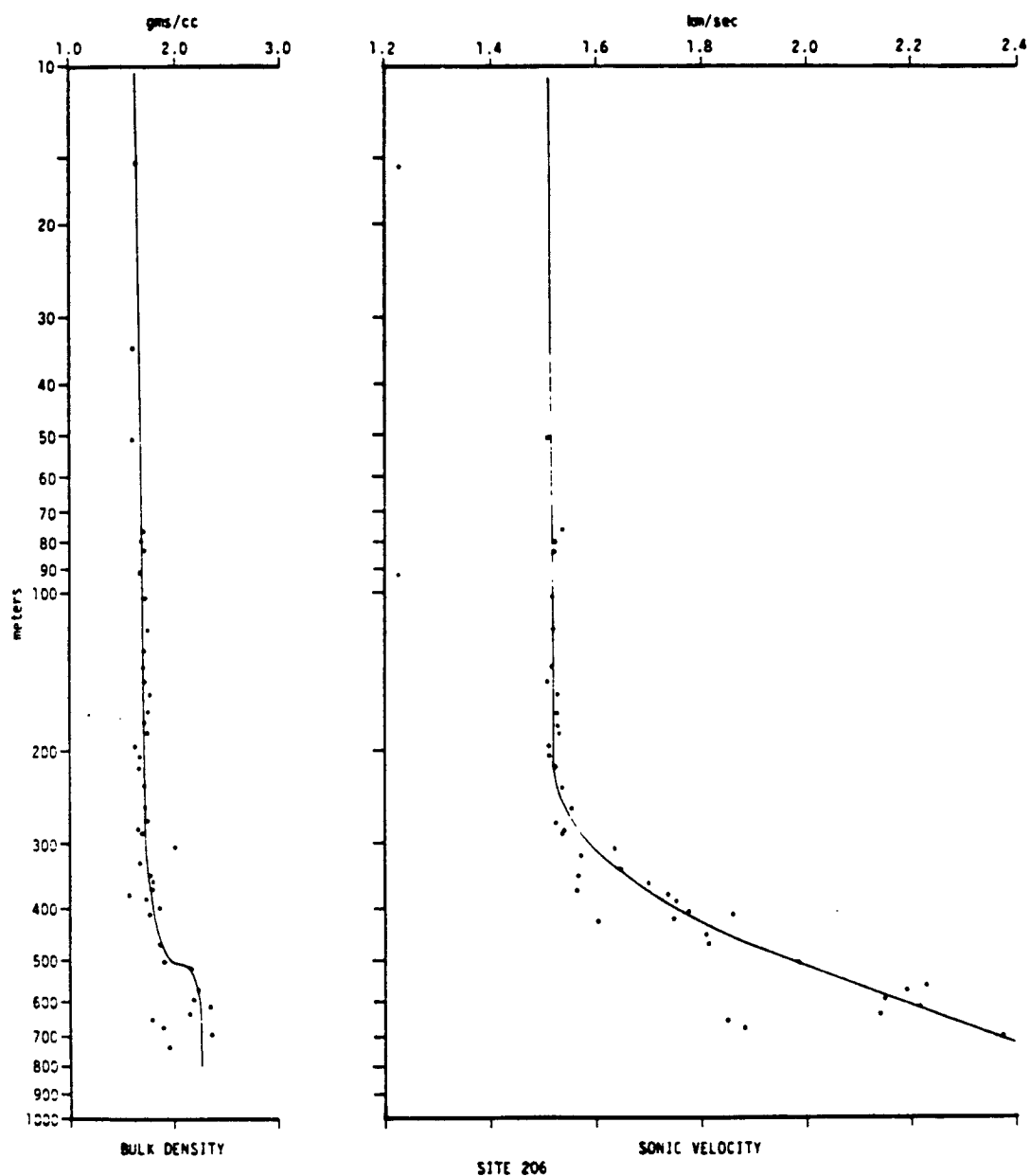


Figure 2.13: Velocity and density vs. depth profiles for sediments from DSDP site 206. The rapid increase in velocity at depth of 250 m does not correspond to changes in the lithological unit and may be attributed to compaction.

range of prediction.

Other examples of rheological transitions from suspensions to unconsolidated load-bearing sediments can be found in the literature. Significant departure of velocity from Wood's equation may be observed in data from Milholland et al. (1980), Hamilton (1978), Shumway (1960), Nafe and Drake (1957), Smith (1974).

2.3.4 Relationships between velocity, density and impedance in sediments

We have shown in the previous section how variability of velocity and porosity or density in sediments was strongly dominated by the state of consolidation of the material. In suspensions, velocity was found to vary little (between 1.48 km/s to 1.8 km/s) with sediment type, whereas porosity could vary between 30 to 99 %. In contrast in unconsolidated load-bearing sediments, velocity was found to vary relatively rapidly over a small range of porosity. This suggests that contrasts in impedance in sediments are primarily attributable to density contrasts in suspensions. In contrast, in unconsolidated sediments impedance variations are attributable to both contrasts of density and contrasts of elastic properties of the load-bearing frame of the material. To illustrate this point, we show in Figure 2.14 the relationship between impedance and density and impedance and velocity in sediments that exhibit a rheological transition from suspension to load-bearing state at 40 % porosity. For suspensions, impedance-density and impedance-velocity relationships shown in Figure 2.14 were calculated using Wood's relation. In unconsolidated sediments we assumed a linear dependence of velocity on porosity similar to that shown in our experiment on spherical particles (Figure 2.9). Relationships shown in figure 2.14 are in qualitative agreement with data from DSDP site 574 shown in Figure 2.15. Note the dominant effect of density on impedance in suspensions and the comparable effect of velocity and density on impedance in compacted sediments.

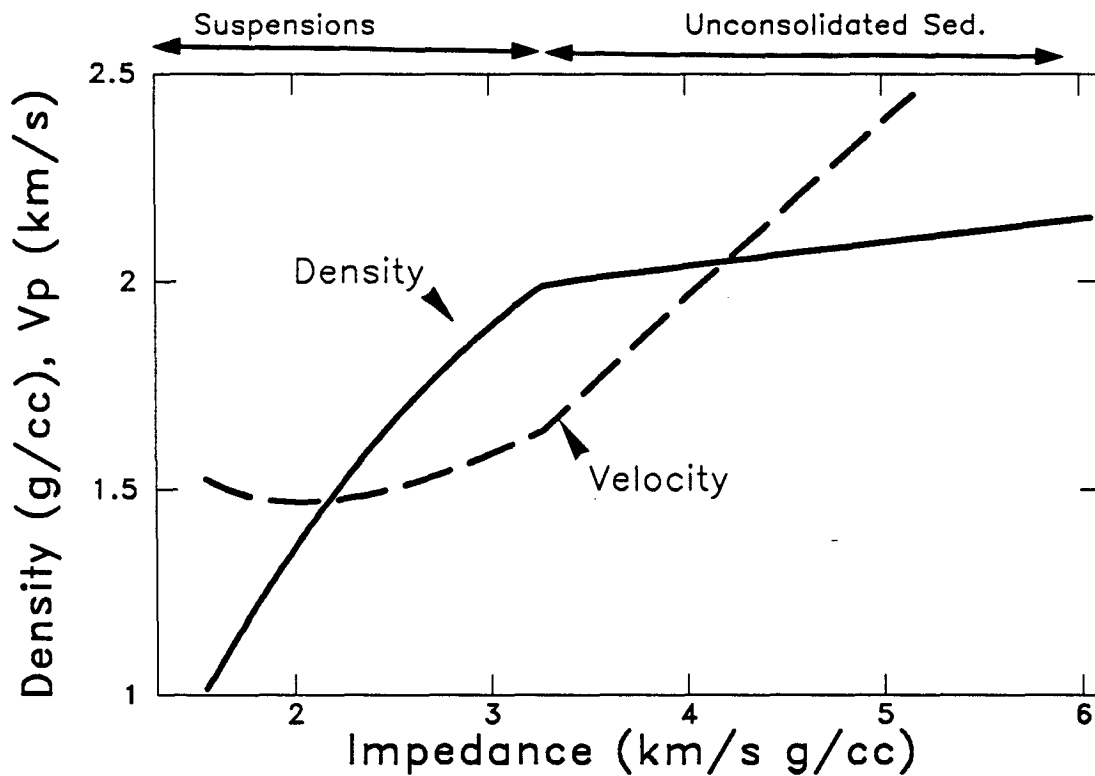


Figure 2.14: Impedance vs. density and velocity relationship in suspension and load-bearing sediments. In suspension, impedance variations are mostly dominated by density variations. In unconsolidated sediments, impedance contrasts are attributed to both velocity and density. Calculations are based on Wood's relation for suspensions. In unconsolidated sediments we assumed a linear dependence of velocity on porosity similar to that shown in Figure 2.11 for spherical particles.

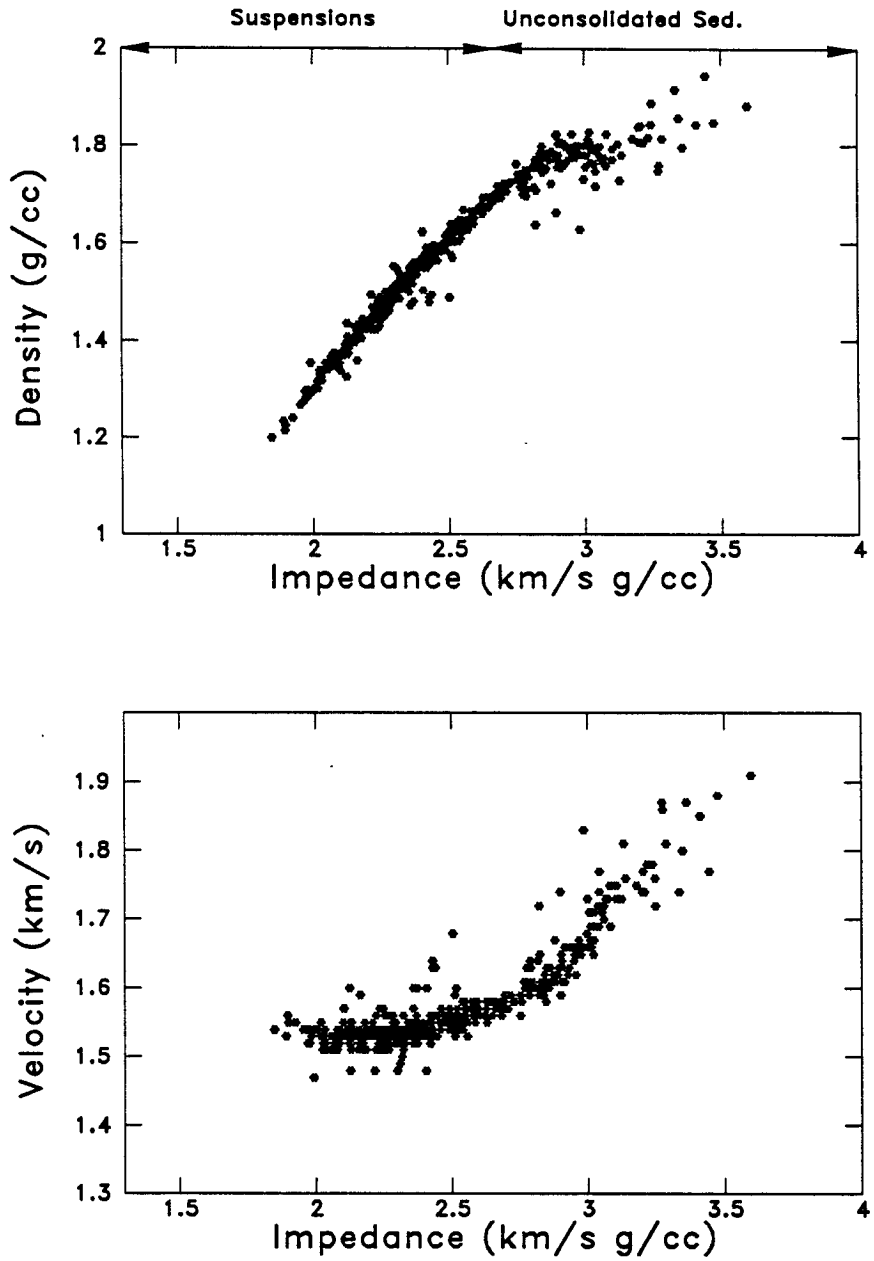


Figure 2.15: Impedance vs. density and velocity relationship for DSDP data, site 574. Variations of impedance are primarily due to density contrasts in suspended sediments and contrasts in impedance can be attributed to velocity variations in unconsolidated sediments.

2.4 Conclusion

This study was aimed at investigating the influence of consolidation on acoustic properties of sediments. We found that the velocity-porosity relationship carries the imprint of the state of consolidation of the sediment. In suspensions, the velocity-porosity relationship is in reasonable agreement with the Wood-isostress model. We noticed that when departure from the Wood-Isostress relation occurs, it may be primarily attributed to velocity dispersion and to a smaller extent to rigidity and stiffness of a skeleton frame for sediments composed of electrically charged particles. Upon compaction, we noticed that when significant mechanical interactions occur between grains in contact, velocity departs abruptly from the Wood-Isostress relation. We evaluate that such transitions from a suspension to a load-bearing state for sediment should occur when the material attains its loose packing configuration (typically for porosity ranging from 30 to 60 % for granular materials).

Acknowledgements

This work was supported by the Office of Naval Research under contract N00014-84-K-0560.

References

- Akal, T., 1972, The relationship between the physical properties of underwater sediments that affect bottom reflection: *Marine Geology*, **13** , 251-266.
- Ament, W. S., 1953, Sound propagation in gross mixtures: *J. Acoust. Soc. Am.*, **25**, 638-641.
- Batchelor, G. K., R.W. O'Brien , 1977, Thermal or electrical conduction through a granular material: *Proc. R. Soc. Lond. A.*, **355** , 313-333.
- Beard, D. C., and P. K. Weyl, 1973, Influence of texture on porosity and permeability of unconsolidated sand: *Bull. AAPG* **57**, 349-369.

- Bell, D. W., and D. J. Shirley, 1980, Temperature variation of the acoustical properties of laboratory sediments: *J. Acoust. Soc. Am.*, **68**, 227-231.
- Berryman, J.G., 1980, Confirmation of Biot's theory: *Appl. Phys. Lett.*, **37**, 382-384.
- Biot, M.A., 1956, Theory of propagation of elastic waves in a fluid saturated porous solid, 1. Low-frequency range: *J. Acoust. Soc. Am.*, **28**, 168-178.
- Biot, M.A., 1956, Theory of propagation of elastic waves in a fluid saturated porous solid, 2. Higher frequency range: *J. Acoust. Soc. Am.*, **28**, 179-191.
- Birch, F., 1960, The velocity of compressional waves in rocks to 10 kilobars, 1: *J. Geophys. Res.*, **65**, 1083-1102.
- Carmichael R.C., 1981, *Handbook of physical properties of rocks*, C.R.C press.
- Cumberland. D. J., R. J. Crawford, 1987, *The packing of particle*, *Handbook of powder technology*, Elsevier.
- Domenico, S. N., 1977, Elastic properties of unconsolidated porous sand reservoirs: *Geophys.*, **42**, 1339-1368.
- Finney, J. L., 1970, Random packing and the structure of simple liquids - 1. The geometry of random close packing: *Proc. Roy. Soc. Lond.*, **A319**, 479-493.
- Gabriels, P., R. Snieder, and G. Nolet, 1987, In situ measurements of shear-wave velocity in sediments with higher mode Rayleigh waves: *Geophys. Prosp.*, **35**, 187-196.
- Geertsma J. and D. C. Smit, 1961, Some aspect of elastic wave propagation in fluid-saturated porous solids: *Geophys.*, **26**, 169-181.
- Gray, W.A., 1968, *The packing of solid particles*, Chapman and Hall, Ltd., London.
- Goodwin, J. W., R. W. Hughes, S. J. Partridge, and C. F. Zukovski, 1986, The elasticity of weakly flocculated suspension. *Chem. Phys.*, **85**, 559-566.
- Hamdi, F., D. T. Smith, 1982, The influence of permeability on compressional wave velocity in marine sediments: *Geophys. Prosp.*, **30**, 622-640.
- Hamilton, E.L., G. Shumway, H. W. Menard, and C. J. Shipek, 1956, Acoustic and other physical properties of shallow-water sediments off San Diego: *J. Acoust. Soc. Am.*, **28**, 1-15.

- Hamilton, E.L., 1956, Low sound velocities in high porosity sediments: J. Acoust. Soc. Am. , **28**, 16-19.
- Hamilton, E.L., 1971, Elastic properties of marine sediments: J. Geophys. Res.,**76**, 579-604.
- Hamilton E.L., 1978, Sound velocity-density relations in sea-floor sediments and rocks: J. Acoust. Soc. Am., **63**, 366-377.
- Hamilton E.L., 1980, Geoacoustic modeling of the sea floor: J. Acoust. Soc. Am., **68**, 1313-1350.
- Hardin, B. O., F. E. Richard, 1963, Elastic wave velocities in granular soils: J. Soil Mech. Found. Div. ASCE, **89** , SM1, 33-35.
- Lambe, T. W., and R. W. Whitman, 1969, Soil mechanics, Wiley, New York.
- Laughton, A. S., 1957, Sound propagation in compacted ocean sediments: Geophys., **22**, 233-260.
- Milholland P., M.H. Manghnani, S.O. Schlanger, and G.H. Sutton, 1980, Geoacoustical modeling of deep-sea carbonate sediments: J. Acoust. Soc. Am.,**68**, 1351-1360.
- Nafe, J. E., C. L. Drake, 1957, Variation with depth in shallow and deep water marine sediments of porosity, density and the velocities of compressional and shear waves: Geophys., **22**, 523-552.
- Reuss, A., 1929, Berechnung der fließgrenze von mischkristallen auf grund der plastizitätsbedingung für einkristalle: Zeitschrift für Angewandte Mathematik and Mechanik, **9**, 49-58.
- Scott, G. D., and D. M. Kilgour, 1969, The density of random close packing of spheres: Brit. J. Appl. Phys. (J. Phys. D), **2**, 863-866.
- Shirley D. W., and L. D. Hampton, 1978, Shear wave measurements in laboratory sediments: J. Acoust. Soc. Am.,**63**, 607-613.
- Shumway, G., 1958, Sound velocity versus temperature in water-saturated sediments: Geophys. **23**, 494-505.
- Shumway, G., 1960, Sound speed and absorption studies of marine sediments by a resonance method, part II: Geophys., **25**, 659-682.

- Smith D.T., 1974, *Physics of Sound in Marine Sediments*, edited by L. D. Hampton, Plenum, New York.
- Stoll, R.D., 1977, Acoustic waves in ocean sediments: *Geophys.*, **42**, 715-725.
- Stoll, R. D., G. M. Bryan, R. Flood, D. Chayes, and P. Manley, 1988, Shallow seismic experiments using shear waves: *J. Acoust. Soc. Am.*, **83**, 93-102.
- Sutton, G. H., H. Berckhemer, and J. E. Nafe, 1957, Physical analysis of deep sea sediments: *Geophys.*, **22**, 779-812.
- Tucholke, B. E., and D. J. Shirley, 1979, Comparison of in situ compressional wave velocity measurements on sediments cores from the western north Atlantic: *J. Geophys. Res.* , **84**, 687-695.
- Voigt W. 1928, *Lehrbuch der Kristallphysik*, Teubner, Leipzig. Macmillan, New York.
- Wood, A.B., 1941, *A Textbook of Sound*. Macmillan, New York.

Chapter 3

Velocity, porosity, and permeability, in sand, shale, and shaley sand.

Abstract

A microgeometrical model for sand, shale, and shaley sand is proposed to explain and predict the dependence of sonic velocity, porosity, and permeability on clay content and compaction. The geometry used for sand and shaley sand is that of a sand framework with clay dispersed in the pore space whereas shale is modeled as a suspension of sand grains in a shaley matrix. Based on these geometries, the dependence of elastic, storage, and transport properties on clay content is computed. The model predicts the existence of a minimum for porosity and permeability upon increase in clay content, and the existence of a peak in velocity versus clay content. The model results are in good qualitative agreement with laboratory velocity, porosity, and permeability data on unconsolidated sand-clay mixtures and consolidated sandstones. The model is used to interpret relationships between porosity and velocity, and porosity and permeability in sedimentary rocks and explain the existence of highly scattered data in terms of clay content and state of compaction.

3.1 Introduction

The determination of porosity and permeability from P-velocity measurements has been a topic of great interest in reservoir characterization. The primary motivation for using seismic or sonic methods is based on recognizable correlations that exist between (1) velocity and porosity, and (2) porosity and permeability. However, in practice, the determination of porosity from velocity, or permeability from porosity has not always been very accurate because of the considerable amount of scatter in the velocity-porosity and porosity-permeability relationships.

Many studies have revealed that clay content was responsible for much of the scatter observed in velocity-porosity relationship in clastic sedimentary rocks, and empirical relationships have been proposed to account for clay content in velocity-porosity relationships (Tosaya and Nur, 1982; Kowallis et al., 1984; Han et al., 1986). Similarly, field and laboratory observations have revealed that clay content and its location within the rock had an overwhelming influence in porosity-permeability relationships (Neasham, 1977; Heron, 1987). These observations demonstrate that a proper description of the storage and transport properties of reservoirs using seismic or sonic measurements requires a better understanding of the effect of clay content on velocity, porosity, and permeability measurements.

This study is first an investigation of the relationships between P-velocity and clay content, porosity and clay content, and permeability and clay content in clastic sediments using a microgeometrical model for sand, shaley sand, sandy shale and shale. The model is used then to describe how clay content and compaction can be responsible for scatter in velocity-porosity and porosity-permeability relationships.

3.2 The sand-clay model

3.2.1 Topology of the model

Location of clay within a rock dictates in many cases the behavior of elastic mechanical and transport properties of the material. Based on their location, clay can be divided into four groups : (1) intrapore clay such as "pore-filling", "pore-lining" and "pore-bridging" clay, (2) intragranular clay, (3) laminar clay and (4) dispersed matrix clay (Almon, 1979). In the microgeometrical model that is used for sand and shaley sand, clay minerals are strictly located within the sand pore space (intrapore clay). In shale and sandy shale, clay is modeled as the matrix (dispersed matrix clay) in which sand grains are dispersed. Such topology for assemblage of coarse and fine particles has been referred in the field of powder technology (Cumberland and Crawford, 1987) as an "ideal packing" of a binary mixture in which small particles do not disturb the original packing of the coarse particles and vice-versa. This geometrical model is applied to sand, shaley sand, sandy shale, and shale, in order to estimate the variations of porosity, P-velocity and permeability with clay content.

3.2.2 Porosity-clay content relationship

Pore volume of a mixture of coarse and fine particles has been quantified by many authors (McGeary, 1961; Furnas, 1928; Westman and Hugill, 1930) using various notations that have generally not been used for geophysical applications. The equations that describe packing of coarse and fine particles can be rederived using a more appropriate set of notations: specifically when porosity of a binary mixture of sand grains and clay particles is expressed in terms of porosity of its two end members (i.e., pure sand and pure shale), a very simple relationship provides the dependence of the composite's porosity on clay volume fraction (Graton and Frazer, 1935; Thomas and Stieber 1975; Clarke, 1979).

Sand and shaley sand : $c \leq \phi_s$

When clay volume fraction, c , is less than the pure sand porosity, ϕ_s , clay particles fit within the sand pore space, and porosity of the mixture, ϕ , decreases linearly with increasing clay volume fraction (Figure 3.1)

$$\phi = \phi_s - c(1 - \phi_{sh}) \quad \text{for } c < \phi_s \quad (3.1)$$

where ϕ_{sh} is porosity of pure shale and c is the volume fraction of clay including micro and macroporosity of clay. Equation 3.1 holds until shaley materials entirely fills the sand pore space. The porosity at this point, $c = \phi_s$, is the product of sand porosity times shale porosity,

$$\phi = \phi_s \phi_{sh} \quad \text{for } c = \phi_s. \quad (3.2)$$

Sandy shale and shale: $c \geq \phi_s$

When clay volume fraction becomes greater than sand porosity, addition of clay can be accomplished only by expanding the sand lattice. Sand grains become disconnected and porosity of the mixture increases linearly with increasing clay content due to replacement of sand grains by porous shaley material.

$$\phi = c \phi_{sh} \quad \text{for } c > \phi_s. \quad (3.3)$$

These results are summarized in Figure 3.1 in a plot of porosity versus clay volume fraction.

Porosity model applied to unconsolidated sand-clay mixtures

The porosity model results computed using equations 3.1 to 3.3 are compared with porosity data measured on ten different mixtures of Ottawa sand and kaolinite at six confining pressures (Yin et al., 1988). Input parameters, ϕ_s and ϕ_{sh} , necessary to compute porosity are the experimentally measured sand and shale end member porosities at the six corresponding confining pressures.

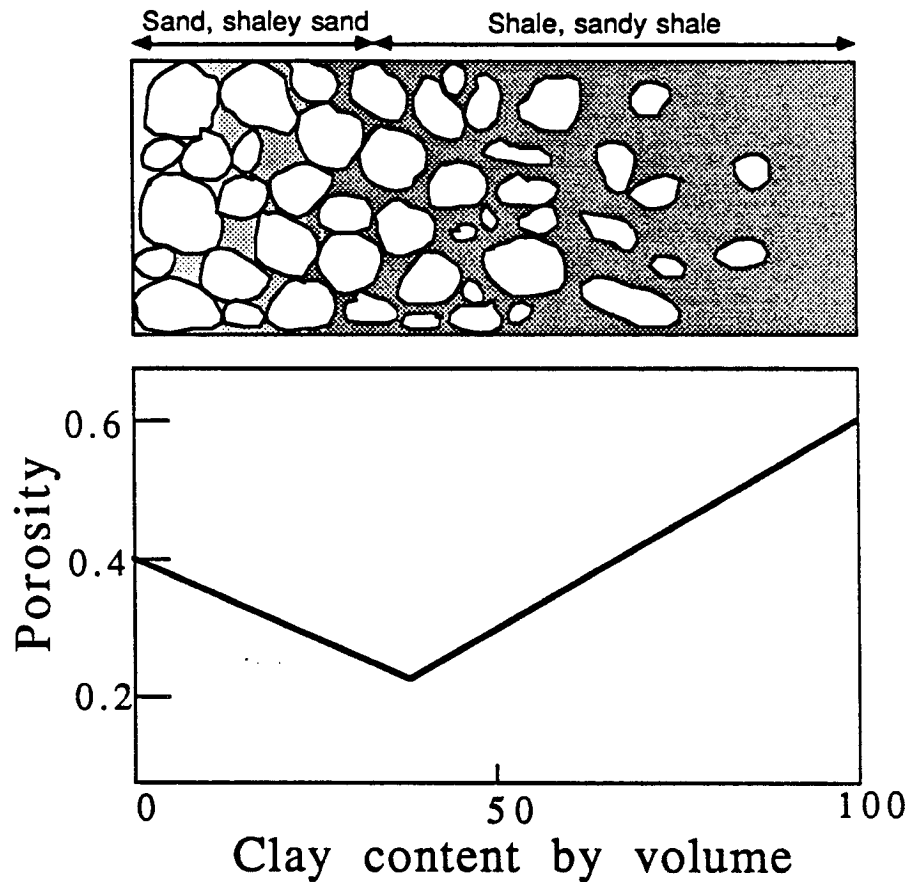


Figure 3.1: Schematic diagram of geometry of sand-clay mixture used in the calculation of porosity vs. clay volume fraction. The controlling factor in the model results is the clay volume fraction c vs. sand porosity ϕ_s . It is considered here that when clay volume fraction is less than sand porosity, clay particles are located within the sand pore space and act as reducing the sediment porosity. When clay volume fraction becomes greater than sand porosity, the sand pore space is entirely filled with clay and any additional clay will tend to disconnect the sand lattice. This results in an increase of the sediment porosity with increasing clay content due to replacement of non porous sand grains by porous clay.

Model results of porosity vs. clay content were converted from clay volume fraction to clay weight fraction using the following relations:

$$w_c = \frac{V_c \rho_c}{V_c \rho_c + V_s \rho_s} = \frac{c (1 - \phi_{sh}) \rho_c}{c (1 - \phi_{sh}) \rho_c + (1 - \phi_s) \rho_s} \quad \text{if } c \leq \phi_s. \quad (3.4)$$

$$w_c = \frac{V_c \rho_c}{V_c \rho_c + V_s \rho_s} = \frac{c (1 - \phi_{sh}) \rho_c}{c (1 - \phi_{sh}) \rho_c + (1 - c) \rho_s} \quad \text{if } c \geq \phi_s \quad (3.5)$$

where ρ_c and ρ_q are the grain densities for clay and quartz (sand forming mineral), respectively and V_c and V_s are the volumes of clay particles and sand grains respectively.

By comparing the model at various pressures (Figure 3.2a) to the experimental data (Figure 3.2b), it can be noticed that the main features of the porosity data versus clay content are captured with the model: (1) the existence of a porosity minimum at $c \approx .2$ to $.4$, (2) the porosity minimum shifts to higher clay content with increasing pressure (from 20 percent clay weight fraction at 0 MPa to 40 percent at 50 MPa). The good qualitative agreement between model and data suggest that the microgeometrical model of bimodal grain size distribution is adequate to describe porosity-clay content relationship in unconsolidated sedimentary mixtures.

3.2.3 Velocity-clay content relationship

The calculation of velocity versus clay content is based on the distinction between two classes of sediments, sand and shaley sand, and shale and sandy shale.

Sand and shaley sand: $c \leq \phi_s$

When clay volume fraction is less than sand porosity, clay particles, according to the model, are located within the pore space of the load bearing sand. Thus, clay must be treated as a component of the pore space that will act to stiffen the pore filling material, and not as part of the matrix. One therefore must expect an increase of velocity of the mixture with increasing clay content due to an increase of the elastic

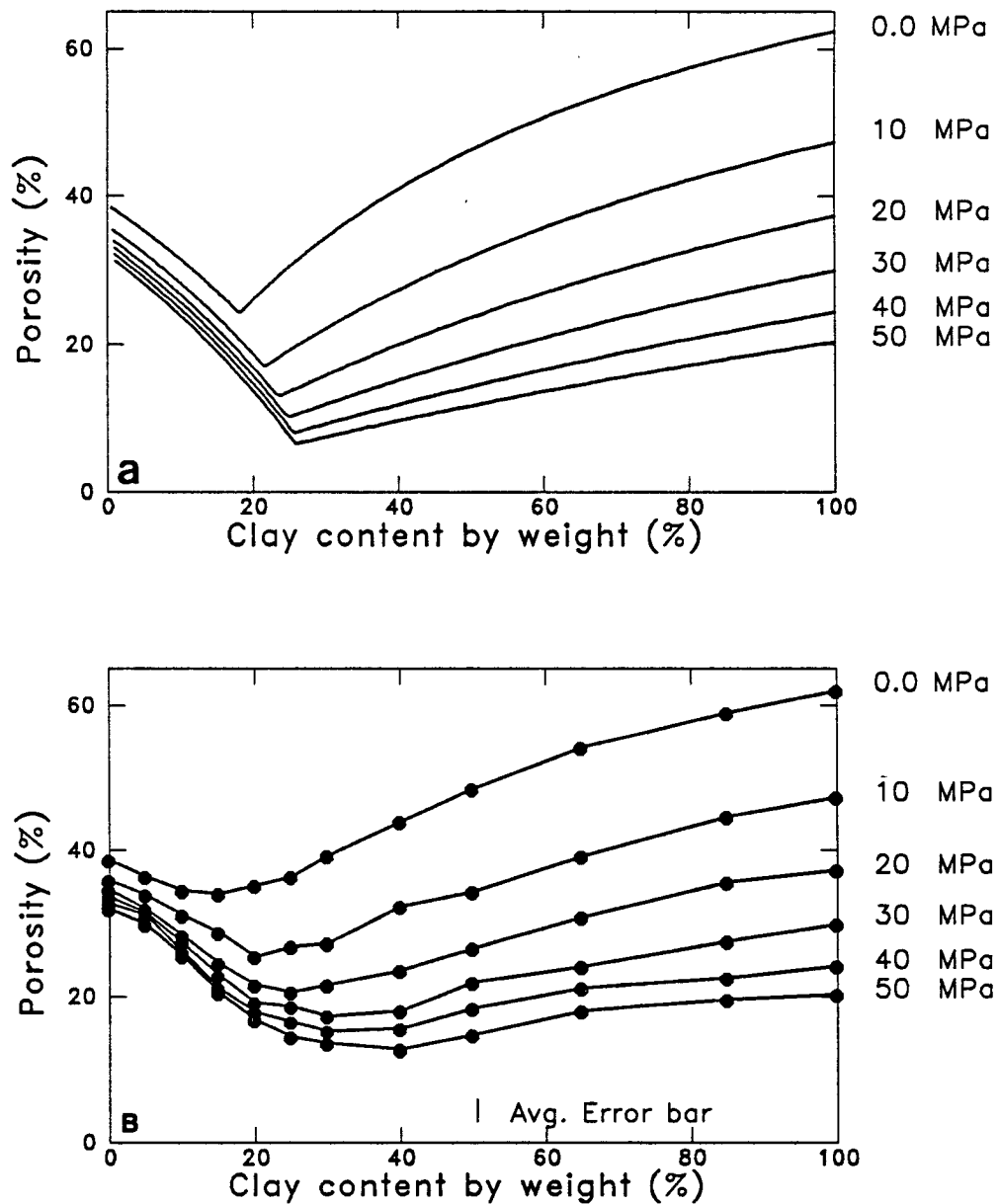


Figure 3.2: Porosity vs. clay weight fraction at various confining pressures. The sand-clay model (Figure a) captures the main trends of unconsolidated sand-clay mixture porosity data (Figure b): (1) existence of a porosity minimum at $c \approx 20$ to 40%, (2) pressure shifts the minimum towards higher clay content and (3) translates the porosity curve towards lower porosity. (data are after Yin et al., 1988).

moduli of the pore filling material (fluid and clay). This effect is computed using a relation similar to Gassmann's (1951) relations where compressional and shear velocity of the mixture, V_p and V_s , respectively, are calculated using the following equations

$$V_p = \sqrt{\frac{K + 4G/3}{\rho}} \quad (3.6)$$

$$V_s = \sqrt{\frac{G}{\rho}} \quad (3.7)$$

where K , G , and ρ , the bulk modulus, the shear modulus, and the density of the sand-clay mixture respectively, can be calculated using the following relations:

$$\frac{K}{K_q - K} = \frac{K_{fr}}{K_q - K_{fr}} + \frac{K_{fl}^*}{\phi_s(K_q - K_{fl}^*)} \quad (3.8)$$

$$G = G_{fr} \quad (3.9)$$

$$\rho = (1 - \phi_s)\rho_q + c(1 - \phi_{sh})\rho_c + (\phi_s - c(1 - \phi_{sh}))\rho_w \quad (3.10)$$

where ρ_q , ρ_c and ρ_w are the density of sand grains (quartz), clay mineral and saturating fluid respectively, K_{fr} , and K_q are the bulk moduli of the solid frame, and the frame forming mineral respectively, and G_{fr} is the shear modulus of the frame. K_{fl}^* is the effective bulk modulus of the pore filling material (fluid and clay). Equation 3.8 which relates the effective bulk modulus of the rock to the effective modulus of the pore filling material is derived in appendix A following a method used by Mavko and Jizba (1989) to estimate "the unrelaxed bulk modulus of saturated rocks". Note that equation 3.8 is identical to Gassmann's relation when replacing ϕ_s and k_{fl}^* by ϕ , the rock porosity, and k_{fl} the fluid bulk modulus respectively. Equation 3.9 is theoretically valid only in the case where the material filling the pore space has a shear modulus equal to zero. Although saturated shale has a finite shear modulus, little variations of shear moduli in the sand-clay mixtures were observed, indicating that the influence of shear modulus of the material filling the sand pore space can be neglected, to a first order approximation.

Sandy shale and shale: $c \geq \phi_s$

When clay volume fraction is greater than sand porosity (in shale and sandy shale), clay particles disconnect the sand lattice and sand grains become suspended in the shaley matrix. Experimental results on fluid-solid suspensions (Kuster and Toksoz, 1974; Marion and Nur, 1989) and similar composite media (Purnell, 1986) show that velocity of the "sand saturated-shale composite" can be accurately described using an isostress model or identically the Reuss (1929) average for bulk and shear moduli:

$$\frac{1}{K} = \frac{c}{K_{sh}} + \frac{1-c}{K_q} \quad (3.11)$$

$$\frac{1}{G} = \frac{c}{G_{sh}} + \frac{1-c}{G_q} \quad (3.12)$$

where K and G denote the bulk and shear moduli respectively and subscripts sh and q refer to saturated shale and quartz grains respectively. Velocity is obtained using equations 3.6 and 3.7 where density, ρ is given by:

$$\rho = (1-c)\rho_q + c(1-\phi_{sh})\rho_c + c\phi_{sh}\rho_w. \quad (3.13)$$

Model results of P-velocity vs. clay volume fraction are schematized in Figure 3.3.

Velocity-clay content relationship in sand-clay mixtures

The velocity model results (Figure 3.4a) are compared with velocity data (Figure 3.4b) measured on the previously mentioned sand-clay mixtures (data from Yin et al., 1988). Computation of velocity for sand-clay mixtures using the isostress and Gassmann's relations (equations 3.6 to 3.13) requires knowledge of the following parameters: K_{fr} , G_{fr} , K_{sh} , G_{sh} , K_{fl} , ϕ_s , and ϕ_{sh} . These input parameters were obtained from experimentally measured pure sand and pure shale velocities and porosities. Besides minor differences that are related to assumptions regarding packing (see following section for discussion), good agreement between calculated velocities in Figure 3.4a and measured velocities in Figure 3.4b is observed. This demonstrates the

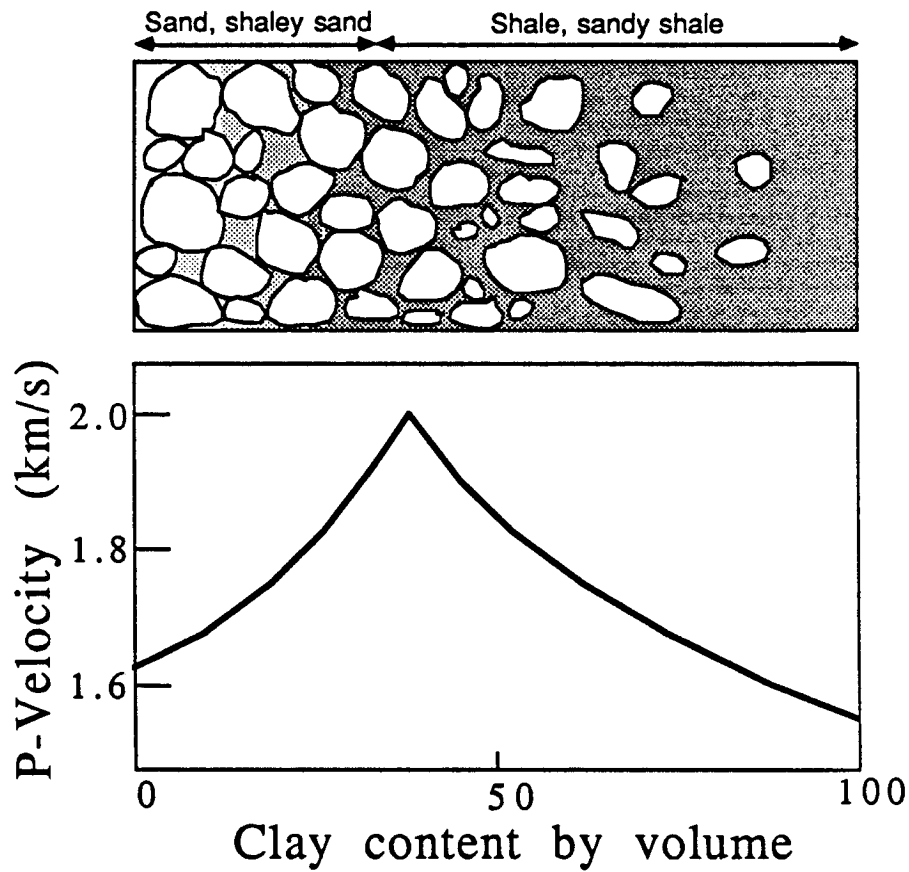


Figure 3.3: Velocity vs. clay volume fraction. When clay volume fraction is less than sand porosity, velocity increases with increasing clay content due to increasing stiffness of the material filling the sand pore space. When clay content becomes greater than sand porosity, velocity decreases with decreasing amount of sand grains due to replacement of stiff sand grains by softer clay particles.

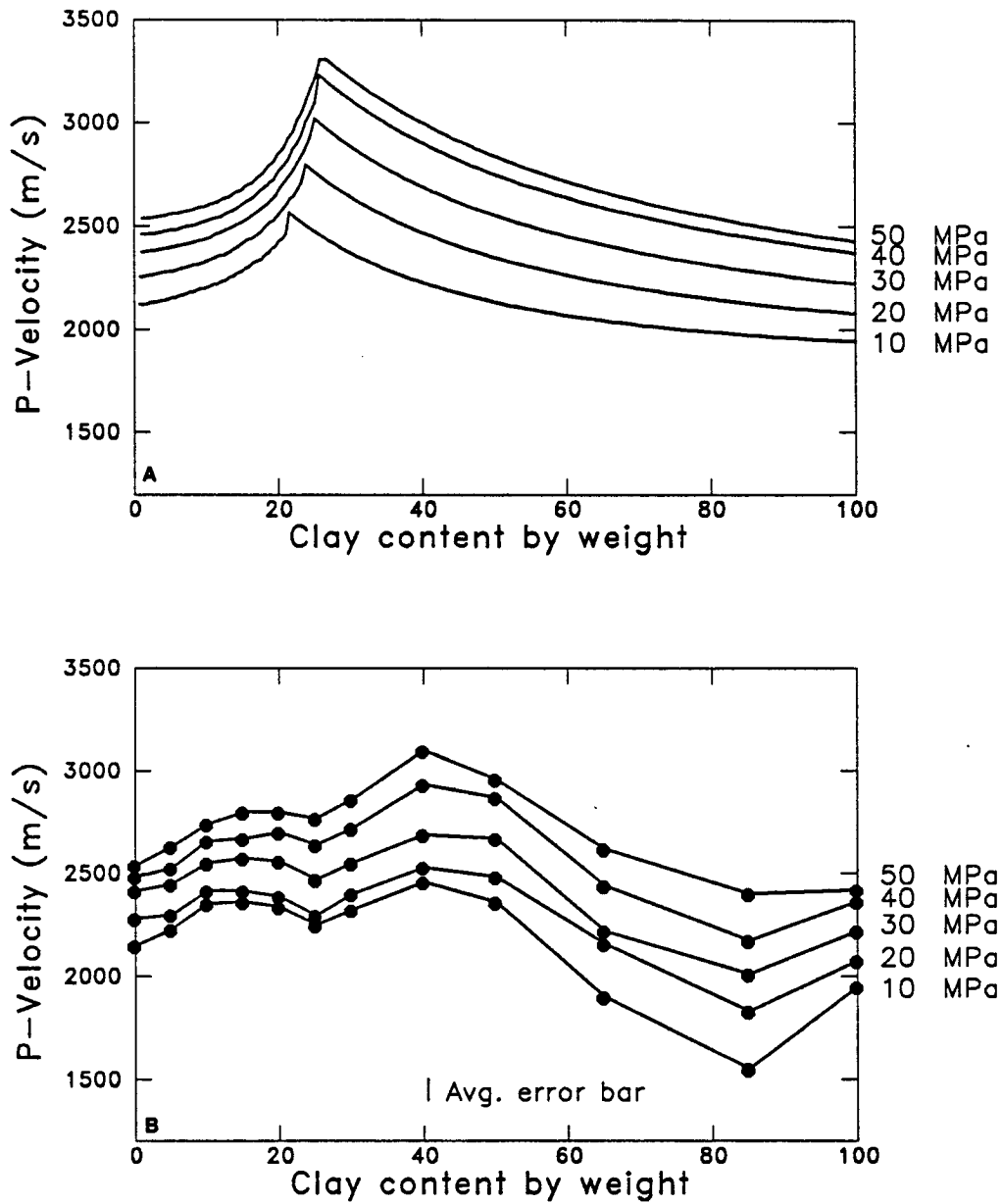


Figure 3.4: Velocity vs. clay weight fraction at various confining pressures. Velocity vs. clay content in Figure a was calculated using Gassmann's relations ($c < \phi_s$) and Isostress model ($c > \phi_s$). Model results reproduce the peak in velocity observed in unconsolidated sand-clay mixtures data in Figure b (data from Yin et al., 1988).

validity of the two concepts used in calculation of velocity, i.e., (1) for shaley sand, clay is considered as a component of the pore space and not as a matrix term and (2) for shale and sandy shale, the sand grains can be considered as suspended in the shaley matrix.

3.2.4 Packing of Sand-Clay mixtures and departure from ideal model for porosity and velocity

It has been shown in previous sections how the sand-clay model could reproduce the main features of porosity and velocity behavior of sand-clay mixtures. However, in a detailed comparison between model and data in Figure 3.5, it can be noticed that the model systematically underestimates porosity and overestimates velocity with respect to data. The nature of this discrepancy is discussed here.

In the sand dispersed-clay model, the assumption is made that addition of clay particles to sand grain packing will not disturb the original sand lattice and vice-versa sand grains will not perturb shale packing. Practicably, this assumption is only valid for either very low or very high clay content. For intermediate clay contents, each component is expected to somewhat disturb the original packing of the other upon mixing.

Specifically, in shaley sands, some clay particles may locate between sand grains and thus expand the sand lattice. This expansion of the sand lattice will tend to increase the porosity of shaley sands relative to the values obtained from equation 3.1. In addition, expansion of sand lattice creates additional pore space to be filled with clay and thus shifts the position of the porosity minimum towards higher clay content. In Figure 3.5a, porosity data recorded at 50 MPascal show that porosity minimum occurs at 42% clay content in volume, instead of 32% as predicted using the simple sand-clay model (dashed line on Figure 3.5a). This suggests that the sand lattice expanded from 32 % at zero clay content to 42% at the minimum due to intergranular clay particles.

Similarly, for shales, the presence of sand grains in the shaley matrix will disturb the original shale packing and increase shale porosity in the neighborhood of sand grains (see Ben Aim and Le Golf (1967) for argument). In Figure 3.5a, porosity at the minimum suggests that shale porosity is increased by 3%, relative to equation 3.3, due to perturbation by the sand grains.

As a consequence, the sand dispersed-clay model can be viewed as a lower bound for porosity. Any departure from this model can be attributed, for shaley sand ($c < \phi_s$) to the presence of intergranular clay that expands the sand lattice porosity, and for shales ($c > \phi_s$) to perturbation in shale packing due to sand grains. To illustrate this point, it is shown in Figure 3.5a that by allowing the sand lattice porosity to expand linearly with clay content from 32 % (i.e. sand porosity) at zero clay content to 42% at the minimum, and shale porosity to decrease linearly with decreasing sand content from 25% at the minimum to 22% at 100% shale, a good fit of the data can be achieved using equations 3.1 to 3.3 (solid line in Figure 5a).

In Figure 3.5b, a comparison between velocity data and velocities estimated using Gassmann's relations for shaley sands and isostress relations for shales is shown. Dashed line corresponds to the simple version of the sand-clay model, while bold line represents velocity of sand-clay mixture calculated using the adjusted porosity model shown by the bold line in Figure 3.5a. Figure 3.5b shows how velocity estimates of sand-clay mixtures is drastically improved upon knowledge of variations of sand lattice porosity with clay content.

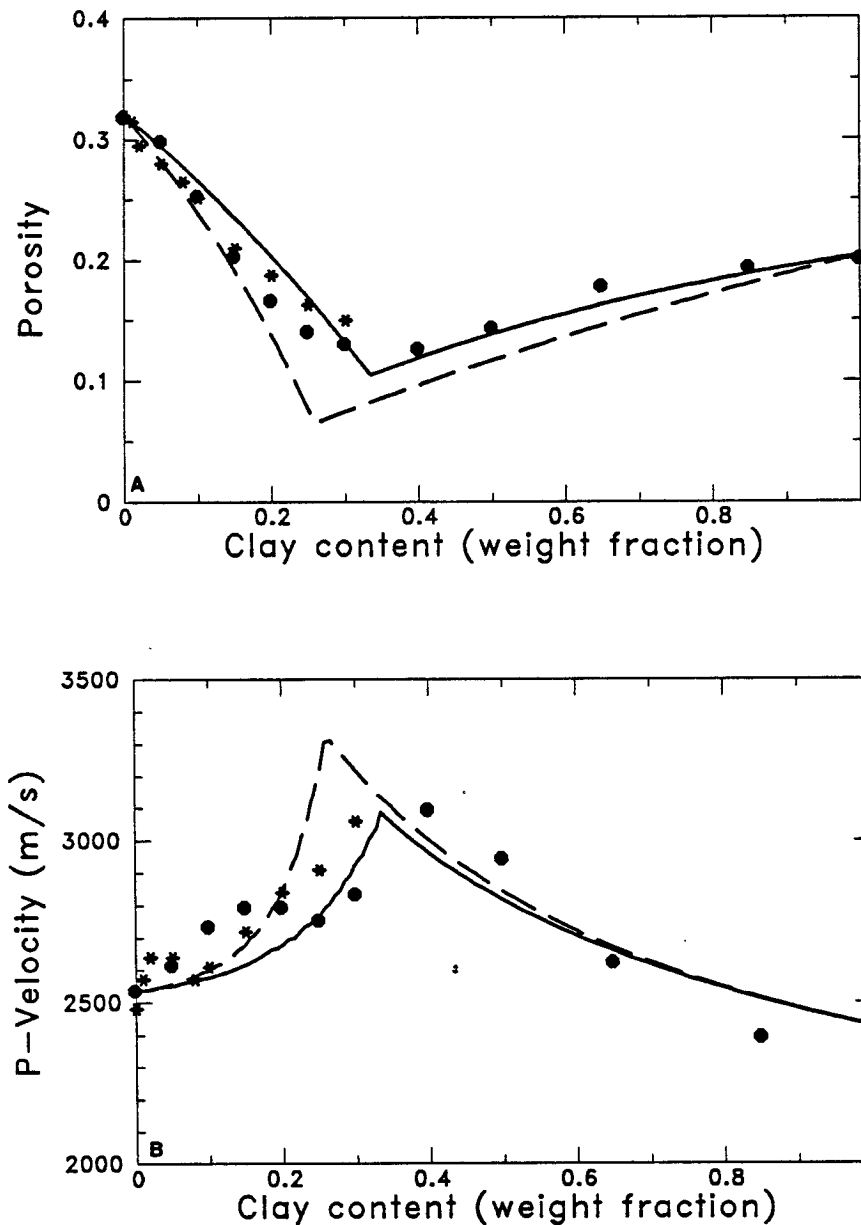


Figure 3.5: Influence of packing on porosity and velocity of sand-clay mixtures. The ideal sand-clay model (dashed line) is in reasonable qualitative agreement with both porosity and velocity data measured at 50 MPascal on two data sets ((●) from Yin et al., 1988; (*) from Han, 1986). However, better data matching is achieved (solid line) by considering that for clay content less than 30 %, the original sand packing is perturbed by introduction of clay particles within the sand lattice. For clay content greater than 30 %, clay packing is perturbed by presence of sand grains.

3.2.5 Permeability-clay content relationship

Permeability of porous materials can be estimated using Kozeny-Carman equations (Carman, 1956):

$$k = \frac{\phi^3}{k_0 T^2 S^2} \quad (3.14)$$

where k , T , ϕ , and S are the permeability, tortuosity, porosity and specific surface area (surface area per unit volume) of the porous material and k_0 is an empirical constant. Clay minerals can reduce considerably permeability of a porous material in many different ways : (1) reduce the porosity, (2) increase the specific surface area, (3) increase the tortuosity, (4) block the pore space due to swelling, (5) clog pore throats. In the particular case of air permeability that is considered here clay is expected to influence permeability through its effect on porosity, tortuosity and specific surface area only. The influence of clay content on porosity of the material has already been described by equations 3.1 to 3.3 in the section concerned with porosity-clay content relationship.

Tortuosity

Tortuosity in porous materials is related primarily to the shape, grain size, and the degree of alignment of the grains forming the rock. In sands and sandstones, tortuosity typically ranges between 1.5 to 2.5. In shale, tortuosity can be one or two orders of magnitude greater than sand tortuosity, depending on the alignment of the particles.

In sand-clay mixtures, tortuosity of the material, T , is the superposition of tortuosity associated with sand grains, T_s , and tortuosity associated with clay particles, T_c :

$$T = T_s T_c. \quad (3.15)$$

In shaley sand, it is assumed as a first order approximation that 1) tortuosity associated with sand grains is the tortuosity of a clean sand T_{sand} , and 2) tortuosity

associated with clay particles depends linearly on the amount of clay located within the pore space. Hence tortuosity can be written as:

$$T = T_{sand} \left(\frac{c}{\phi_s} (T_{shale} - 1) + 1 \right) \quad c < \phi_s \quad (3.16)$$

where the volume fraction of clay, c varies between 0 and ϕ_s , and T_{shale} is the tortuosity of the pure shale. From equation 3.16, tortuosity associated with clay particles ranges from 1 when no clay is present ($c = 0$) to T_{shale} when the pore space is entirely filled with clay ($c = \phi_s$).

For sandy shale it is assumed that tortuosity of the material is primarily dominated by shale tortuosity and that 1) tortuosity associated with clay particles, T_c , is the tortuosity of a pure shale, T_{shale} and 2) additional tortuosity due to sand grains suspended in the shaley matrix is proportional to the amount of sand grains. Tortuosity of the sandy shale can be written as:

$$T = T_{shale} \left(1 + \frac{T_{sand} - 1}{\phi_s - 1} (c - 1) \right) \quad c > \phi_s \quad (3.17)$$

From equation 3.17, tortuosity of the sandy shale decreases linearly with clay content from $T_{sand}T_{shale}$ at $c = \phi_s$ to T_{shale} when $c = 1$.

Specific surface area

The surface area per unit volume of granular materials is approximately inversely proportional to the mean radius of the grains. Because of their small size and platy or fibrous shape, the specific surface area of clay minerals is three to four orders of magnitude greater than the specific surface area of sand. Typical values of surface area per unit weight for clay and sandstone are listed in Table 3.1 (after Knight, 1986).

Table 3.1

Clay type	N_2 ads.	H_2O ads.	Glycol retention
Kaolinite	11 - 70	14 - 54	15 - 25
Illite	96 - 227	52 - 82	70 - 95
Montmorillonite	99 - 141	282 - 491	600 - 844

Sandstone type	N_2 ads.
St. Peter	0.12
Berea	1.2
Tight Gas	3.0

In sand and shaley sands, according to the sand-clay model, increasing amount of clay particles within the sand pore space does not modify the bulk volume of the material. In contrast, surface area of the pore space increases drastically with clay content and specific surface area increases with increasing clay content as:

$$S = S_{sand} + cS_{shale} \quad c < \phi_s \quad (3.18)$$

where S_{sand} and S_{shale} are the specific surface area of sand and shale respectively.

In sandy shales and shales, specific surface area of the material is a linear combination of shale specific surface area and sand grains specific surface area

$$S = S_{sand} \frac{(1 - c)}{(1 - \phi_s)} + cS_{shale} \quad c > \phi_s. \quad (3.19)$$

Permeability model results applied to Gulf Coast sandstones

Combining the influence of clay content on porosity (equations 3.1 to 3.3), tortuosity (equations 3.15 to 3.17), and specific surface area (equations 3.18 and 3.19) in equation 3.14 leads to a relationship between permeability and clay content. This relationship is compared with air permeability data measured on 14 Gulf Coast sandstone samples (Figure 3.6). Data exhibit a rapid decrease in permeability (4 orders of magnitude) with increasing clay content from 3 to 30 %. From 30 to 48 % clay, permeability remains approximately constant (10^{-1} to 10^{-2} millidarcy). This behavior

is well reproduced with the permeability model (solid line) using input parameters listed in table 3.2. Note that for low clay volume fraction (5 to 15 %), the model underestimates permeability. This departure may be attributed to the tortuosity model in which it is assumed that tortuosity within the sand pore space varies linearly with the amount of clay. The validity of this assumption depends certainly upon location of clay particles within the pore space. Such assumption may be reasonable for pore-filling and pore-bridging clay, whereas for pore-lining clay the effect of clay content on tortuosity may be overestimated with such model.

Table 3.2

<i>Mineral Properties</i>	<i>Quartz</i>	<i>Clay</i>
density (g/cc)	2.568	2.77
K (GPa)	38	not needed
G (GPa)	44	not needed

<i>Bulk Properties</i>	<i>Sandstone</i>	<i>Shale</i>
Porosity (%)	32	25
K (GPa)	8.0 (dry)	12.5 (sat.)
G (GPa)	6.5 (dry)	6.0 (sat.)
Tortuosity	1.5	10
S (m^2/gm)	0.15	50

3.3 Influence of clay content on velocity-porosity relationships

The sand-clay model is used here as a starting point to show how the scatter in velocity-porosity relationships can to a large extent be attributed to clay content and compaction in unconsolidated sediments and clastic rocks.

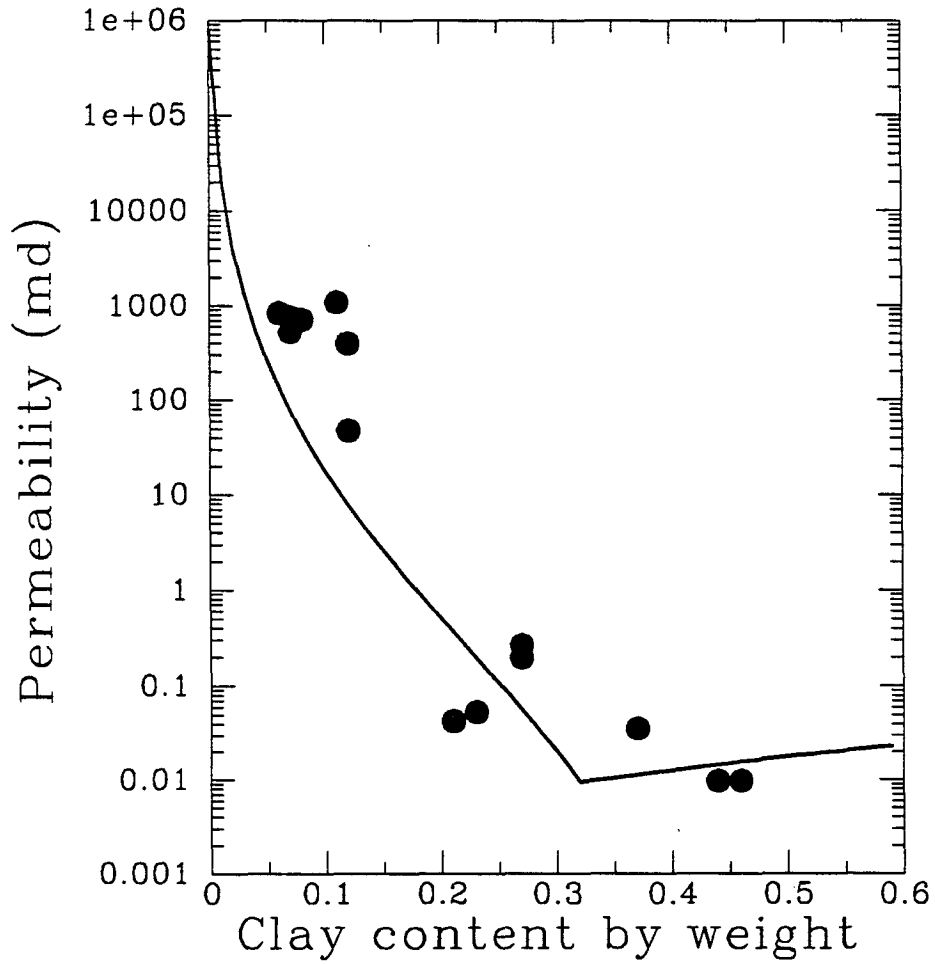


Figure 3.6: Permeability vs. clay content: model results (solid line) and Gulf Coast sandstone data. A rapid decrease in permeability is observed with increasing clay content from 0 to 30% (sand and shaley sands) due to increase in tortuosity and specific surface area with increasing clay content. Once the minimum is reached, permeability is rather insensitive to clay content (shale and sandy shale).

3.3.1 Unconsolidated sand-clay mixtures

Important differences in porosity and velocity behavior between sand and shaley sands ($c < \phi_s$), and shale and sandy shale ($c > \phi_s$) were observed experimentally in sand-clay mixtures and predicted using the sand-clay geometrical model. From Figures 3.2 and 3.4 it can be noted that that sands and shaley sands exhibit an increase in velocity and decrease in porosity with increasing clay content. In contrast, shales and sandy shales exhibit a decrease in velocity and increase in porosity with increasing clay content. Velocity data in sand, shaley sand, sandy shale and shale consequently display an overall decrease in velocity with increasing porosity as shown in Figure 3.7. However, when conventional velocity-porosity transforms (Wood, Wylie time average, or Raymer) are applied to these data, a considerable amount of scatter remains unaccounted for. Based on the systematic study of influence of clay content and pressure on porosity and velocity, it is shown in the following section that the scatter generally observed in velocity-porosity relationships has a deterministic physical cause and can be related to clay content and compaction.

The influence of clay content on velocity-porosity relationship becomes clear by looking at the data at a constant value of confining pressure (Figure 3.8). In view of the understanding of the effect of clay content on velocity and porosity we schematically outlined in Figure 3.8 the dependence of velocity on porosity for shaley sand (dashed line) and a steeper dependence for sandy shale (solid line). It can also be noted that the two trends intersect at a singular point, the point at which clay volume fraction is equal to sand porosity. These observations demonstrate how the scatter observed at a constant pressure is primarily related to clay content.

The sand-clay model is also used to investigate the effect of pressure on the velocity-porosity relation in sand-clay mixtures. In Figure 3.9, computed velocity versus computed porosity are shown at 0, 5, and 50 MPa. Note in this figure that the effect of pressure is to shift the velocity-porosity trend to higher values of velocity

and lower values of porosity. In addition, because shales compact more with pressure than sands, the shaley sand and sandy shale trends tend to separate with increasing pressure. Confining pressure therefore enhances the general trend of decreasing velocity with increasing porosity, whereas clay content is responsible for the scatter around the main trend.

Based on the results above, it appears that a significant improvement in understanding of the complexity of the relationship between velocity and porosity in unconsolidated sedimentary mixtures may be achieved by incorporating information on depth (or equivalently pressure) and shale content. In an attempt to determine accurately porosity from velocity measurements, it can be noticed in Figure 3.9 that an estimate of pressure at which velocity is measured could theoretically reduce the number of possible porosity values to two. One value would correspond to the porosity in a shaley environment. The other value would represent porosity of a shaley sand. If, in addition, an estimate of shale content is available, then the determination of porosity from velocity may be accurate to within 3 percent porosity units (Figure 3.8).

3.3.2 Unconsolidated marine sediments

The need to determine the physical properties of unconsolidated sediments and especially deep water sediments from seismic methods is obvious primarily because of the ineffectiveness of drilling and coring procedures in these soft materials. The main motivation for using seismic method is the existence of recognized correlation between acoustic velocity and porosity in sediments. This relationship can be used as a starting point to determine other physical properties, related to porosity, from acoustic measurements. However, in practice, the determination of porosity from acoustic measurements has not always been very accurate, essentially because of the considerable amount of scatter in the velocity-porosity relationship, as illustrated in Figure 3.10 (core data from the Deep Sea Drilling Project, compiled by Nobes et

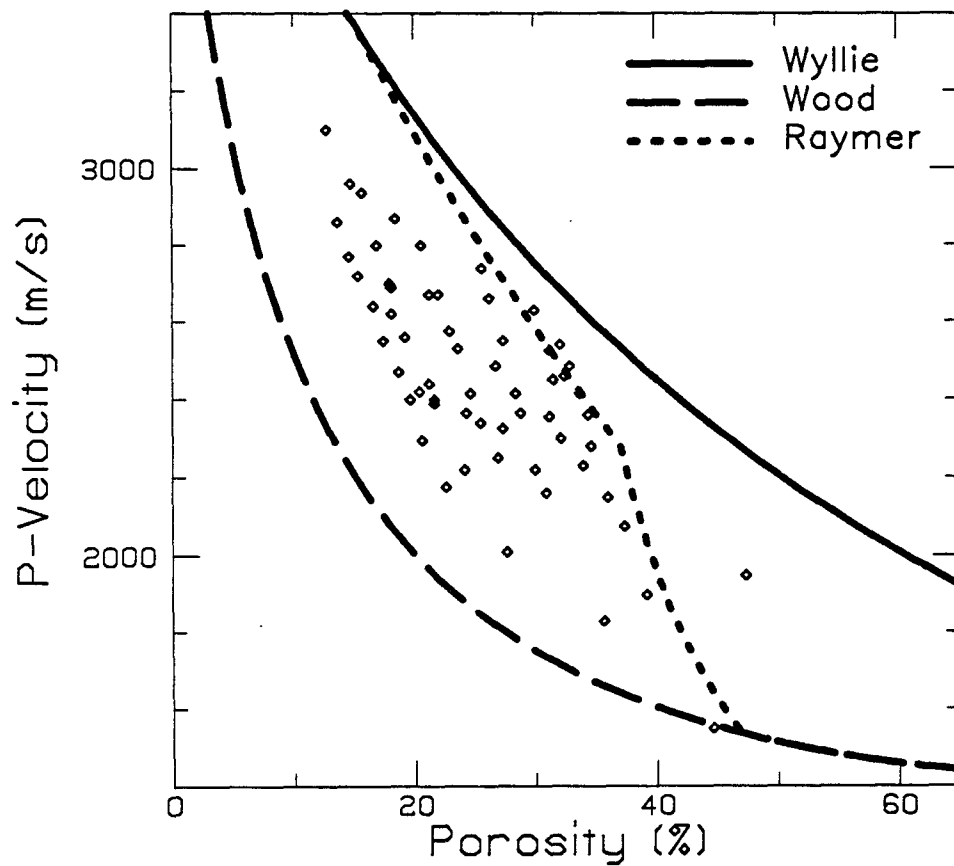


Figure 3.7: Comparison between traditional velocity-porosity relations and data (\diamond) for sand-clay mixtures. Velocity-porosity transforms are calculated for a mineralogical composition of 50% quartz and 50% clay. Conventional velocity-porosity transforms fail to explain the large scatter in velocity-porosity relation. Data are from Yin et al. (1988)

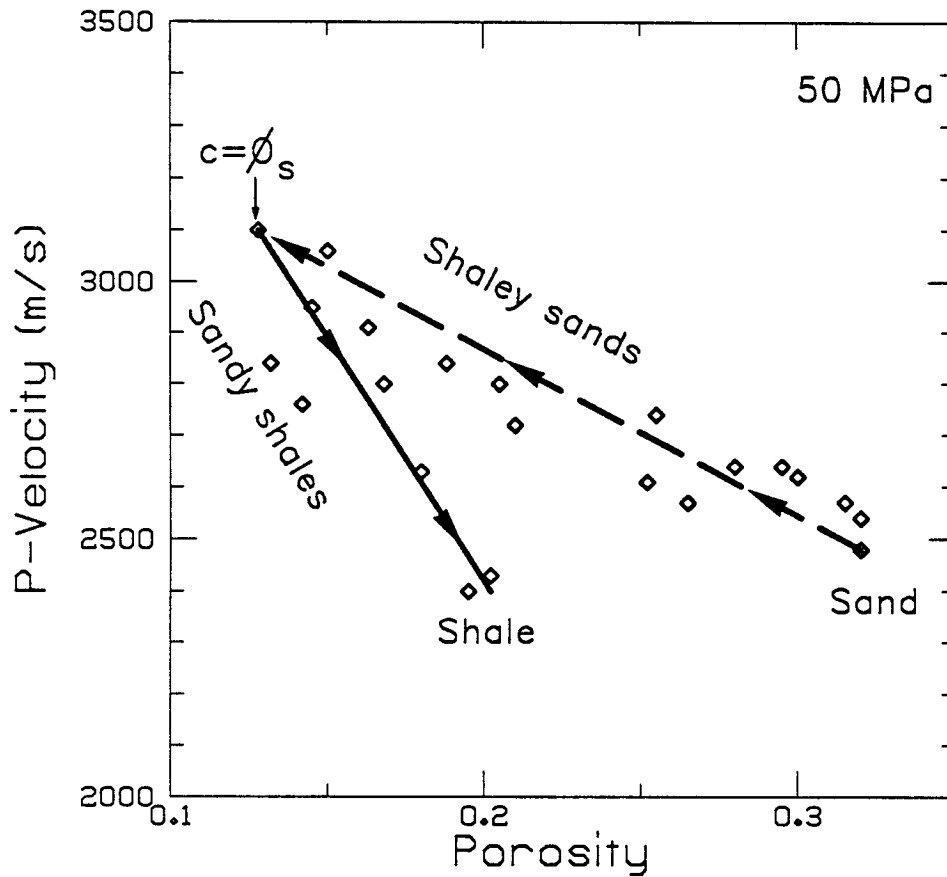


Figure 3.8: Influence of clay content on velocity-porosity relationship at a constant confining pressure (50 MPa). Distinct trends for shaley sand and for shale are schematically superposed on experimental data on sand-clay mixtures(\diamond). The trends intersect when clay content equals sand porosity at $c = \phi_s$. Arrows indicate increasing shaliness. Data are from Yin et al. (1988) and Han (1986).

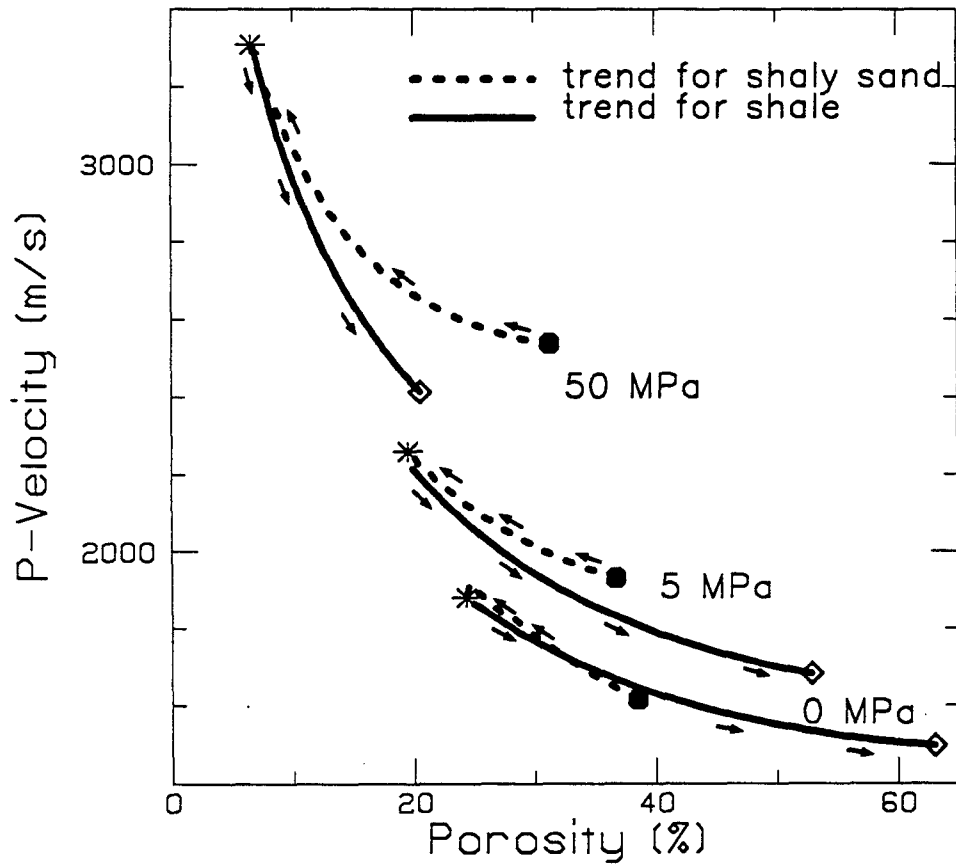


Figure 3.9: Calculated velocity and porosity using the sand-clay model at various pressures. At each pressure, solid and dashed lines represent trends for shale and shaly sand respectively. Clean sand, pure shale, and the singular point at which $c = \phi$, are represented by ●, ◇, ∗ respectively. Arrows indicate increasing shaliness. The combined effect of pressure and clay content creates scatter in the velocity-porosity relationship in sand-clay mixtures.

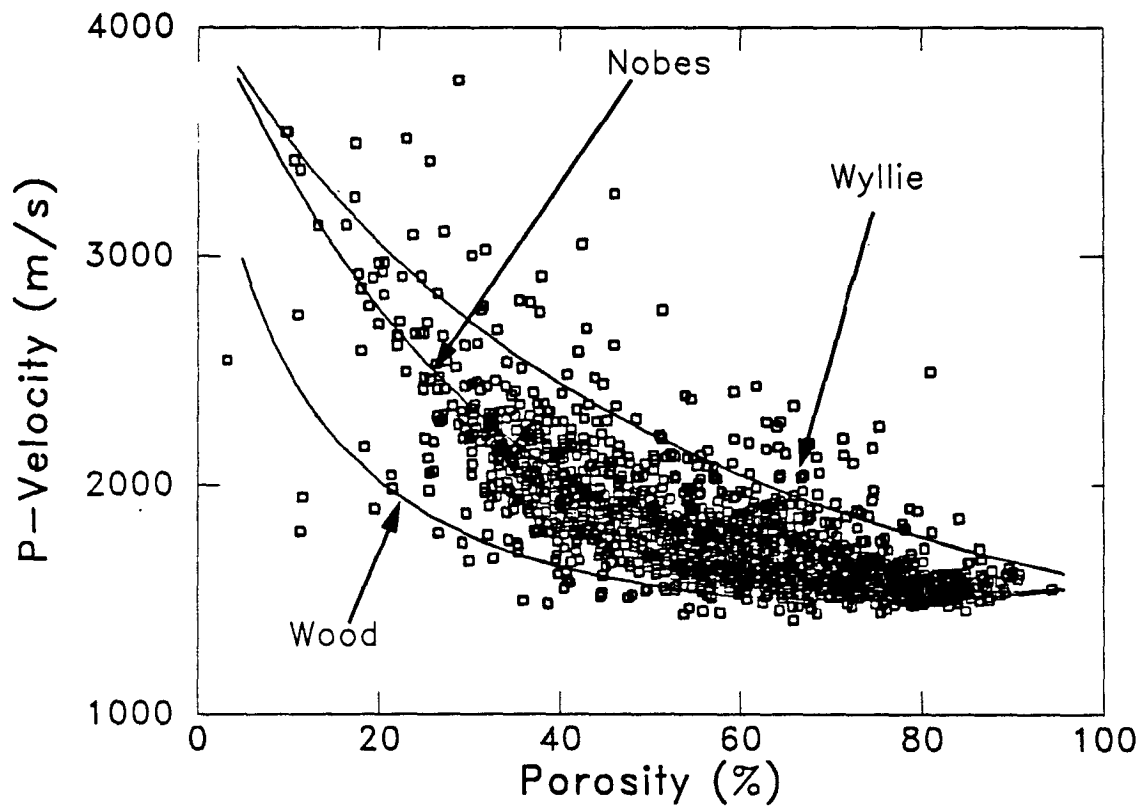


Figure 3.10: Velocity and porosity data in marine sediments, mostly in shaley environments. Data are from the Deep Sea Drilling Project (Nobes et al., 1986). The model results (Figure 3.9) reveal that much of the observed "scatter" in the data may be attributed to clay content and compaction.

al. (1986)).

Comparison between experimental data (Figure 3.7) and model (Figure 3.9) and sediment data (Figure 3.10) suggests that a large fraction of the scatter in velocity-porosity relations in these marine sediments might be attributed to the effect of compaction and existence of sedimentary mixtures similar to sand-clay mixtures. Thus, to be accurate, determination of porosity from velocity measurements needs to be constrained with parameters such as overburden pressure, and clay content that have a recognized effect on both velocity and porosity.

3.3.3 Gulf Coast sandstones

In the previous sections, we have shown the possible relevance of the sand-clay model to explain the dependence of velocity, porosity, and permeability of unconsolidated sedimentary mixtures on clay content. Because the sand-clay model is essentially based on geometrical considerations, its use can be extended to consolidated material as well, providing that such material features the geometrical characteristics of our model (i.e. presence of dispersed clay).

The sand-clay model is tested on consolidated rocks using a data set of 21 samples of Gulf Coast sandstone (after Han et al. 1986). This data set was chosen for three reasons: 1) Gulf Coast sandstones feature detrital "intrapore" clay, 2) clay content in this data set ranges from 5 to 50 percent and hence covers the range of sand, shaley sand and sandy shale in our model and 3) cores were collected from depths of 10,000 to 16,000 feet which allows investigation of the effect of overburden pressure on physical properties. Figure 3.11 shows results of the comparison between the porosity, P-velocity data measured under saturated conditions at 40 MPa (differential pressure) and the sand-clay model. In Figure 3.11a, data exhibit a decrease in porosity with increasing clay content. A porosity minimum is reached when clay volume fraction is equal to 32 percent. This behavior is closely matched with the porosity model (solid line) using equations 3.1 and 3.3 with $\phi_s = 32\%$ and $\phi_{sh} = 25\%$. In Figure 3.11b, P-

velocity data show an increase in velocity from 0 to 30 % clay volume fraction followed with a decrease from 30 to 55 %. This peak in velocity is reproduced with the model (solid line) using input parameters listed in Table 3.2. These parameters were chosen to best fit end-members (pure sand and pure shale) porosity and velocity data. The scatter around the model results in Figure 11a and 11b may be primarily attributed to the effect of compaction. It can be noticed that shallow samples (data marked as • corresponding to depths ranging between 10,000 and 13,000 feet) are fairly well described with the model's solid line, whereas deeper samples (data marked as o corresponding to depths ranging between 13,000 and 17,000 feet) are characterized by lower porosities and higher velocities due to compaction.

In Figure 3.12, the relationship between porosity and velocity is similar to that shown in Figure 3.8 for sand-clay mixtures. Gulf Coast sandstones exhibit a moderately scattered velocity-porosity relationship. However, even in this favorable case, determination of porosity from velocity measurements using a single linear fit would be accurate to at least 10 porosity units. In contrast, the superposition of the sand-clay model results (solid line) on the porosity-velocity data indicates clearly the dependence of velocity on porosity for shaley sand and a steeper dependence for sandy shales. The velocity-porosity relationship at different depths, also shows that the influence of pressure is to shift the trend for shaley sand to higher values of velocity and lower values of porosity. Based on this information, porosity can be estimated with 2-3 % accuracy, provided information exists about shaliness (from Gamma Ray) and depth.

3.3.4 Consolidated sediments

The following example is aimed at showing how the characteristic trends of the sand-clay model may be identified in sonic well-log data (Smith and Gidlow, 1987). In Figure 3.13a, the two distinct sandstone and shale trends that were observed in experimental data (Figure 3.8) and model (Figure 3.9) are identified in sonic log

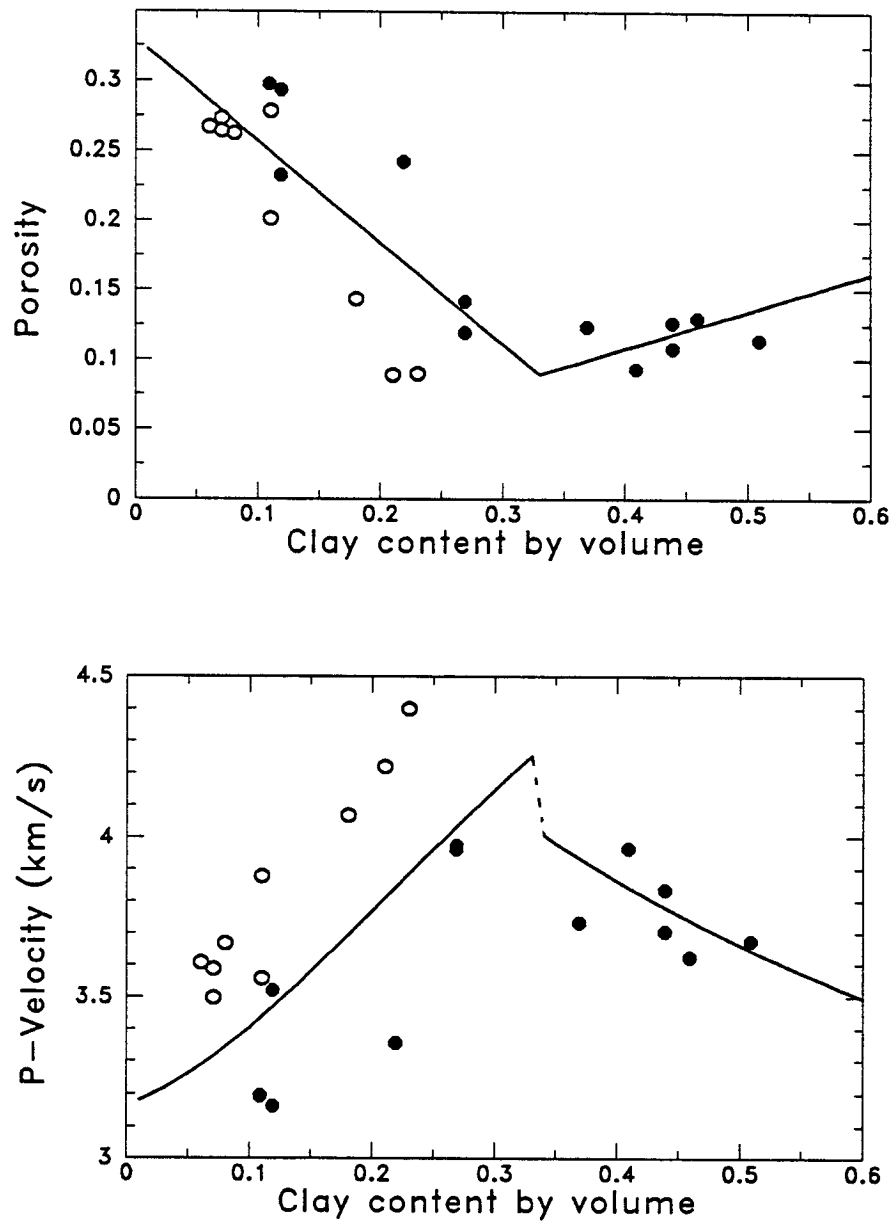


Figure 3.11: Gulf Coast sandstones (data from Han et al., 1986) exhibit the characteristic trends of sand-clay mixtures: minimum in porosity (Figure a), and peak in velocity (Figure b) versus clay content. The scatter around the main trends is attributed to compaction (data marked as ● were recovered at depth ranging between 10,000 and 13,000 feet and data marked as ○ were recovered between 13,000 and 17,000 feet).

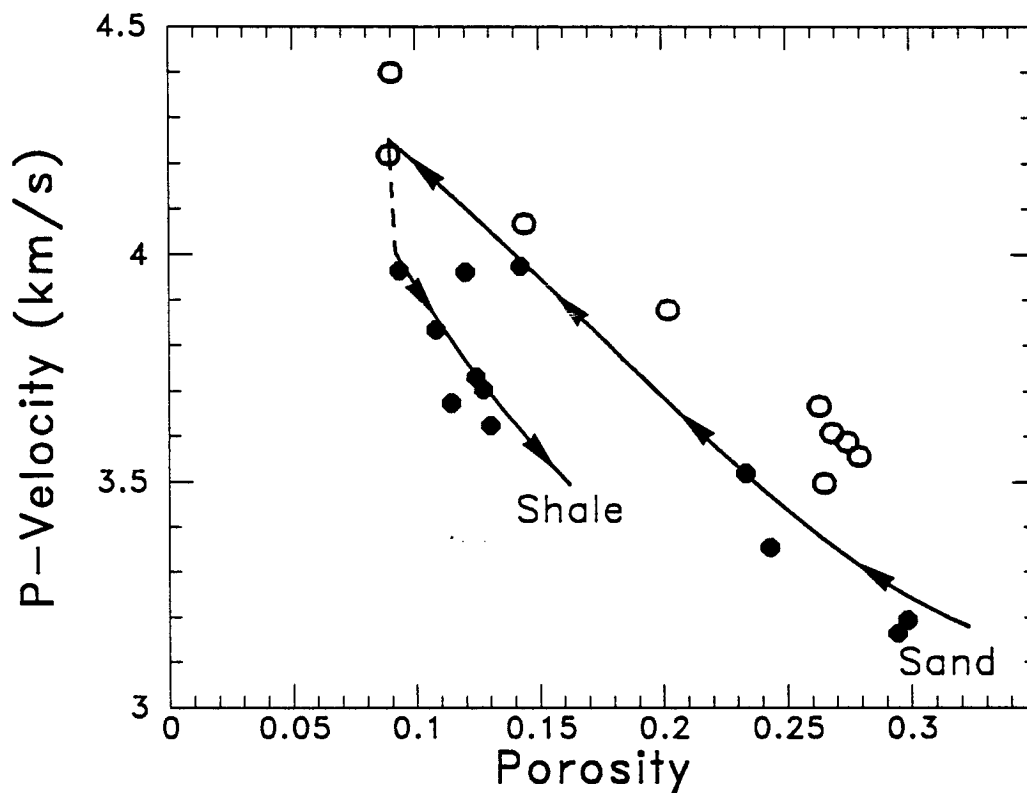


Figure 3.12: Scatter in the velocity-porosity relationship has a deterministic cause and is related to clay content and compaction. By superposing the sand-clay model on the Gulf Coast sandstone data, distinct trends for shaley sand and for shale can be observed. The trends intersect when clay content equals sand porosity at $c = \phi_s$. The effect of compaction (\bullet : low depth, \circ : high depth) is to create additional apparent scatter in the velocity-porosity relationship. Arrows indicate increasing shaliness.

velocity and density data from consolidated marine sediments. For comparison, the sand-clay model for velocity and density calculated at three different depths (or pressure) is shown in Figure 3.13b. Velocity and density were calculated using equations 3.8 to 3.13. Input parameters listed in Table 3.3 were determined to best fit the end-member data (clay-free sandstone, pure shale). The model is found to reproduce not only trends for shales and sandstones but also their associated scatter and the region of sparse data (middle left-hand portion of graph) that results from the paucity of sonic log measurements in the upper part of the sediment column.

Table 3.3

Depth	ϕ_s (%)	ϕ_{sh} (%)	V_{psand} (m/s)	V_{pshale} (m/s)	V_{sand} (m/s)	V_{shale} (m/s)
1	24	12	3900	3100	2200	1400
2	20	8	4350	3200	2700	1700
3	15	4	4800	3700	3200	2000

3.4 Influence of clay content on porosity-permeability transform

Linear relationships between the logarithm of permeability and porosity have been observed commonly in many reservoirs and used as a tool to derive empirically permeability from porosity measurements. However, the considerable amount of scatter in the porosity-permeability relationship suggests that porosity alone is insufficient to account for large variations of permeability and that other parameters such as mineralogy should be incorporated in the porosity-permeability transforms (Heron, 1987).

The superposition of the sand-clay model (solid line) on permeability (logarithm) vs. porosity data for Gulf Coast sandstones illustrates the combined effect of porosity and clay content on air permeability in Figure 3.14. For comparison, Kozeny-Carman

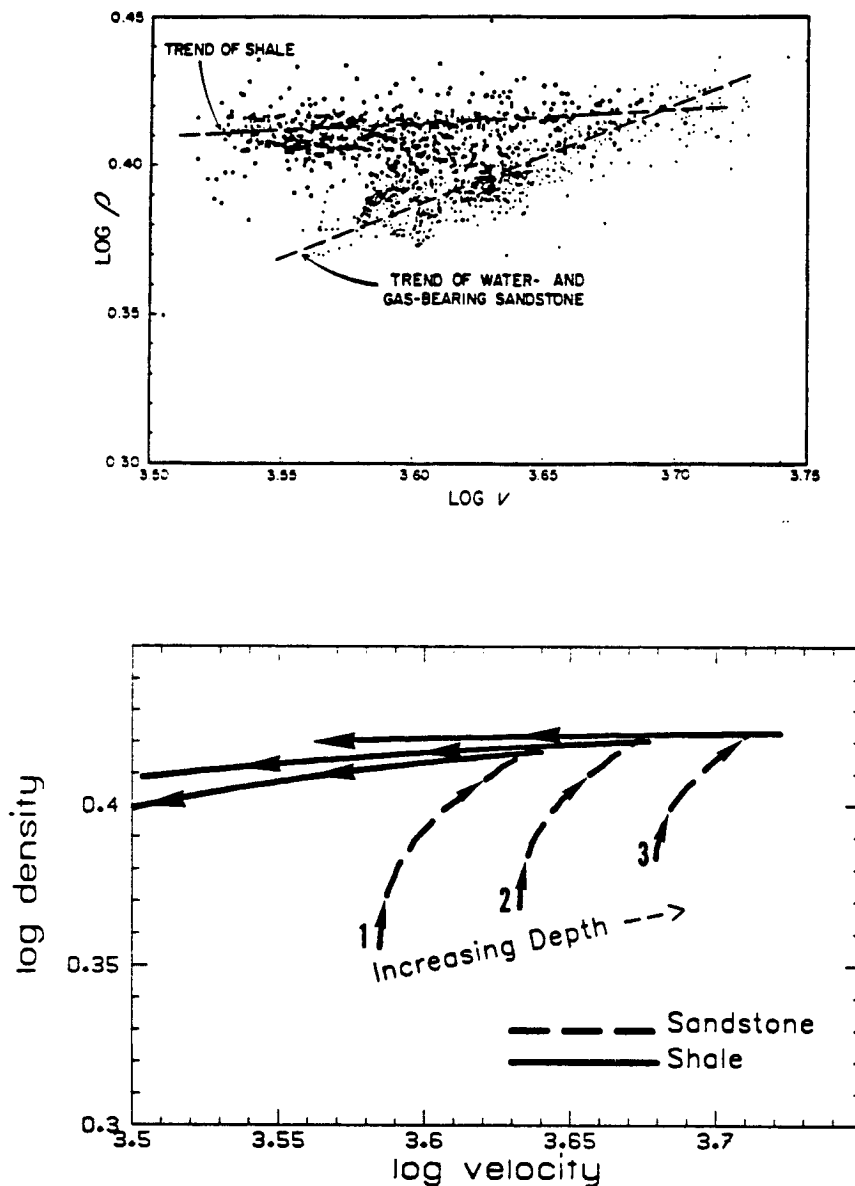


Figure 3.13: Shale and sandstone sonic log data (Figure a from Smith and Gidlow, 1987) are explained using the sand-clay model (Figure b). The model reproduces the trend for shale and sandstone observed in the log data and the scatter around the trends. Arrows indicate increasing shaliness.

equation calculated for pure sand and pure shale (dashed line) shows the effect of porosity on permeability. In clean sandstones, because of the absence of clay, Kozeny-Carman relation is a reasonably good model for the effect of porosity on permeability (Bourbie and Zinszner, 1985). In contrast, in shaley sandstones the rapid decrease of permeability over a small range of porosity indicates that clay content has an overwhelming effect on permeability . The reasonable agreement between the sand-clay model and the data in Figure 3.14 suggests that in shaley sands, the slope of the permeability-porosity relationship reflects primarily the influence of clay content on both permeability and porosity. Dispersion of data around the main trend is primarily attributed to the location of clay within the pore space (pore-lining vs. pore-filling and pore-bridging).

3.5 Summary

A microgeometrical model for sand and shaley sand with "intrapore clay", and sandy shale and shale with dispersed sand grains was proposed to describe porosity, P-velocity and permeability vs. clay content behavior in unconsolidated sand-clay mixtures and some clastic rocks. In the case where the sand-clay model is validated from core or well-log observations, improvement in the determination of (1) porosity from sonic measurements and (2) permeability from porosity may be achieved by incorporating clay content and compaction. Finally, information from well-logs can be combined with seismic measurements and the sand-clay model to obtain spatial variations of porosity, permeability and shaliness.

Acknowledgement

This work was supported by the Office of Naval Research under contract N00014-84-K-0560.

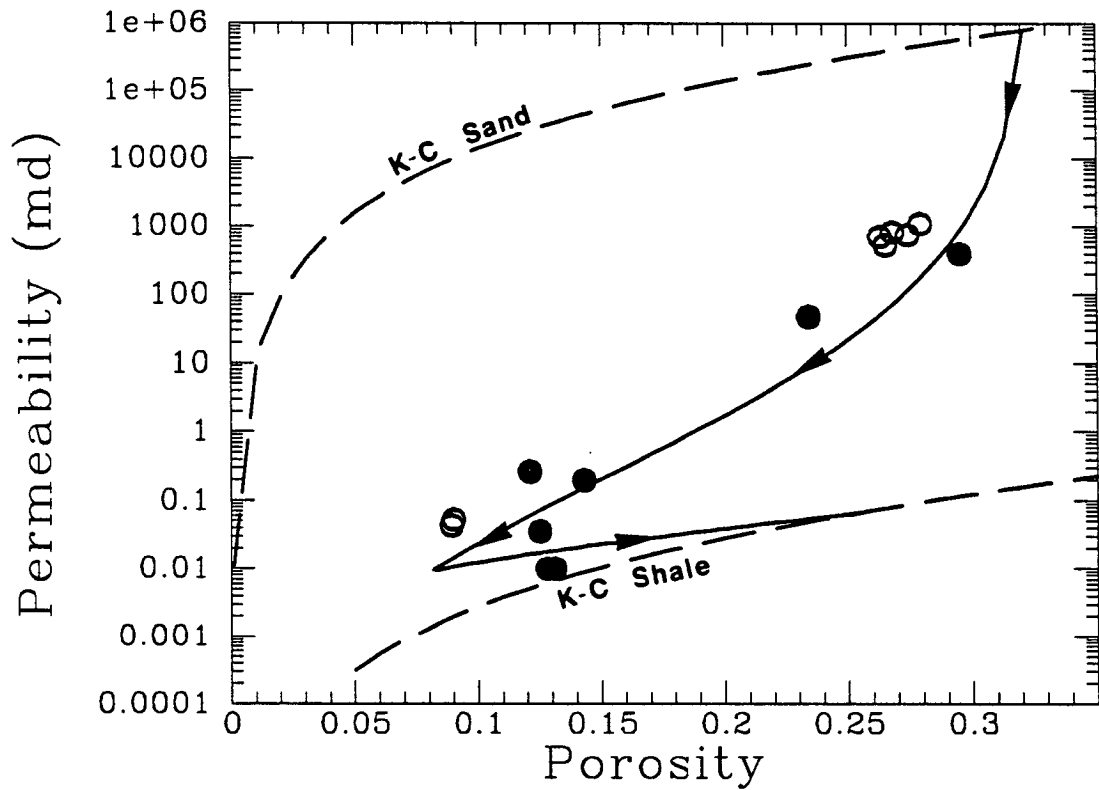


Figure 3.14: Permeability vs. porosity data in Gulf-Coast sandstones reflect the primary influence of clay content on both permeability and porosity. Kozeny-Carman relations for pure sand and pure shale are also shown (dashed lines) to illustrate the effect of porosity on permeability.

Appendix A

The influence of intrapore clay on elastic moduli of rocks is computed in this appendix. The method used follows that of Mavko and Jizba (1989) for the derivation of "undrained bulk modulus of saturated rocks".

The effective modulus is computed using the Betty-Rayleigh reciprocity theorem (Jaeger and Cook, 1969) applied to the case of a saturated rock submitted to two different sets of traction (Figure A1).

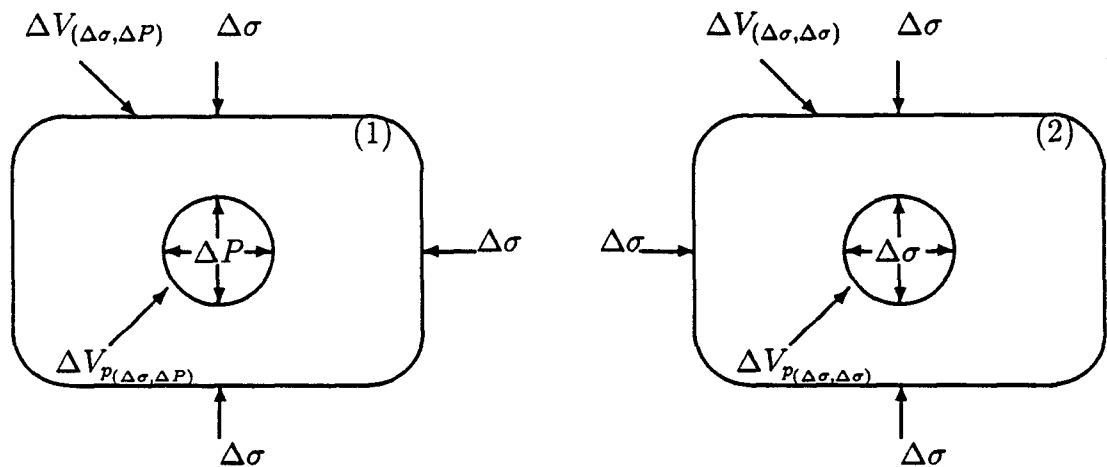


Figure A.1: Sets of traction and displacements used in calculation of elastic moduli of the saturated rock using the Betty-Rayleigh reciprocity theorem.

In the first case, (1), the bulk volume of the rock, V , is subjected to confining stress, $\Delta\sigma$, and the pore volume, V_p , is subjected to pore pressure, ΔP . In the second case, (2), pore pressure and confining pressure are both set equal to $\Delta\sigma$.

According to the reciprocity theorem, the product of one set of traction times the

displacement created by another set of traction is invariant:

$$\Delta\sigma_{(1)} \Delta V_{(2)} = \Delta\sigma_{(2)} \Delta V_{(1)} \quad (3.20)$$

In the case of Figure A.1 this leads to the following equation

$$\Delta\sigma \Delta V_{(\Delta\sigma, \Delta P)} - \Delta\sigma \Delta V_{P(\Delta\sigma, \Delta P)} = \Delta\sigma \Delta V_{(\Delta\sigma, \Delta\sigma)} - \Delta P \Delta V_{P(\Delta\sigma, \Delta\sigma)} \quad (3.21)$$

where ΔV and ΔV_p are the change of bulk volume and pore volume respectively in the confining and pore pressure conditions listed in the subscript.

By definition,

$$\Delta V_{(\Delta\sigma, \Delta P)} = \Delta\sigma \frac{V}{K^*} = \text{Change of undrained bulk volume} \quad (3.22)$$

$$\Delta V_{(\Delta\sigma, \Delta\sigma)} = \Delta\sigma \frac{V}{K_0} = \text{Change of mineral bulk volume} \quad (3.23)$$

$$\Delta V_{P(\Delta\sigma, \Delta\sigma)} = \Delta\sigma \frac{V_p}{K_0} \quad (3.24)$$

Combining equations 3.22, 3.23, and 3.24 to equation 3.21 leads:

$$\Delta\sigma \frac{\Delta\sigma V}{K^*} - \Delta\sigma \Delta V_{P(\Delta\sigma, \Delta P)} = \Delta\sigma \frac{\Delta\sigma V}{K_0} - \Delta P \frac{\Delta\sigma V_p}{K_0} \quad (3.25)$$

After dividing by $V(\Delta\sigma)^2$

$$\frac{1}{K^*} - \frac{\Delta V_{P(\Delta\sigma, \Delta P)}}{V \Delta\sigma} = \frac{1}{K_0} - \frac{1}{K_0} \frac{\Delta P V_p}{\Delta\sigma V} \quad (3.26)$$

The term $(\Delta P/\Delta\sigma)$ that represents the stress induced pore pressure can be calculated using the superposition theorem (see Figure A.2).

From Figure A.2, The change of pore volume under the stress conditions (1) is equal to the sum of change of pore volume under conditions (2) and (3).

$$\Delta V_{P(\Delta\sigma, \Delta P)} = \Delta V_{P(\Delta\sigma - \Delta P, 0)} + \Delta V_{P(\Delta P, \Delta P)} \quad (3.27)$$

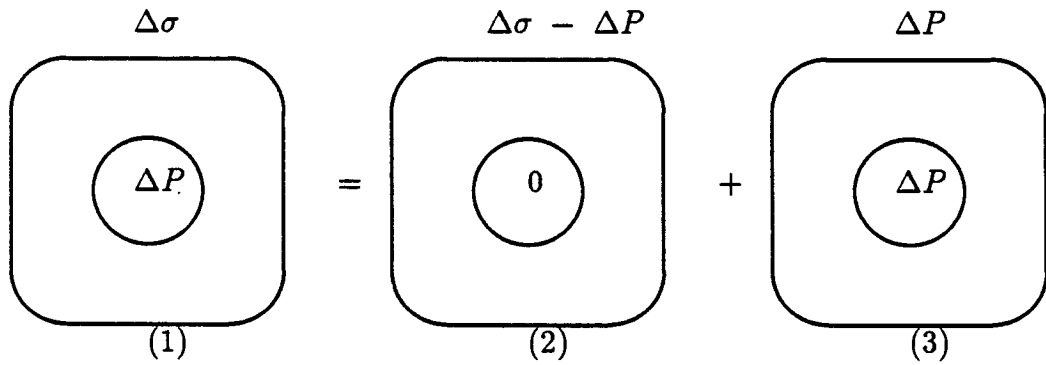


Figure A2: Superposition of state of stress for calculation of stress induced pore pressure $\Delta P/\Delta\sigma$.

By definition, $\Delta V_{p(\Delta\sigma-\Delta P,0)}$ can be written as (after Zimmerman et al., 1986):

$$\Delta V_{p(\Delta\sigma-\Delta P,0)} = \frac{V_p(\Delta\sigma - \Delta P)}{K_{pc}} \quad (3.28)$$

where K_{pc} , the pore stiffness under confining pressure is related to bulk and mineral stiffnesses, K_b and K_o , respectively following the relation:

$$\frac{1}{K_{pc}} = \left(\frac{1}{K_b} - \frac{1}{K_o} \right) \frac{V}{V_p} \quad (3.29)$$

Combining equations 3.27 and 3.28 gives

$$\Delta V_{p(\Delta\sigma,\Delta P)} = \frac{V_p(\Delta\sigma - \Delta P)}{K_{pc}} + \frac{V_p\Delta P}{K_o} \quad (3.30)$$

and after dividing by $V_p\Delta\sigma$

$$\frac{\Delta V_{p(\Delta\sigma,\Delta P)}}{V_p\Delta\sigma} = \frac{1}{K_{pc}} - \frac{\Delta P}{\Delta\sigma} \left[\frac{1}{K_{pc}} - \frac{1}{K_o} \right] \quad (3.31)$$

Finally combining equations 3.29 and 3.31 gives for the stress induced pore pressure:

$$\frac{\Delta P}{\Delta \sigma} = \left[1 + \frac{V_p}{V} \left(\frac{\Delta V_{p(\Delta \sigma, \Delta P)}}{\Delta P V_p} - \frac{1}{K_0} \right) / \left(\frac{1}{K_b} - \frac{1}{K_0} \right) \right]^{-1} \quad (3.32)$$

The term $(\Delta V_{p(\Delta \sigma, \Delta P)}/V_p \Delta P)$ represents the pore volume compressibility under confining pressure, $\Delta \sigma$, and pore pressure, ΔP . In the case where clay is located within the pore space, pore volume, V_p , is filled with a certain amount of fluid, V_{fl} , and clay, V_{cl} ,

$$V_p = V_{fl} + V_{cl} \quad (3.33)$$

Let's consider here that clay particles are dispersed in the pore space and do not interact with pore wall. Then the change of pore volume is simply the sum of the changes of fluid volume and clay volume:

$$\Delta V_p = \Delta V_{fl} + \Delta V_{cl} \quad (3.34)$$

Hence

$$\frac{\Delta V_p}{V_p} = \frac{\Delta V_{fl}}{V_{fl} (1 + V_{cl}/V_{fl})} + \frac{\Delta V_{cl}}{V_{cl} (1 + V_{fl}/V_{cl})} \quad (3.35)$$

x and $1 - x$ being the volume fraction of clay and fluid in the pore space respectively, equation 3.35 becomes after dividing by ΔP

$$\frac{\Delta V_p}{V_p \Delta P} = \frac{1}{K_p} = \frac{1}{K_{fl}^*} = \frac{x}{K_{cl}} + \frac{1-x}{K_{fl}} \quad (3.36)$$

which relates the bulk stiffness of the pore space, K_p to the bulk stiffness of its constituents (i.e., fluid and clay). By combining equations 3.26, 3.32 and 3.36, we obtain an expression for the bulk modulus of a clay-bearing saturated rock.

$$\frac{1}{K^*} = \frac{1}{K_0} - \left(\frac{1}{K_{fl}^*} - \frac{1}{K_0} \right) \left(1 - \frac{1}{\phi_s + \left(\frac{1}{K_{fl}^*} - \frac{1}{K_0} \right) / \left(\frac{1}{K_b} - \frac{1}{K_0} \right)} \right) \quad (3.37)$$

with ϕ_s being equal to V_p/V . By rearranging equation 3.37, one obtain equation 3.8.

References

- Almon, W., R., 1979, A geologic appreciation of shaley sands: SPWLA Symposium, paper WW.
- Ben Aïm, R., and Le Goff, P., 1967, Effet de paroi dans les empilements désordonnés de spheres et application à la porosité de mélanges binaires: Powder Technol., **1**, 281-290.
- Bourbie, T. and Zinszner, B., 1985, Hydraulic and acoustic properties as a function of porosity in Fontainebleau sandstone, J. Geophys. Res., **90**, 11,524-11,532.
- Carman, P., C., 1956, Flow of gasses through porous media, New York, Academic Press.
- Clarke, R. H., 1979, Reservoir properties of conglomerates and conglomeratic sandstones: AAPG Bull., **63**, 799-803.
- Cumberland D. J. and Crawford R. J., 1987, The packing of particles , Handbook of powder technology, Elsevier.
- Fisk, H. N., McFarlan, E., Kolb, C. R., and Wolbert, L. J., 1954, Sedimentary framework of the modern Mississippi delta: J. Sed. Pet., v. 24, 76-99.
- Furnas, C. C., 1928, The relation between specific volume, voids, and size composition in systems of broken solids of mixed sizes: U.S. Bur. Mines, Rept. Investigations, 2894, 1-10.
- Gassmann, F., 1951, Elastic waves through a packing of spheres: Geophysics, **16**, 673-685.
- Graton, L. C. and Frazer, H. J., 1935, Systematic packing of spheres - with particular relation to porosity and permeability. J. Geol., **43**, 785-909.
- Heron, M., M., 1987, Estimating the intrinsic permeability of clastic sediments from geochemical data : SPWLA Symposium, paper HH.
- Han, D., Nur, A., and Morgan, D., 1986, Effect of porosity and clay content on wave velocity in sandstones: Geophysics, **51**, 2093-2107.
- Jaeger J. C., and N. G. Cook, 1979, Fundamental of rock mechanics. Chapman and Hall ltd.
- Knight, R., 1986, Mineralogy, Petrology, and Geochemistry of clay minerals, class notes, Stanford University.

- Kowallis, B., Jones, L. E. A. and Wang H. F., 1984, Velocity-porosity-clay content; systematics of poorly consolidated sandstones: *J. Geophys. Res.*, **89**, 10355-10364.
- Kuster, G. T., and Toksöz, M. N., 1974, Velocity and attenuation of seismic waves in two-phase media, Part II: Experimental results: *Geophysics*, **39**, 607-618.
- McGeary, R. K., 1961, Mechanical packing of spherical particles: *J. Am. Ceram. Soc.*, **44**, 513-522.
- Marion, D. P., and Nur A., 1989, Percolation of electrical and elastic properties of granular materials at the transition from a suspension to a loose packing: *Physica A*, **157**, 575-579.
- Mavko, G. and D, Jizba, 1989, Estimating Grain-scale effects on bulk and shear dispersion in rocks, unpublished.
- Neasham, J. W., 1977, The morphology of dispersed clay in sandstones and its effect on sandstone shaliness, pore space and fluid flow properties: 52nd Annual Fall Technical Conference and Exhibition of the Society of Petroleum Engineers of AIME, Denver, SPE paper 6858.
- Nobes, D.C., Villinger, H., Davis, E. E., and Law, L. K., 1986, Estimation of marine sediments bulk physical properties at depth from sea-floor geophysical measurements: *J. Geophys. Res.*, **91**, 14033-14043.
- Purnel, G. W., 1986, Observation of wave velocity and attenuation in two-phase media: *Geophysics*, **51**, 2193-2199.
- Raymer, D. S., Hunt, E. R., and Gardner, J. S., 1980, An improved sonic transit time-to-porosity transform: Presented at the Soc. Prof. Well-log Anal. 21st Ann. Mtg., paper P.
- Reuss, A., 1929, Berechnung der fließgrenze von mischkristallen auf grund der plastizitätsbedingung für einkristalle: *Zeitschrift für Angewandte Mathematik and Mechanik*, **9**, 49-58.
- Smith, G. C., and Gidlow, P. M., 1987, Weighted stacking for rock property estimation and detection of gas: *Geophys. Prosp.*, **35**, 993-1014.
- Thomas, E., C. and Stieber, S. J., 1975, The distribution of shale in sandstones and its effect upon porosity, SPWLA meeting paper T.
- Tozaya, C. and Nur, A., 1982, Effect of the diagenesis of clays on compressional velocity in rocks: *Geophys. Res. Lett.*, **9**, 5-8.

- Westman, A. E. R., and Hugill, H. R., 1930, The packing of particles: *J. Am. Ceram. Soc.*, **13**, 767-779.
- Wood, A.B., 1941, *A textbook of sound*: Macmillan Publ. Co.
- Wyllie, M. R. J., Gregory, A. R., and Gardner, L. W., 1956, Elastic wave velocities in heterogeneous and porous media: *Geophysics*, **21** , 41-70.
- Yin, H., Han D. H. and Nur A., 1988, Study of velocity and compaction on sand-clay mixtures, *Stanford Rock and Borehole Project*, Vol 33.
- Zimmerman, R. W., W. H. Somerton, and M. S. King, 1986, Compressibility of Porous Rocks, *J. Geophys. Res.*, **91**, 12765-12777.

Chapter 4

Elastic properties of granular materials and the effect of coordination number

Abstract

The dependence of elastic moduli of granular materials on the average number of contacts per grains is studied experimentally. The distribution of contacts of a random packing of conductive spheres is first inferred from conductivity measurements where large conductive beads are mixed with smaller non-conductive beads. These results are combined with measurements of porosity and P velocity on the packing of conductive spheres to determine the influence of number of contacts on elastic moduli of the material. Static elastic moduli are found to vary linearly with the number of contacts following an Effective-Medium theory type of relation. In contrast, dynamic moduli are rather insensitive to the number of contacts. These results show that the ratio of static to dynamic moduli in granular materials may be directly related to the number of contacts and the differing sensitivity of static and dynamic moduli to the number of contacts.

4.1 Introduction

The determination of in-situ mechanical properties of soils and other unconsolidated granular materials is essential in civil engineering and reservoir production tasks for prediction of slope stability, ground subsidence, sanding during production, etc. Information about elastic properties of such materials may be provided by in situ measurements or laboratory mechanical tests on cores. However such measurements are expensive and sparsely collected. Furthermore, drilling conditions in such materials are not always optimal. Core recovery can be low and chances to restore in situ conditions for mechanical testing are rather small. Because seismic or acoustic methods have a much broader spatial coverage and can be implemented in any type of environments, their use as an alternate solution to determine elastic properties of unconsolidated materials has been suggested for many years. There has been consequently a growing interest in understanding the elastic behavior of granular materials and the relationships between seismically or acoustically derived elastic moduli (dynamic) and mechanically measured moduli (static). Laboratory experiments have shown that dynamic elastic stiffnesses are invariably greater than the statically measured ones. In consolidated materials, the discrepancy between static and dynamic elastic moduli and specially the pressure dependence of the ratio of static to dynamic moduli has been primarily attributed to presence of microcracks (King, 1969, Simmons and Brace, 1965). In favor of this argument, it was experimentally observed that upon crack closure with confining pressure, the ratio of static to dynamic moduli eventually approach unity at high pressure (Cheng and Johnston, 1981).

In unconsolidated materials, the ratio of dynamic to static moduli is considerably larger than in consolidated materials and can typically range from 1 to 100 (Smith, 1974). Such discrepancy between static and dynamic moduli has two main causes: (1) dynamic measurements record principally elastic deformation of grains in contact whereas static measurements are sensitive to both elastic deformation and inelastic

behavior, such as irreversible sliding and rolling of grains. As a result, static compressibilities are larger than dynamic ones. (2) Purely elastic deformation of granular materials is not "felt" identically by static and dynamic measurements. Even at elevated pressures or during the unloading phase of a pressure cycle (when inelastic behavior are not dominant), it is experimentally observed that the ratio of static to dynamic moduli is still significantly lower than 1.

In this paper, we focus attention on the mechanisms responsible for the discrepancy between static and dynamic elastic moduli in granular materials when the deformation is purely elastic. In section 4.2, elastic theory applied to solid bodies in contact (Hertz-Mindlin theory) is used to investigate the elastic response of granular materials under applied stress. The generalization of Hertz-Mindlin theory from two grains in contact to packing of grains suggests that in addition to contact stiffness, the average number of contacts per grain greatly influences elastic behavior of the material. We therefore analyse in greater details, in sections 4.3 and 4.4, the dependence of elastic moduli on average number of contact based on results from percolation theory and laboratory experiments. Section 4.3 is a short review on percolation theory and its possible application to granular materials. Section 4.4 is concerned with the experimental determination of the average number of contact per grains of a random packing of spheres and the relationship between elastic moduli and number of contacts. Combination of elasticity and percolation theories is finally used in section 4.5 to interpret the difference between static and dynamic moduli in granular materials in term of average number of contact per grain.

4.2 Contact models for granular materials

When two solid grains are brought into contact, they touch initially at a contact point. Upon loading, grains deform in the vicinity of their contact over an area that is proportional to the applied load. In order to predict how the area of contact grows

with applied load, Hertz applied the theory of linear elasticity to two solid bodies in contact and derived a relationship between elastic deformation and normal stress (Landau and Lifshitz, 1959). Cattaneo (1938), Mindlin (1949), and Walton (1978) extended Hertz's theory to the case of tangential deformations acting on the surface area of contact between grains. Finally, generalization of the elastic solution from two spheres in contact to a random packing of spheres was derived by Digby (1981) and Walton (1987). We review here these contact models and their main characteristics.

4.2.1 Hertz' contact theory

Hertz's theory describes elastic deformation of solid bodies in contact when forces between bodies are normal to the contact surfaces. Assumptions are made that: (1) grain surfaces are continuous and contacts are non-conforming (point contact), (2) the strains are small, (3) each solid can be considered as an elastic half space (radius of contact small with respect to the dimension of the particle and the relative radii of curvature of the surfaces), and (4) surfaces are frictionless. Although Hertz's contact theory can be applied to relatively complicated contact geometry such as ellipsoidal area of contact, the discussion will be restricted here to identical spherical bodies in contact. Based on Hertz' calculations, a normal force, N , acting on two identical spheres of radius, R , in contact will create a circular area of contact of radius, a

$$a = \left(\frac{3(1 - \nu)NR}{8\mu} \right)^{1/3} \quad (4.1)$$

where ν and μ are intrinsic Poisson's ratio and shear modulus of spheres respectively. The application of a normal force also results in a small displacement, h , between the centers of the two spheres (see Figure 4.1) :

$$h = 2 \left(\frac{a^2}{R} \right) = 2 \left(\frac{3(1 - \nu)N}{8\mu\sqrt{R}} \right)^{2/3} \quad (4.2)$$

From these equations, one can define for each contact, a normal compliance, C_n , that depends on the surface area of contact and the elastic properties of the particles

$$C_n = \frac{1}{2} \frac{dh}{dN} = \frac{2}{3} \left(\frac{9(1-\nu)^2}{64\mu^2 RN} \right)^{1/3} = \frac{1-\nu}{4\mu a} = \frac{1}{S_n} \quad (4.3)$$

The validity of Hertz's theory was verified experimentally by Hertz himself, using optical interference fringes between two glass lenses in contact. Other studies (Fessler and Ollerton, 1957) have also tested the validity of the cube root relationship between surface area of contact and load (equation 4.1) at sufficiently high enough loads such that roughness of the surfaces had a negligible effect on the results.

Relationships derived for the deformation of two spheres in contact under normal stress were extended to a random packing of spheres by Brandt (1955) assuming that: (1) for each sphere, contacts are distributed with a uniform probability over the surface of the sphere, (2) that all the contacts deform identically, and (3) that forces acting on contacts are purely normal to the contact. The average force, $\langle N \rangle$, exerted on each contact can then be related to the hydrostatic pressure, P , using the relation:

$$\langle N \rangle = \frac{4\pi R^2 P}{c(1-\phi)} \quad (4.4)$$

where c is the average number of contacts per sphere for the packing, and ϕ is the porosity of the packing. From this, the average strain at each contact resulting from the application of hydrostatic pressure P on the random packing is given by:

$$\left\langle \frac{h}{R} \right\rangle = \left(\frac{3\pi(1-\nu)P}{2\mu(1-\phi)c} \right)^{2/3} \quad (4.5)$$

Based on assumptions (1) to (3), the bulk modulus, K of the packing can be related to the average normal strain $\langle h/R \rangle$ and hydrostatic pressure, P :

$$P = K \left\langle \frac{h}{R} \right\rangle \quad (4.6)$$

Combining equations 4.5 and 4.6 gives an expression for effective bulk modulus of a random packing of spheres as a function of applied stress, P , packing parameters, c

and ϕ , and elastic moduli of the grains, μ and ν :

$$K = \left(\frac{4\mu^2 c^2 (1 - \phi)^2 P}{9\pi^2 (1 - \nu)^2} \right)^{1/3} \quad (4.7)$$

4.2.2 Mindlin's contact theory

When a tangential force is superimposed on the normal force that presses solid bodies against each other, no sliding motion should occur if the magnitude of the tangential force T is smaller than the limiting friction force, fN . Nevertheless, the effect of the tangential force is to cause the bodies to deform in shear and points of the area of contact will undergo small relative motion so called "slip" in an annulus of internal radius, c , and external radius, a , with

$$\frac{c}{a} = \left(1 - \frac{T}{fN} \right)^{1/3} \quad (4.8)$$

Cattaneo (1938) and Mindlin (1949) have shown that the effect of the tangential force T , is to create a tangential displacement, δ , between the centers of the two spheres occurs (see Figure 4.2)

$$\delta = \frac{3fN(2 - \nu) \left[1 - (1 - T/fN)^{2/3} \right]}{8\mu a} \quad (4.9)$$

where f is the coefficient of friction of the material of the spheres. The corresponding tangential compliance for a given sphere can be written as

$$C_t = \frac{1}{2} \frac{d\delta}{dT} = \frac{2 - \nu}{8\mu a (1 - T/fN)^{1/3}} = \frac{1}{S_t} \quad (4.10)$$

Note that because the distribution of normal pressure is not affected by tangential tractions, the shape of the area of contact is not modified by the tangential traction. Consequently, the expression for the normal displacement, h , created by the normal force, N is identical to that obtained by Hertz in equation 4.2.

These results for two spheres in contact were generalized to ordered packing of spheres and applied to compute elastic moduli of packings (Gassmann, 1951; Duffy and Mindlin, 1957; Dereziwicz, 1958, Walton, 1975).

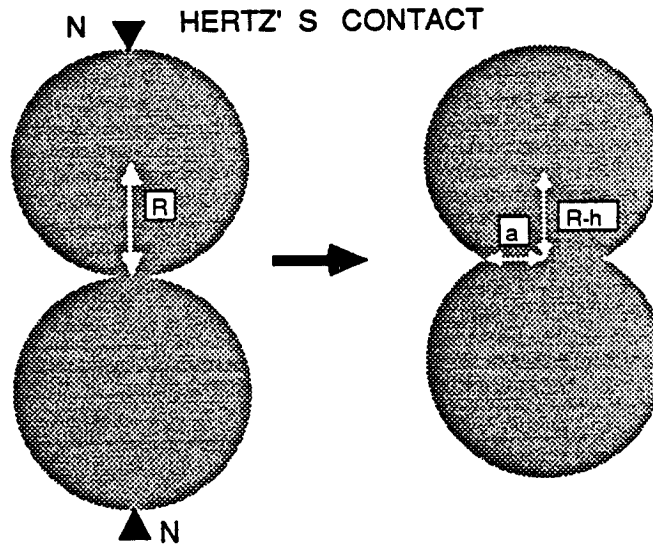


Figure 4.1: Hertzian contact. Application of normal forces to two bodies in contacts creates a circular surface area of contact of radius, a , and a normal displacement, h between the centers of the spheres.

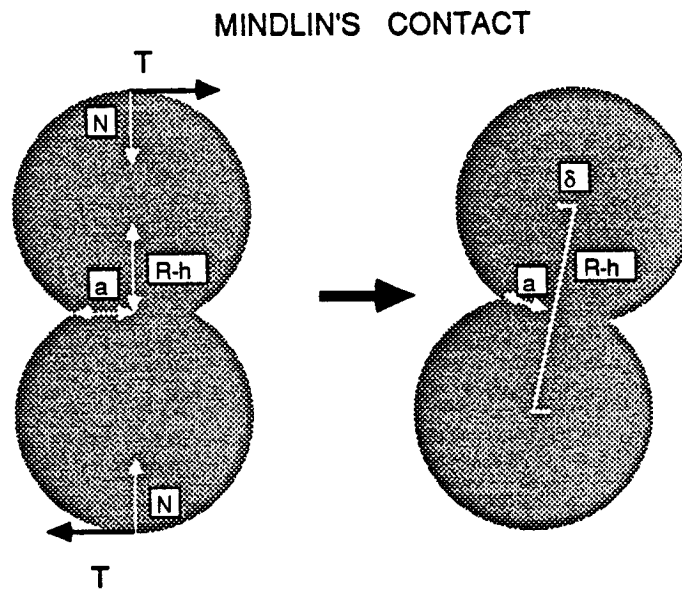


Figure 4.2: Mindlin contact. The superposition of a tangential force on a Hertzian contact generates a lateral displacement, δ between the centers of the spheres.

4.2.3 Walton's contact model

Walton (1978) treated the case of the oblique compression of two elastic spheres. This case differs from that treated by Mindlin in the sense that both normal and tangential forces are applied simultaneously to the contact, resulting in a different deformed state. In his calculations Walton imposes that grains are in perfect adhesion and shows that if slip occurs in the region of contact, it is in the form of sliding. For the case of infinitely rough spheres in contact, Walton's results for normal and tangential displacements between the centers of the two spheres are:

$$h = \left(\frac{3\pi BN}{4\sqrt{R}} \right)^{2/3} \quad (4.11)$$

and

$$\delta = \left(\frac{3\pi(2B + C)T}{8a} \right) \quad (4.12)$$

where

$$B = \frac{1}{4\pi} \left(\frac{1}{\mu} + \frac{1}{\lambda + \mu} \right) \quad (4.13)$$

and

$$C = \frac{1}{4\pi} \left(\frac{1}{\mu} - \frac{1}{\lambda + \mu} \right) \quad (4.14)$$

where λ and μ are the Lamé's constants for the grains.

4.2.4 Effective moduli of a packing of spheres under hydrostatic pressure

Based on the theoretical results for compression of two spheres under oblique force, Walton derived an expression for the elastic moduli of a random packing of spheres under hydrostatic state of stress assuming that: (1) the displacements of the sphere centers are consistent with the applied uniform field, (2) the packing is statistically isotropic (3) and contacts are distributed uniformly over the surface of the grain. In this derivation which is quite similar to that developed by Digby (1981) for a random

packing of spheres bonded together, the effective bulk modulus is given by:

$$K = \frac{1}{6} \left(\frac{3\phi^2 c^2 P}{\pi^4 B^2} \right)^{1/3} \quad (4.15)$$

The shear modulus is given by:

$$G = \frac{5B + C}{10(2B + C)} \left(\frac{3\phi^2 c^2 P}{\pi^4 B^2} \right)^{1/3} \quad (4.16)$$

Although Walton's expressions for bulk and shear moduli (equations 4.15 and 4.16) are derived for a certain type of contact model (Walton, 1978), the method of generalization from two spheres in contact to a random packing of spheres can be applied to other types of mechanical contacts providing that assumptions (1) to (3) are satisfied. More specifically, one can relate elastic moduli of a random packing of spheres to the average normal and tangential stiffnesses at each contact, S_n and S_t respectively, and number of contacts, c , using the relation (After Winkler, 1983):

$$K = \frac{c}{12\pi R} S_n \quad (4.17)$$

$$G = \frac{c}{20\pi R} \left(S_n + \frac{3}{2} S_t \right) \quad (4.18)$$

Expressions for normal and tangential stiffness for various contact models are summarized in table 4.1, where a , the average contact radius between grains in contact is related to normal load using equations 4.1 and 4.4.

Table 4.1

Contact models	S_n	S_t
Hertz	$\frac{4\mu a}{1-\nu}$	—
Mindlin	$\frac{4\mu a}{1-\nu}$	$\frac{8\mu a(1-T/fN)^{1/3}}{2-\nu}$
Walton	$\frac{4\mu a}{1-\nu}$	$\frac{8\mu a}{2-\nu}$
Digby	$\frac{4\mu a}{1-\nu}$	$\frac{8\mu b}{2-\nu}$

Note that in the limit where the tangential force is negligible with respect to the normal force, Mindlin and Walton's expressions for tangential compliances are similar and the ratio (S_n/S_t) (or identically the ratio (K/G)) is independent of the applied load and is only related to elastic parameters of the grains.

In the case of wave propagation ($\Delta T, \Delta N \ll N$), the various contact models predict that elastic moduli are linearly related to a , the surface area of contact between grains. Hence elastic moduli are expected to vary as the cube root of confining pressure. This power law dependence has been verified experimentally for ordered packings of spheres (Johnson, 1955) and attempts to apply this relationship to sediments have been made by Brandt (1955). However, for sediments or soils, elastic moduli were found to vary more rapidly with confining pressure (power law exponent greater than $1/3$ in marine sediments, unconsolidated sands, and glass beads (Murphy, 1982)). It is important to note that, according to equations 4.17 and 4.18, a dependence of elastic moduli to the cube root of confining pressure can only be achieved in the particular cases where the average number of deforming contacts, c , remains constant with pressure. As such condition is unlikely to apply to sediments as they deform during compaction, there is a need to estimate better variations of the number of deforming contacts with pressure in order to understand relationships between elastic moduli and pressure in unconsolidated granular materials.

From equations 4.17 and 4.18, we notice that elastic moduli should vary linearly with number of contacts, and should vanish when the average number of contacts is equal to zero. In contrast, experimental results in Chapter 2 on elastic and electrical properties of granular materials at the transition from suspension to compacted state suggest that elastic moduli of granular materials vanish when the average number of contact per grain is greater than zero. Furthermore, the analogy between the elastic and the electrical response of granular material observed in this experiments suggests that the dependence of elastic moduli, M , on number of contacts, c may not be of

the form $M(c) = c$ as suggested by equations 4.17 and 4.18, but instead could be of the form of a percolation type relation (see next section).

From this a more general expression for elastic moduli, M of granular materials may be given by:

$$M \propto F(c)H(S_n, S_t) \quad (4.19)$$

where $H(S_n, S_t)$ describes the dependence of elastic moduli of the materials on contact stiffnesses, and $F(c)$ describes the dependence of elastic moduli on number of contacts, c , to be determined experimentally.

4.3 Percolation Theory and Granular Materials

This section is a short review of percolation theory and its possible application to transport and elastic properties of granular materials. More specifically, we present the relationships between number of contacts and elastic and electrical properties of lattice networks and granular materials.

4.3.1 Percolation and electrical conductivity

Percolation theory has been widely used to explain transport properties in inhomogeneous media (see Etopim proceedings by Lafait and Tanner, 1989). Classical percolation results of conductivity through lattice networks (Kirkpatrick, 1973; Powell, 1979) have been particularly useful for the understanding and prediction of electrical conduction in particulate materials. From experiments on random packing of spheres (Ottavi et al., 1978 ; Maliaris and Turner, 1971), electrical conduction through particulate materials was found to be analogous to conduction through lattice networks. Using the lattice network analogy, spheres of the random packing are equivalent to sites or nodes of the lattice and contacts between spheres are similar to bonds between sites of the lattice (Figure 4.3). It has been recognized that for both lattice network and particulate materials, the influence of sites or grains and bonds or contacts on

conductivity was significantly different. Because of the distinction between bonds and sites, percolation mechanisms were divided into two categories: bond and site percolation.

Bond percolation

Bond percolation mechanisms can be described simply by considering a resistor network in which a fraction of the resistors is removed randomly (i.e. their resistance is set to infinity) while the remainder is conductive. In such system, there exists a critical fraction of resistors or bonds, p_c below which the probability of finding a conductive path is zero. Below this critical threshold, conductivity is equal to zero. Above this critical threshold, conductivity increases with the increasing fraction of conducting bonds or resistors (see Figure 4.4) and two domains can be distinguished (after Kirkpatrick, 1973).

Close to threshold: Close to threshold, p_c , a power law of the form

$$k(p) = (p - p_c)^t \quad (4.20)$$

relates conductivity to fraction of conductive bonds with a percolation exponent, t which is typically of the order of 1.8 ± 0.2 and a number of bonds at threshold close to 1.5.

Far from threshold: Far from threshold, an accurate analytical solution for conductivity can be obtained using Effective Medium Theory (EMT). Consider a resistor network submitted to a voltage applied along one axis of the network. The average effect of this random network can be represented by an homogeneous effective medium made of resistors of resistance r . The value of r is obtained by requiring that when some perturbations are created in the system by replacing some resistances r by resistances r_i , the extra voltage induced must average to zero. Based on such an argument, Kirkpatrick (1973) has shown that the dependence of the average resistance

of the network, r , to the fraction of conducting bonds, p , is of the form:

$$r = 1 - \left(\frac{1 - p}{1 - 2/c} \right) = \left(\frac{zp - 2}{z - 2} \right) \quad (4.21)$$

where c is the maximum number of bonds meeting at a node, or identically for granular materials, the maximum number of contacts per spheres. It can be noticed, from EMT, that resistance of resistor network vanishes when the average number of resistor meeting at a node is less than two. Similarly, for conducting granular materials, one might expect the "effective medium conductivity" to go to zero when the average number of contact per grain is less than two.

Site percolation

In a site percolation, a fraction of sites (or nodes) is randomly selected to be conducting while the remainder is isolating. Under a critical number of sites present p_s^c , the lattice is disconnected and non conductive. The behavior near and far from threshold, p_s^c , is quite similar to a bond percolation problem. Near threshold, a relation of the form of equation 4.20 holds for conductivity, but the site exponent t can be slightly different from the bond exponent (Kirkpatrick, 1973). Far from threshold, conductivity varies linearly with number of sites present following an EMT type of relation similar to equation 4.21.

In granular materials, site percolation relations are appropriate to model conductivity in mixtures of conducting and non-conducting particles (Ottavi et al., 1978). Bond percolation on the other hand is more relevant to model influence of number of conductive contacts in a conducting granular material and will be used in the following section to model conductivity measurements in conducting granular materials.

4.3.2 Percolation and elasticity

Applying the concept of percolation theory to elasticity was first proposed by De Gennes (1976) to describe elastic behavior of Gels. The analogy between resistor and

elastic networks was more recently confirmed from computer simulations on networks (Feng and Sen, 1984; He and Thorpe, 1985; Schwartz et al., 1985). Experiments were also performed to investigate the analogy between electrical and elastic properties of 2D and 3D percolating systems (Benguini, 1984; Deptuck et al., 1985). The common feature of these studies was to invariably find that the critical exponent, t (in equation 4.20), was significantly higher in the elastic case than in the electrical case. These observations were used to argue that elastic networks were a new class of percolating systems (Bergman and Kantor, 1984; Kantor and Webman, 1984; Bergman, 1985; Feng et al., 1984).

In order to estimate when the percolation threshold for elasticity should occur, a method based on calculating the number of zero frequency modes of the system was proposed by Philipps (1979) and Thorpe (1983). Percolation is expected to take place when the number of zero-frequency modes goes to zero or identically when the number of degrees of freedom of the system is equal to the number of constraints. As the constraint counting method suggests, transition depends upon the degrees of freedom and number of constraints attached to each particle of the system and consequently depends on the topology of the elastic network and the kinds of interacting forces between particles. This method was compared against simulations on different types of elastic networks and was found to predict quite accurately elastic percolation thresholds (He and Thorpe, 1985, Schwartz et al., 1985).

Far from the percolation threshold, EMT was found to describe quite accurately the dependence of elastic moduli of elastic networks on number of elastic bonds present (Feng et al. 1985; Garboczi and Thorpe, 1985). The method used by Kirkpatrick, to calculate the effective resistance of a resistor network, was adapted to elastic networks by replacing resistors by elastic springs and voltage by strain (Feng, 1985).

Using the analogy between lattice network and granular materials (Figure 4.3)

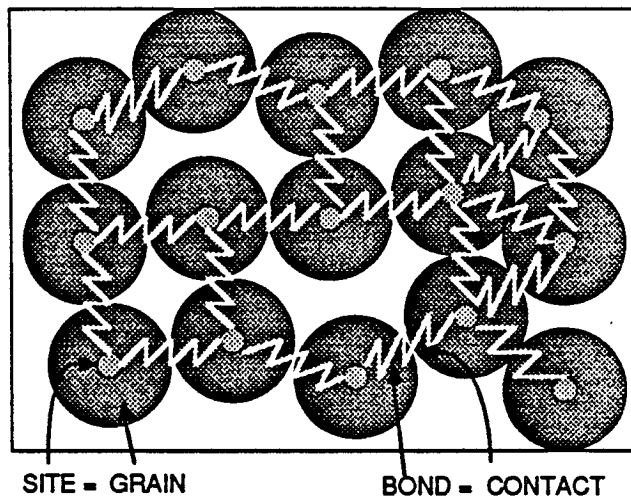


Figure 4.3: Analogy between resistor networks and granular materials: Grains are analogous to sites, and contacts are similar to bonds.

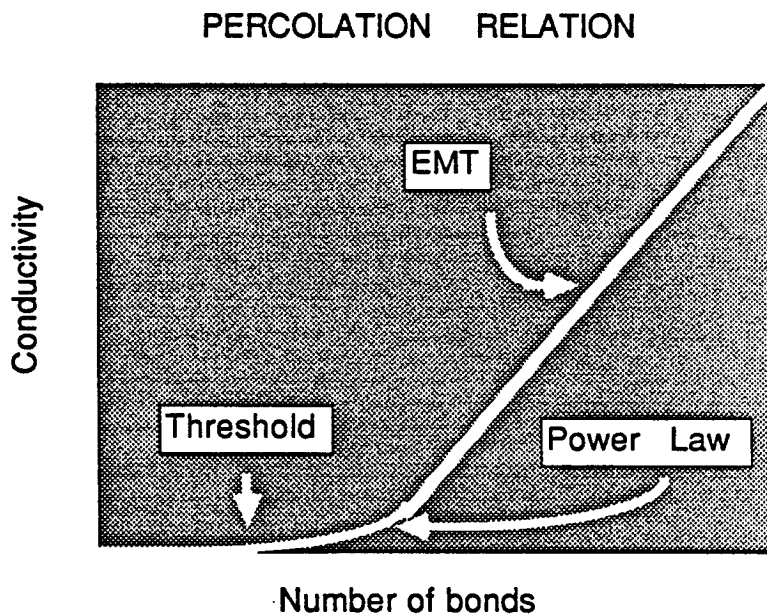


Figure 4.4: In a percolation type of relation, close to threshold, a power law describes dependence of conductivity on number of contacts. Far from threshold, behavior of conductivity is described by Effective Medium Theory.

we would like to determine whether or not results developed for elastic networks may also apply to granular materials. More specifically, we would like to test the applicability of Effective Medium Theory to the dependence of elastic properties on the number of contacts.

4.4 Dependence of Elastic Moduli on Number of Contacts

As mentioned in the first section on contact models, the elastic moduli, M , of granular materials depend primarily on contact stiffness, S and number of contact or bonds per grains, c :

$$M = H(S_n, S_t) F(c_p) \quad (4.22)$$

From Walton and Digby's models for granular materials it is assumed that $F(c_p) = c_p$, whereas from computer simulations on elastic networks $F(c_p)$ may follow a bond percolation type of relation similar to equations 4.20 and 4.21. In an attempt to define an expression for $F(c_p)$ and understand the functional dependence of elastic moduli of granular materials on the number of contact per grain, it is first necessary to estimate variations of the number of contacts with confining pressure. Because direct measurements of the number of contacts are technically difficult and limited to random packings at rest (Bernal and Mason, 1960, Smith et al., 1929), variation of number of contacts with pressure have been determined indirectly from conductivity measurements using the sensitivity of electrical conduction through granular materials to the number of contacts (Batchelor and O'Brien, 1977, Ottavi et al., 1978). To determine the functional dependence of elastic moduli on number of contacts, the experimental investigation is conducted in two phases.

(1) Electrical conductivity is first measured on mixtures of large conducting spheres and small non-conducting spheres at various pressures. From these measurements, we first infer the variations with pressure of the average number of contacts of the

aggregate of conducting spheres.

(2) P-velocity, porosity, and electrical conductivity are then measured simultaneously on the packing of large conducting spheres. From these measurements and the results from part (1), we investigate the relationship between elastic moduli and number of contacts.

4.4.1 Experimental Procedure

Experiments were conducted on 11 samples. Samples were prepared by mixing various proportions of conducting silver coated glass beads with non-conducting regular glass beads. Silver coated glass particles (Potter Industry brand) were 75 microns diameter spheres (the same kind as the ones described in the experimental set-up in Chapter 2). The diameter of the non-conducting glass spheres ranged between 1 and 4 microns and their density was 2.37 g/cm³. Each sample weighed 100 g and silver coated glass spheres weight fraction ranged between 0 and 100 % with increment of 10 %. Samples were placed in a 2.54 cm. diameter teflon tube with two electrode-piezoelectric transducer, attached to sample end-plugs. Experiments were carried out during loading and unloading pressure cycles with uniaxial pressure ranging from 0 to 3.5 MPa. Changes of sample length with pressure were recorded using three micrometers positioned at 120 degree.

Initial porosity, ϕ_0 , of the sample was computed using the relation

$$\phi_0 = \frac{V_0 - (W_s/\rho_s + W_g/\rho_g)}{V_0} \quad (4.23)$$

where V_0 is the initial bulk volume of the sample computed from the length and diameter of the sample, W_s and W_g are silver coated glass beads and glass beads mass in grams, and ρ_s and ρ_g are the densities in g/cm³ of silver coated glass beads and glass respectively. Changes of porosity upon pressure increase were measured from changes of the sample length, l using the relation:

$$\frac{l_0}{l_p} = \frac{1 - \phi_p}{1 - \phi_0} \quad (4.24)$$

where l_p and ϕ_p are the length and porosity of the sample at pressure p .

Compressional wave velocity, V_p , was measured at ultrasonic frequency using the pulse transmission technique (Birch, 1960). The central frequencies of P transducers was 0.9 MHz. P-wave first arrival times were picked within an accuracy of $0.05 \mu\text{s}$ leading to a reading measurement error less than 0.3 percent.

Electrical conductivity was measured using a multimeter (H.P. 3478 A) connected to the sample stainless steel end-plugs electrodes. Resistance of the sample was measured with an accuracy of 4×10^{-4} Ohms.

4.4.2 Number of deforming contacts versus pressure

Conductivity of granular materials, according to Batchelor and O'Brien (1977) theoretical work on transport properties in granular materials, depends primarily on the number of conducting contacts and surface area of contact. However, in the special case of an aggregate of silver coated glass beads, electrical conduction is a surface conduction mechanism and variations of surface area of contact with pressure have a negligible effect on the pressure dependence of conductivity. Consequently, conductivity measurements vs. pressure of an aggregate of silver coated glass beads are primarily a measure of number of conducting contact vs. pressure. To determine experimentally how the number of contacts of a random packing of conducting spheres varies with pressure, some perturbations were created artificially in the system of conducting beads by introducing smaller non conducting particles in the aggregate. Upon mixing of small and large particles, some small particles are introduced at grain contact between large particles and their effect is to reduce the average number of conducting bonds of the system. As a result, conductivity decreases, according to bond percolation relationships, as

$$\frac{k}{k_{max}} = \left(\frac{n-2}{c-2} \right) \quad (4.25)$$

where c is the the average number of conducting bonds of the aggregate of conducting spheres, and n is the remaining number of conducting bonds after mixing of conducting and non-conducting particles. When the number of small particles introduced in the system is such that the number of remaining conducting contacts approaches percolation threshold, conductivity varies as

$$\frac{k}{k_{max}} = \left(\frac{n - 1.5}{c} \right)^t \quad (4.26)$$

where t is the percolation exponent that ranges from 1.6 to 2. Figure 4.5 shows the experimental conductivity data during loading cycle at various pressures. Data are shown for 11 samples corresponding to 11 different mixtures of conductive and non-conductive spheres. The data were normalized at each pressure to conductivity of the packing of purely conductive spheres. Figure 4.5 shows that at each pressure conductivity vanishes at the same fraction of conductive spheres (40 %) suggesting that pressure does not create any additional contact near percolation threshold. However, near threshold, the shape of the curve of conductivity vs. fraction of conducting spheres is slightly different at each pressure: conductivity increases relatively less at high pressure than at low pressure. According to equation 4.26, such variations of normalized conductivity can be related to the increase with pressure of c , the average number of conducting bonds of the aggregate of conducting spheres. Thus, based on equation 4.26, we can infer the distribution of conductive contacts, c , vs. pressure for the random packing of conductive spheres during both loading and unloading of pressure. Figure 4.6 shows the results of determination of c at various pressure using the following relationship

$$\frac{c_p}{c_{p=3.5}} = \left(\frac{k_{(p=3.5, f=50)}}{k_{(p, f=50)}} \right)^{1/t} \quad (4.27)$$

where $k_{(p, f=50)}$ and $k_{(p=3.5, f=50)}$ are the normalized conductivity measured at pressure p and 3.5 MPa respectively, for a mixture composed of 50 % of conducting beads. The choice of a mixture composed of 50 % of conducting beads is dictated by the

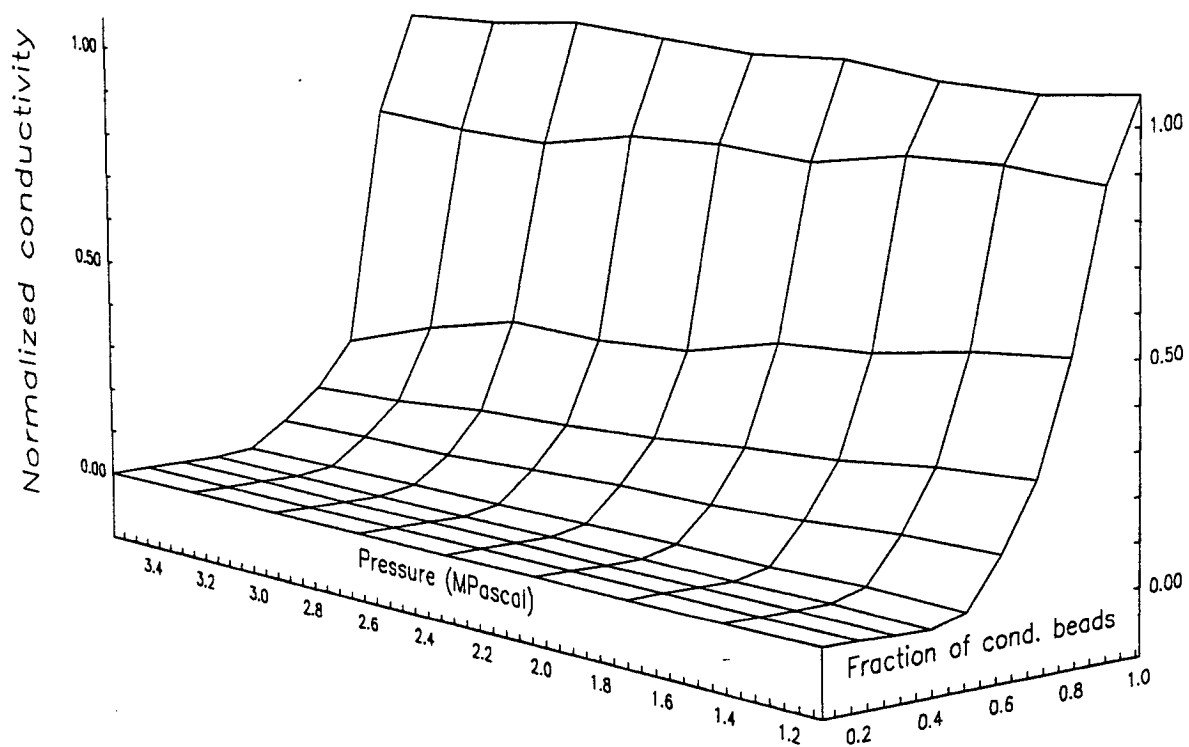


Figure 4.5: Conductivity data vs. pressure for various mixtures of large conductive beads and small non conductive particles. Percolation threshold is invariant with pressure whereas close to threshold, normalized conductivity increases more rapidly at low pressures.

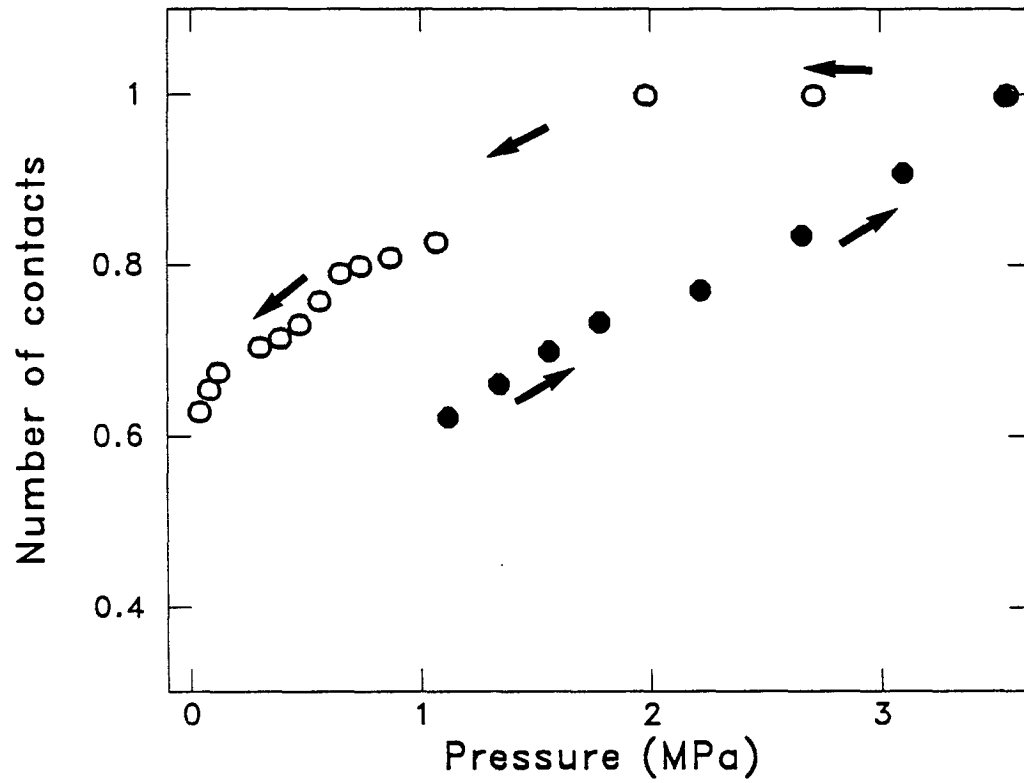


Figure 4.6: Variations of number of contacts with pressure during loading (\bullet) and unloading (\circ) phases of a pressure cycle. Number of contacts was determined from conductivity measurements using a percolation exponent of 1.8.

condition that equation 26 is only valid close to threshold. Calculations were carried out with a percolation exponent, t equal to 1.8.

During loading, number of contacts is found to increase quasi-linearly with pressure, whereas during unloading number of contacts remains constant from 3.5 to 2 MPa before some contacts start to disappear. Such hysteresis might be related to deformation mechanisms that take place during loading and unloading of granular materials. During loading, increase in packing density and hence increase in number of contacts can be primarily attributed to grain sliding and rolling. During unloading, deformation is essentially due to elastic deformation of grains in contact and decrease of number of contacts with decreasing pressure may be related to loading history for each contact: contacts that were formed early during the loading phase might have been submitted to higher level of deformation than contacts that were formed at the end of the loading phase. Hence, during unloading, "young" contacts are likely to disappear more rapidly than "old" contacts.

4.4.3 Dependence of elastic moduli on number of contacts

In this section, we consider the measurements taken during unloading phase and we assume that during this phase, deformation of the material is purely elastic. From equation 4.22, the dependence of elastic moduli on number of contacts, $F(c_p)$ can be obtained from the ratio $M/H(S_n, S_t)$ where M is the experimentally measured elastic moduli, and $H(S_n, S_t)$ represents the influence of contact stiffnesses on elastic moduli.

Using the derivative of porosity data with respect to pressure we calculate the static uniaxial strain modulus, M_s of the material at various pressures. From P-velocity data and density measurements we calculate a dynamic uniaxial strain modulus, M_d .

By combining equations 4.17 and 4.18 with equation 4.22, values of $F(c_p)$ nor-

malized to $F(c_{p=3.5})$ can be computed using the following relationship

$$\frac{F(c_p)}{F(c_{p=3.5})} = \frac{M_p}{M_{p=3.5}} \left(\frac{P}{3.5} \frac{c_{p=3.5}}{c_p} \right)^{1/3} \quad (4.28)$$

Note that because of the uncertainty in the determination of number of contact, and assumptions underlying equations 4.17 and 4.18, equation 4.28 represents only a first order approximation for the functional dependence of elastic moduli on the number of contacts. Values of $F(c_p)$ normalized to $F(c_{p=3.5})$ are plotted versus number of contacts $c_p/c_{p=3.5}$ in Figure 4.7 for static (o) and dynamic (●) moduli. We find that dependence of static uniaxial strain moduli on number of deforming contacts is linear and of the form:

$$\frac{F(c_p)}{F(c_{p=3.5})} \approx \frac{c_p - c_c}{c_{p=3.5} - c_c} \quad (4.29)$$

where c_c is the the number of contacts when $F(c_p) = 0$. The similarity between equation 4.29 and 4.21 suggest that dependence of static elastic moduli on number of contacts may be described using an effective-medium type of relation as suggested by results of simulations on elastic networks. In contrast, we find that dynamic elastic moduli are rather insensitive to variations in the number of contacts with pressure. This would suggest that once a rigid connected path is created at percolation threshold, additional contacts create redundant paths for wave propagation.

These results tend to show that static and dynamic elastic moduli exhibit a differential sensitivity to the number of contacts . Static moduli are sensitive to existence of any new contacts created by pressure and dependence of moduli on number of contacts may be described using EMT. In the dynamic case, however, waves are insensitive to generation of new contacts. This suggests that the ratio of static to dynamic moduli might be sensitive to number of contacts.

4.5 Ratio of Static to Dynamic Moduli

Experimental results of static and dynamic moduli and their ratio are shown in

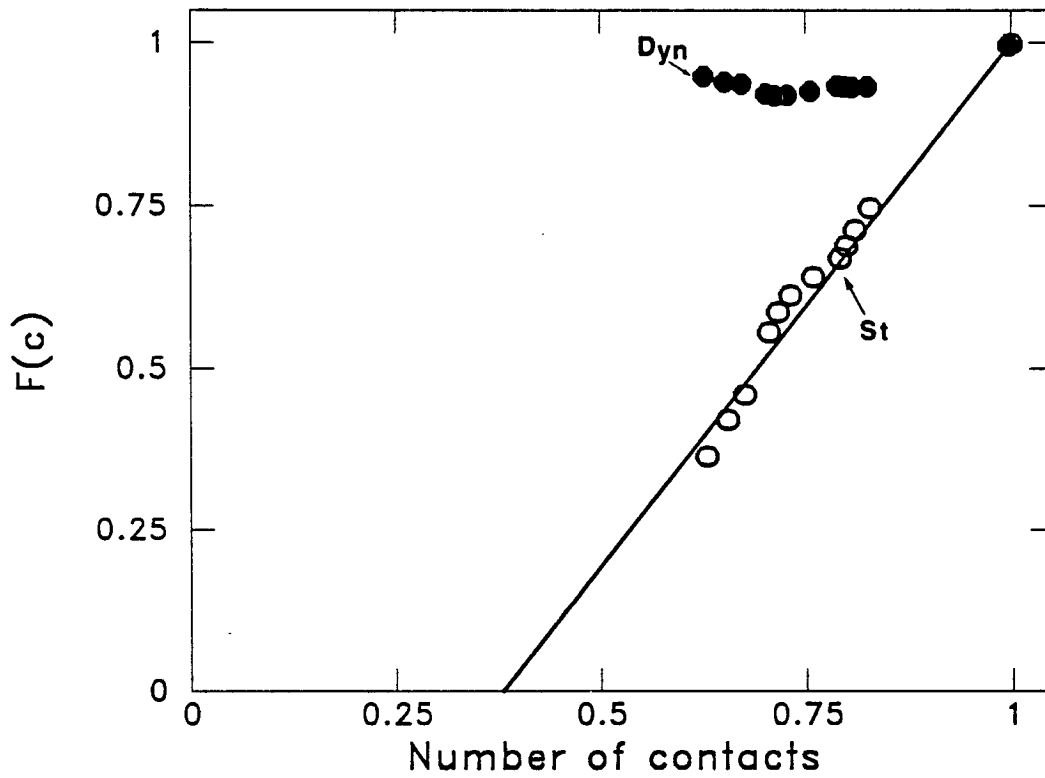


Figure 4.7: Dependence of elastic moduli on number of contacts during unloading. Static uniaxial strain modulus (\circ) varies linearly with number of contacts following an EMT type of relation. Dynamic uniaxial strain modulus (\bullet) is rather insensitive to number of contacts.

Figures 4.8 and 4.9 for the aggregate of silver coated glass beads. Measurements are shown for loading and unloading pressure cycles. During the loading pressure cycle, granular materials undergo deformation which is a combined effect of elastic deformation at grain contacts and inelastic deformation such as grain sliding and rolling. Because dynamic measurements are only recording the elastic part of the deformation whereas static measurements include both elastic and inelastic deformation, the ratio of static to dynamic measurements can be very low during loading (as low as 0.15 at low stress). Experimental results show also that the ratio of static to dynamic moduli increases with pressure from 0.15 at 0.01 MPa to 0.33 at 3.5 MPa. During the unloading pressure cycle, deformation is expected to be dominated by elastic deformation at grain contacts and one would expect the ratio of static to dynamic moduli to be close to 1. Experimental results, on other hand, show values of ratio of static to dynamic moduli between 0.4 at 0.01 MPa to 0.8 at 3.0 MPa. Results from previous section suggest that discrepancy between static and dynamic elastic moduli during unloading may be related to dependence of moduli on average number of contacts. To illustrate this point, the ratio of static to dynamic uniaxial strain moduli is plotted versus the average number of contacts determined from conductivity measurements in Figure 4.10. We find that the ratio of moduli increases approximately linearly with increasing number of contacts.

From the previous section results we propose to model the dependence of ratio of static to dynamic moduli on number of contacts, c , using the following relations for static and dynamic moduli:

$$M_s = H(S_n, S_t) c_{max} \left(\frac{c - c_c}{c_{max} - c_c} \right) \quad (4.30)$$

and

$$M_d = H(S_n, S_t) c_{max} \quad (4.31)$$

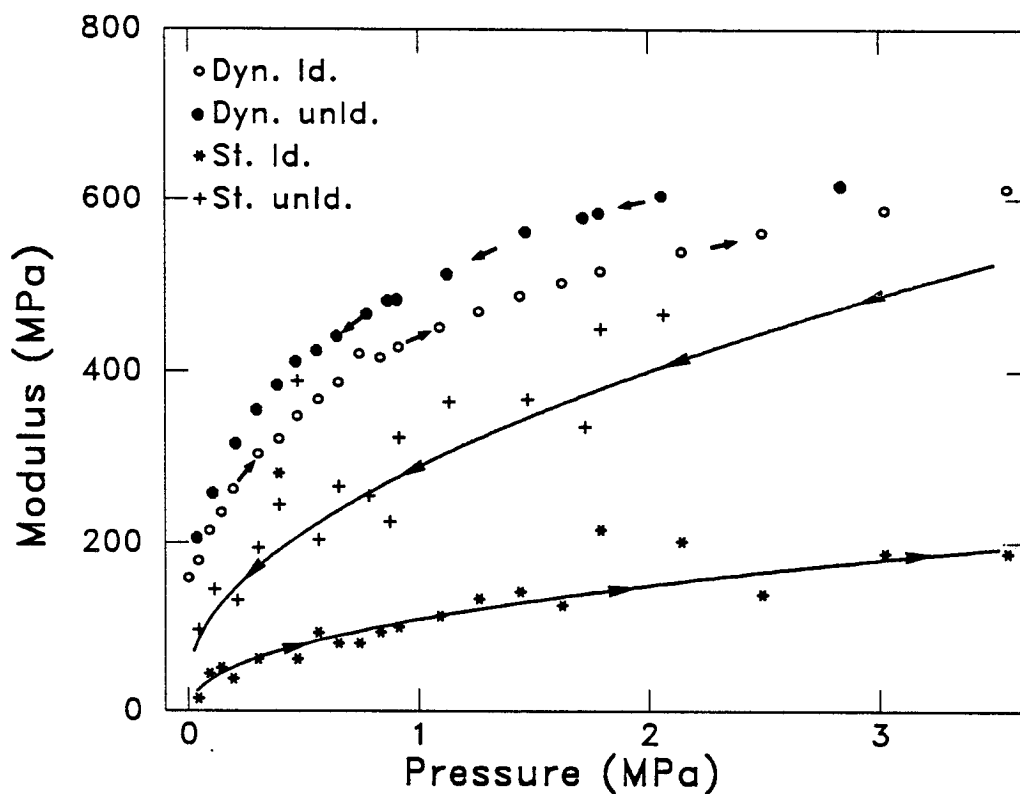


Figure 4.8: Static and dynamic uniaxial strain moduli during loading and unloading of a pressure cycle. During loading, static deformation is a combination of elastic deformation of grains in contact and inelastic deformation due to grain sliding and rolling, whereas dynamic measurements essentially record elastic deformation. Hence dynamic moduli are greater than static ones during loading. During unloading, deformation is essentially elastic and static and dynamic moduli should coincide. Note at 3.5 MPa the presence of a discontinuity between static moduli measured during loading and unloading. This discontinuity is due to a change of slope in the stress-strain relationship between the end of the loading phase and the beginning of the unloading phase.

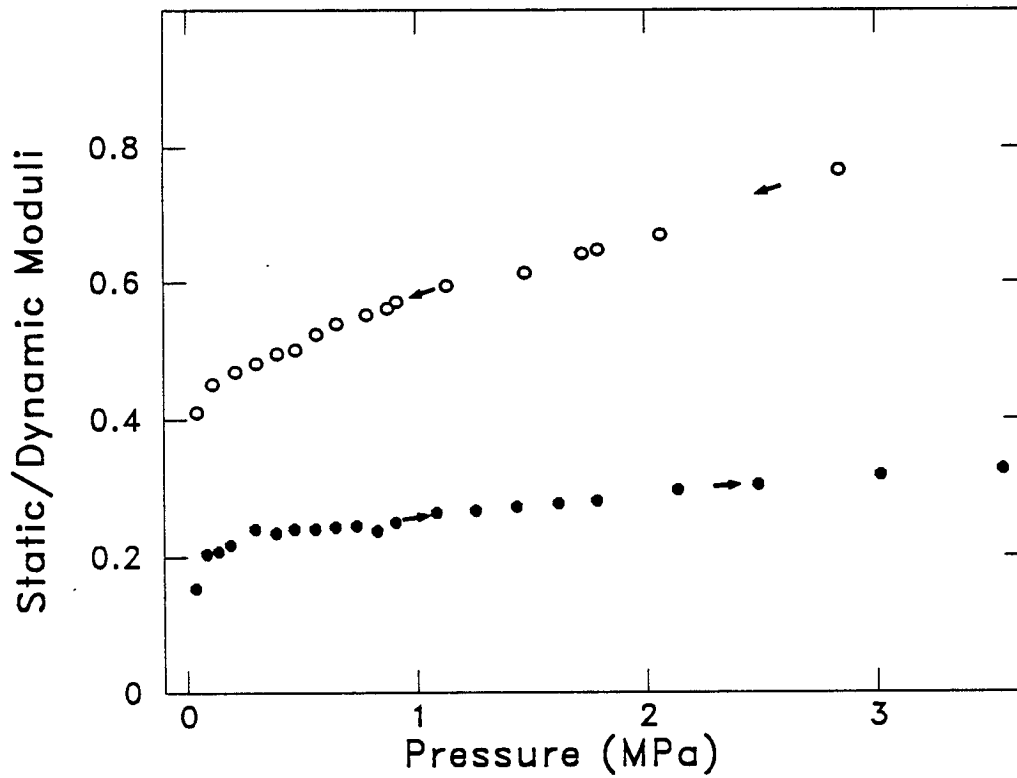


Figure 4.9: Ratio of static to dynamic moduli versus pressure during loading and unloading. The increase of the ratio with pressure during loading suggests that the ratio of elastic to inelastic deformation increases with pressure.

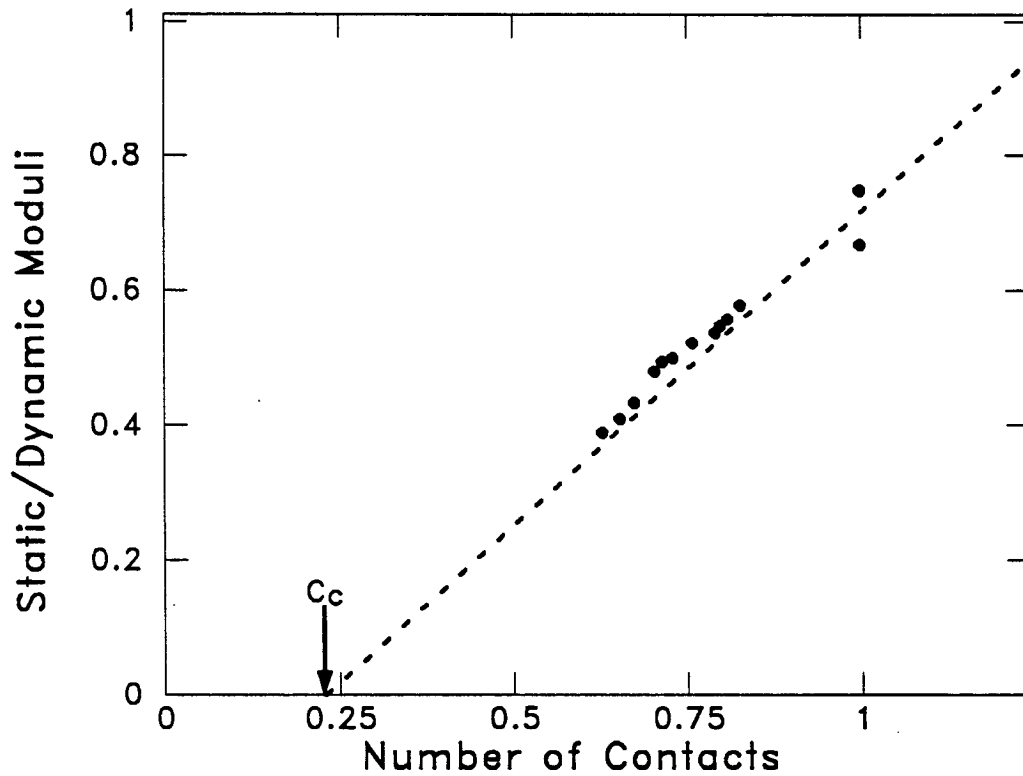


Figure 4.10: Ratio of static to dynamic uniaxial strain moduli vs. number of contacts (normalized to the number of contact at 3.5 MPa) during unloading. The ratio is found to vary approximately linearly with number of contacts. The ratio is expected to go to 1 when all the grain contacts are deforming contacts.

where c_{max} is the number of contact neighbors of the material, c is the number of deforming contacts, and c_c is the number of deforming contacts at threshold. This gives for the ratio of static to dynamic moduli:

$$\frac{M_s}{M_d} = \left(\frac{c - c_c}{c_{max} - c_c} \right) \quad (4.32)$$

This relationship illustrates that at high pressure, when number of contacts is equal to number of contact neighbors or similarly when all the contacts are deforming, c is equal to c_{max} , and the ratio of static to dynamic moduli goes to 1. Inversely, at low stress, the number of deforming contacts is much smaller than the number of contact neighbors and the ratio of static to dynamic moduli is low.

4.6 Conclusion

We have shown experimentally that in granular materials, (1) the average number of contacts per grain is varying with pressure and variation of the number of deforming contacts may be partly responsible for the departure of moduli from a cube root dependency on pressure. (2) Static moduli are strongly dependent on the number of contacts following an Effective Medium Theory relationship where elastic moduli increase linearly with increasing number of contacts above a certain percolation threshold. (3) Dynamic moduli are rather insensitive to variations of number of contacts once a connected path of deforming contacts is created. (4) The discrepancy between static and dynamic elastic moduli may be related to a different sensitivity of static and dynamic moduli on the number of contacts.

References

- Batchelor, G. K., and O'Brien, R. W., 1977 Thermal and electrical conduction through a granular material: Proc. R. Soc. Lond. A, **355**, 313-333.
- Benguini L., 1984, Experimental study of the elastic properties of a percolating system: Phys. Rev. Lett., **53** , 2028-2030.
- Bergman, D. J., and Y. Kantor 1984, Critical properties of an elastic fractal, Phys. Rev. Lett., **53**, 511-514
- Bergman, D. J., 1985, Elastic moduli near percolation: universal ratio and critical exponent: Phys. Rev. B, **31**, 1696-1698.
- Bernal, J. D., and Mason, J., 1960, Co-ordination of randomly packed spheres: Nature, **188**, 910-911.
- Birch, F., 1960, The velocity of compressional waves in rocks to 10 kilobars, 1: J. Geophys. Res., **65**, 1083-1102.
- Brandt, H., 1955, A study of the speed of sound in porous granular media: J. Appl. Mech. ASME, **22**, 479-485.
- Cattaneo C., 1938, Sul contatto di due corpi elastici: distribuzione locale degli sforzi. Accademia dei leici, Rendiconti, **27**, ser. 6, 342-348, 434-436, 474-478.
- Cheng, C. H., and Johnston, D. H., 1981, Dynamic and static moduli: Geophys. Res. Lett., **8**, 39-42.
- De Gennes, P. G., 1976, On a relation between percolation theory and the elasticity of gels: J. Phys., Lett., **37** , L1-L2.
- Deptuck, D., Harrison, J. P., and Zawadski, P., 1985, Measurement of elasticity and conductivity of a three-dimensional percolation system: Phys. Rev. Lett, **54**, 913-916.
- Dereziewicz, H., 1958, Stress-strain relations for a simple model of a granular medium: J. Appl. Mech, **25**, 402-405.
- Digby, P. J., 1981, The effective elastic moduli of porous granular rocks: J. Appl. Mech, **48**, 803-808.
- Duffy, J. and Mindlin, R. D., 1957, Stress-strain relations and vibrations of a granular medium: J. Appl. Mech., **24** 585-593.

- Feng, S., and Sen, P. N., 1984, Percolation on elastic networks: new exponent and threshold: *Phys. Rev. Lett.*, **52**, 216-219.
- Feng, S., Sen, P. N., Halperin, B. I., and Lobb, C. J., 1984, Percolation on two-dimensional elastic networks with rotationally invariant bond-bending forces: *Phys. Rev. B*, **30**, 5386-5389.
- Feng, S., 1985, Percolation properties of granular elastic networks in two dimensions: *Phys. Rev. B*, **32**, 510-513.
- Feng, S., Thorpe, M. F., and Garboczi, E., 1985, Effective medium theory of percolation on central-force elastic networks: *Phys. Rev. B*, **31**, 276-280.
- Fessler, H., and E. Ollerton, 1957, Contact stresses in toroids under radial loads: *Brit. J. Appl. Mech.*, **29**, 387.
- Garboczi, E. J., and Thorpe, M. F., 1985, Effective medium theory of percolation on central elastic networks. II. Further results: *Phys. Rev. B*, **31**, 7276-7281.
- Gassmann, F., 1951, Elastic waves through a packing of spheres: *Geophysics*, **16**, 673-685.
- He, H., and Thorpe, M. F., 1985, Elastic properties of glasses: *Phys. Rev. Lett.*, **54**, 2107-2110.
- Johnson, K. L., 1955, Surface interaction between elastically loaded bodies under tangential forces: *Proc. R. Soc. Lond. A*, **320**, 531-548.
- Kantor, Y., and Webman, I., 1984, Elastic properties of random percolating systems: *Phys. Rev. Lett.*, **52**, 1891-1894.
- King, M. S., 1969, Static and dynamic elastic moduli of rocks under pressure, 11th Proc. U.S. Symp. Rock Mech., 329-351.
- Kirkpatrick, S., 1973, Percolation and conduction, *Rev. Mod. Phys.*, **45**, 574-588.
- Lafait, J., and D. B. Tanner, 1989, Proceedings of the second international conference on electrical, transport, and optical properties of inhomogeneous media, North Holland.
- Landau, L. D., and Lifshitz, E. M., 1959, Theory of elasticity, Perg. Press.

- Maliaris A., and Turner, D. T., 1971, Influence of particle size on the electrical resistivity of compacted mixtures of polymeric and metallic powders: *J. Appl. Phys.*, **42**, 614-618.
- Marion, D. P., and Nur A., 1989, Percolation of electrical and elastic properties of granular materials at the transition from a suspension to a loose packing: *Physica A*, **157**, 575-579.
- Mindlin, R. D., 1949, Compliance of elastic bodies in contact, *Trans. ASME*, **71**, A-259.
- Murphy, W., 1982, Effect of microstructure and pore fluid on the acoustic properties of granular sedimentary materials: Ph.D. dissertation, Stanford Univ.
- Ottavi, H., Clerc, J., Giraud, G., Rouusenq, J., Guyon, E., and Mitescu, C. D., 1978, Electrical conductivity of a mixture of conductive and insulating spheres: an application of some percolation concepts: *J. Phys. C*, **11** 1311-1328.
- Phillips, J. C., 1979, Topology of covalent non-crystalline solids I: short-range order in chalcogenide alloys: *J. Non-Cryst. Solids*, **34**, 153-181.
- Powell, M. J., 1979, Site percolation in randomly packed spheres: *Phys. Rev. B*, **20**, 4194-4198.
- Schwartz, L. M., Feng, S., Thorpe, M. F., and Sen, P. N., 1985, Behavior of depleted elastic networks: Comparison of effective-medium and numerical calculations: *Phys. Rev. B*, **32**, 4607-4617.
- Simmons, G., and Brace, W. F., 1965, Comparison of static and dynamic measurements of compressibility of rocks, *J. Phys. Res.*, **70**, 5649-5667.
- Smith, D. T., 1974, Acoustic and mechanical loading of marine sediments, *Physics of sound in marine sediments*, Plenum New York.
- Smith, W. O., Foote, P. D., and Busang P. F., 1929, Packing of homogeneous spheres: *Phys. Rev.*, **34**, 1271-1274.
- Thorpe, M. F., 1983, Continuous deformations in random networks: *J. Non-Cryst. Solids*, **57** 355-370.
- Walton, K., 1975, The elastic moduli of model sediments: *Geophys. J. R. Astr. Soc.*, **43**, 293-306.

Walton, K., 1978, The oblique compression of two elastic spheres: *J. Mech. Phys. Solids*, **26**, 139-150.

Walton, K., 1987, The effective elastic moduli of a random packing of spheres: *J. Mech. Phys. Solids*, **35**, 213-226.

Winkler, K. W., 1983, Contact stiffness in granular porous materials: comparison between theory and experiments: *Geoph. Res. Let.*, **10**, 1073-1076.

Chapter 5

Effect of pore-filling material on velocity in rocks

Abstract

A method is proposed to estimate the dependence of P and S velocities in rocks on elastic properties of the pore-filling material. The method differs from Gassmann's relations in that it can account for saturating materials that feature non-zero shear stiffness. The method results are in good agreement with experimental data and Gassmann's relations when tested for prediction of velocity in water saturated rocks from velocity measured on dry rocks. The method is also used to predict the temperature dependence of velocity 1) in frozen rocks at the ice-water phase transition, and 2) in heavy hydrocarbon saturated rocks at the hydrocarbon solid-liquid phase transition.

5.1 Introduction

One of the main factors which controls compressional and shear velocities in porous rocks is the type of pore-filling material and more specifically, the compressibility of this material. There are situations in rocks where the pore-filling material may undergo a phase transition due to changes in pressure and/or temperature. In permafrost soils, P and S velocities decrease with increasing depth due to increasing temperature gradient that causes ice to melt within the pore space (Anderson and Morgenstern, 1973; Timur, 1968). Similarly in heavy hydrocarbon saturated rocks, P and S velocities decrease rapidly with increasing temperature in the vicinity of the hydrocarbon melting point (Tosaya et al., 1987; Wang, 1988). In order to predict such changes of velocity with temperature it is important to be able to quantify the effect of bulk and shear moduli of the pore-filling material on elastic moduli of the rock. The Biot-Gassmann relationships (Biot, 1961; Gassmann, 1951) have been commonly used to predict P and S velocities of a liquid saturated rock given the dry rock velocities, the elastic moduli of the liquid, and the elastic moduli of the rock forming minerals. However, Biot-Gassmann's relations are inadequate to describe the influence of a pore-filling material which features non-zero shear stiffness such as ice or solid hydrocarbons.

In this chapter we present a method to quantify the effect of pore-filling elastic moduli on P and S velocities in rocks. The first section describes the method, its assumptions and the domains of its application. In the second section the method is tested against laboratory velocity measurements for the determination of velocity in water saturated rocks using the knowledge of velocity measured on the dry rock. In the third and fourth sections the method is applied to predictions of temperature dependence of velocity in rocks: 1) at permafrost temperatures and 2) saturated with heavy hydrocarbons and the method results are compared with laboratory P and S velocity data.

5.2 The Bound Averaging Method

In rocks, the dependence of elastic properties on porosity is not a simple relationship as was shown in Chapters 2 and 3. It depends on mineralogy, pore geometry, clay content, etc. In order to estimate the possible range of variability of elastic moduli in rocks, theoretical bounds have been derived. Voigt (1928) introduced the concept of the extreme upper bound for elastic moduli by considering the case of elastic deformation of a two phase composite in which strain would be equal throughout the material. Given the rock porosity, ϕ , and the elastic moduli of the mineral and fluid phase, M_m and M_f respectively, the upper bound, M^+ , for elastic moduli can be calculated from the relation:

$$M^+ = (1 - \phi)M_m + \phi M_f \quad (5.1)$$

Reuss (1929) treated the case of a composite in which stress is distributed equally throughout the material and derived a lower bound, M^- , for elastic moduli of two phase composite:

$$M^- = \left[\frac{(1 - \phi)}{M_m} + \frac{\phi}{M_f} \right]^{-1} \quad (5.2)$$

Hashin and Shtrikman (1963) narrowed the Voigt and Reuss bounds using a variational principle for stress and strain. Hashin-Shtrikman bounds, $M^{(HS)}$ were found to be the best possible bounds for bulk modulus given the porosity and elastic moduli of the mineral and fluid phases. Results are for a rock of porosity ϕ , and fluid and mineral elastic moduli, M_f and M_m , respectively:

$$\frac{M^{(HS)} - M_f}{M_m - M_f} = (1 - \phi) \left(1 + \frac{\phi(M_m - M_f)}{M_f + F} \right)^{-1} \quad (5.3)$$

where F is related to the rock bulk and shear moduli, K and G respectively using:

$$F = \frac{4}{3}G_m \text{ for } K^{(HS^+)} \quad (5.4)$$

$$F = \frac{4}{3}G_f \text{ for } K^{(HS^-)} \quad (5.5)$$

$$F = \frac{G_m(9K_m + 8G_m)}{6(K_m + 2G_m)} \text{ for } G^{(HS^+)} \quad (5.6)$$

$$F = \frac{G_l(9K_f + 8G_f)}{6(K_f + 2G_f)} \text{ for } G^{(HS^-)} \quad (5.7)$$

Figure 5.1 shows the Voigt-Reuss (VR) bounds and Hashin-Shtrikman (HS) bounds for a rock in which the mineral phase is composed of quartz ($K = 38 \text{ GPa}$, $G = 44 \text{ GPa}$) and the pore space is saturated with water ($K = 2.2 \text{ GPa}$, $G = 0 \text{ GPa}$). We can notice from this figure that upper and lower bounds are too far apart to be of practical use for direct determination of elastic moduli of the rock given its porosity and elastic moduli of mineral and fluid phases. Yet, for a given porosity, the value of modulus relative its upper and lower bounds carries information regarding the stiffness of the pore space. Closeness to the upper bound may correspond to a rock with stiff pores or vuggy porosity whereas, proximity to the lower bound may be representative of a rock whose porosity is primarily in the form of cracks or uncemented grain contacts. Thus, we can conceive to describe elastic moduli, M , of a rock as a weighted arithmetic average between upper and lower bounds, M^+ and M^- respectively, using the following relation:

$$M = M^- + w(M^+ - M^-) \quad (5.8)$$

where the weighting average, w , that takes values between 0 and 1, is a measure of pore stiffness.

For a given rock, upper and lower bounds will be dependent on the fluid elastic moduli. However, it will be assumed here that the type of fluid filling the pore space does not affect the rigidity of the pore structure. Thus, the weighting factor, w , will be unaffected by the fluid type and is assumed to be invariant for a given rock. Hence one can estimate the elastic moduli, M_1 , of a rock saturated with a fluid of type 1 from the measured elastic moduli, M_0 , of the same rock saturated with a fluid of

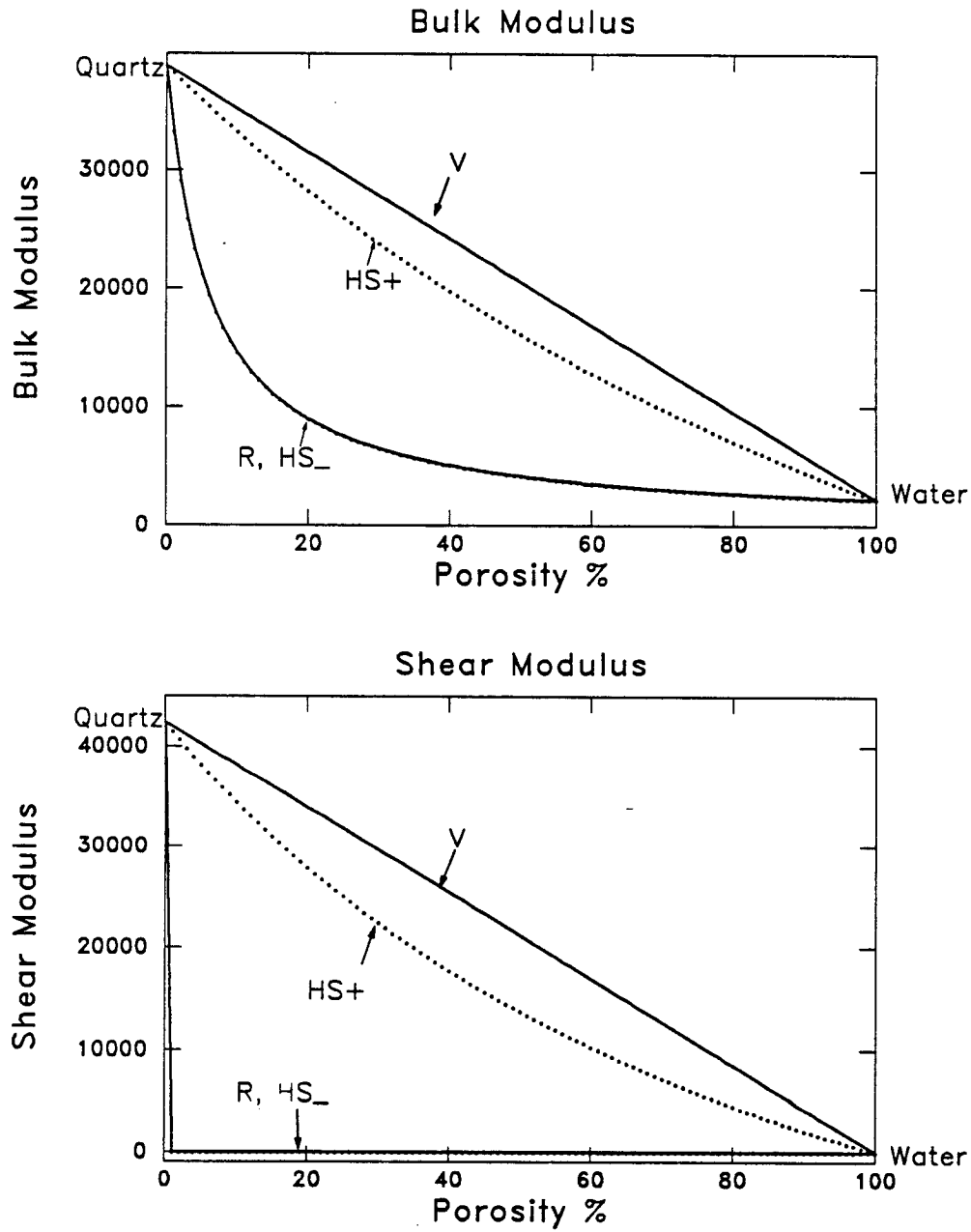


Figure 5.1: Veugt (V), Reuss (R) and Hashin-Shtrikman upper and lower bounds, (HS_+) and (HS_-) respectively, for a Quartz-Water composite. Note that upper and lower bounds are too far apart to be of practical use for determination of elastic moduli from porosity.

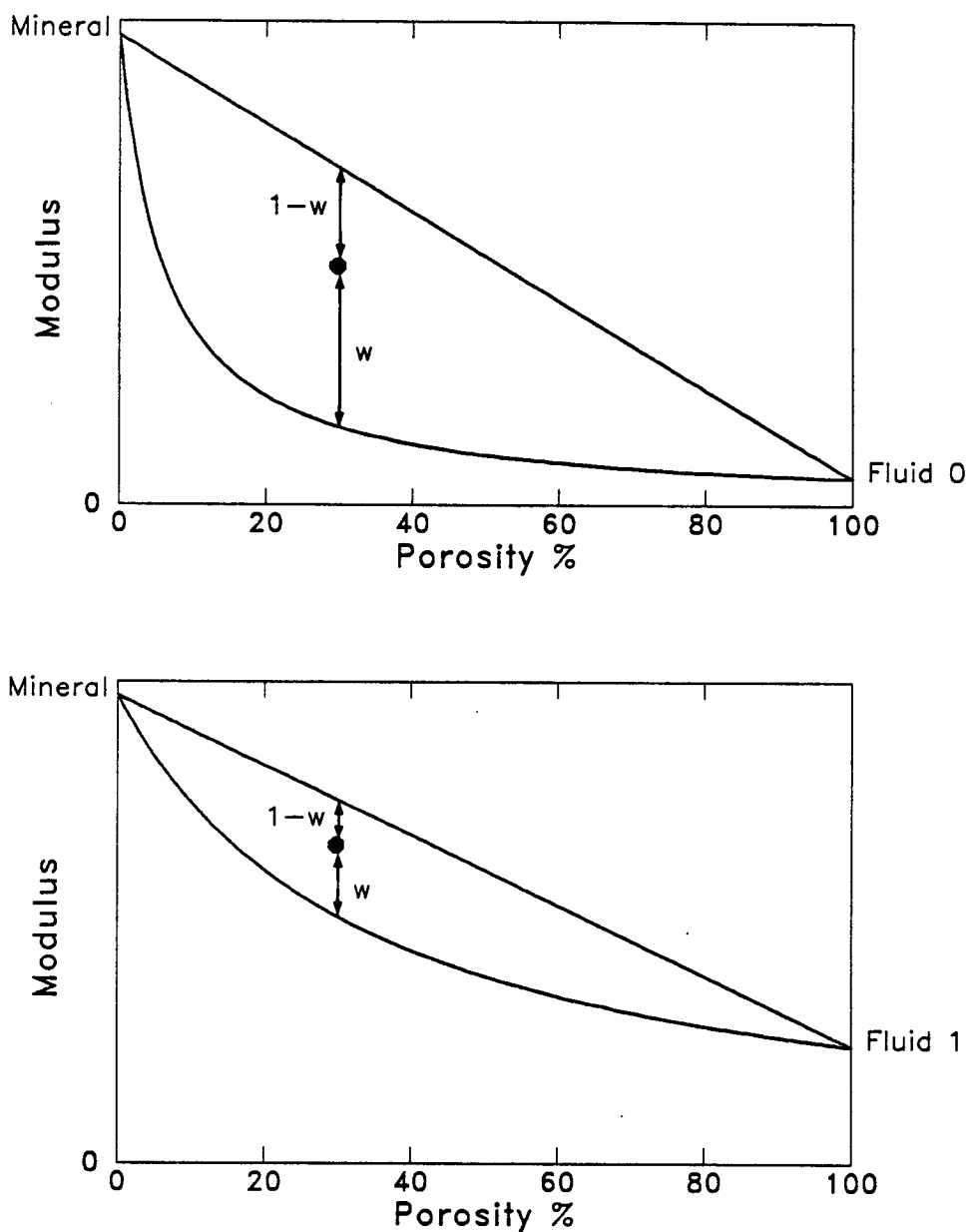


Figure 5.2: In the Bound Averaging Method, the relative value of modulus (●) with respect to upper and lower bounds does not depend on the type of fluid filling the pore space. Hence the weighting factor, w that relates modulus to its upper and lower bound is invariant for a given rock at a given porosity. Elastic moduli of a rock saturated with "Fluid 1" may therefore be determined from elastic moduli of the same rock saturated with "Fluid 0", given the rock forming mineral moduli, and Fluid 0 and Fluid 1 elastic moduli.

type 0, as illustrated in Figure 5.2. Equation 5.8 can be written for the two types of pore-filling fluid as

$$M_0 = M_0^- + w(M_0^+ - M_0^-) \quad (5.9)$$

$$M_1 = M_1^- + w(M_1^+ - M_1^-) \quad (5.10)$$

where M_0 is the measured modulus, M_1 is the modulus to be determined, and M_0^+ , M_0^- , M_1^+ , M_1^- are calculated upper and lower bounds for given mineral elastic moduli and elastic moduli of "fluid 0" and "fluid 1". Combining equations 5.9 and 5.10 allows for determination of M_1 from measured modulus M_0 and calculated bounds, M_0^+ , M_0^- , M_1^+ , and M_1^- :

$$M_1 = M_1^- + (M_0 - M_0^-) \left(\frac{M_1^+ - M_1^-}{M_0^+ - M_0^-} \right) \quad (5.11)$$

This Bound Averaging Method (BAM) is first tested using the Self-Consistent analytical solution for Spherical pores embedded in rock matrix (SCS) as a starting model. According to self consistent treatment, elastic moduli of a rock with spherical pores are related to the elastic moduli of the rock forming minerals and pore-filling fluid, M_m and M_f , respectively by the relations (after Watt, 1976)

$$\frac{M - M_f}{M_m - M_f} = (1 - \phi) \left(1 + \frac{\phi(M_m - M_f)}{M_f + F} \right)^{-1} \quad (5.12)$$

where F is related to the rock bulk and shear moduli, K and G respectively using

$$F = \frac{4}{3}G \quad (5.13)$$

when M represents bulk modulus, K , and

$$F = \frac{G(9K + 8G)}{6(K + 2G)} \quad (5.14)$$

when M represents shear modulus, G .

Equations 5.12 to 5.14 are first used to estimate bulk and shear moduli of a water saturated rock as a function of porosity. This relationship is then used as the starting point to test our method. The main objective is to use BAM to estimate elastic

moduli of frozen rocks from SCS elastic moduli of water saturated rocks and compare BAM results with the self-consistent prediction for frozen rocks.

We also investigate how the method results depend on the type of bounds used by carrying calculations with VR and HS bounds respectively.

SCS calculations were carried out for a water saturated quartzite at room temperature using the following input parameters: $K_m = 38 \text{ GPa}$, $G_m = 44 \text{ GPa}$, $K_f = 2.2 \text{ GPa}$, $G_f = 0.0 \text{ GPa}$. Elastic moduli of frozen quartzite were predicted from BAM and SCS using the following parameters for ice: $K_f = 11.0 \text{ GPa}$, $G_f = 4.4 \text{ GPa}$. Results are shown in Figure 5.3. Good agreement is found between BAM predictions and SCS solution for elastic moduli of a frozen quartzite with best results for porosity ranging between 0 and 40 %. Note also that the two bounding methods, i.e., HS and VR, give very similar results for porosities less than 40 %. For porosities greater than 40 %, the use of HS bounds produces a better match of the SCS relation than VR bounds.

5.3 From dry to saturated rock

In this section BAM and Gassmann's relations (1951) are compared with laboratory data of P and S velocity measurements on clay free sandstones in dry and saturated conditions (data from Han et al., 1986). In Gassmann's relations saturated elastic moduli may be derived from dry moduli using the relations:

$$K_{sat} = K_{dry} + \frac{(1 - \frac{M_{dry}}{M_m})^2}{\frac{\phi}{M_f} + \frac{(1-\phi)}{M_m} - \frac{M_{dry}}{M_m^2}} \quad (5.15)$$

$$G_{sat} = G_{dry} \quad (5.16)$$

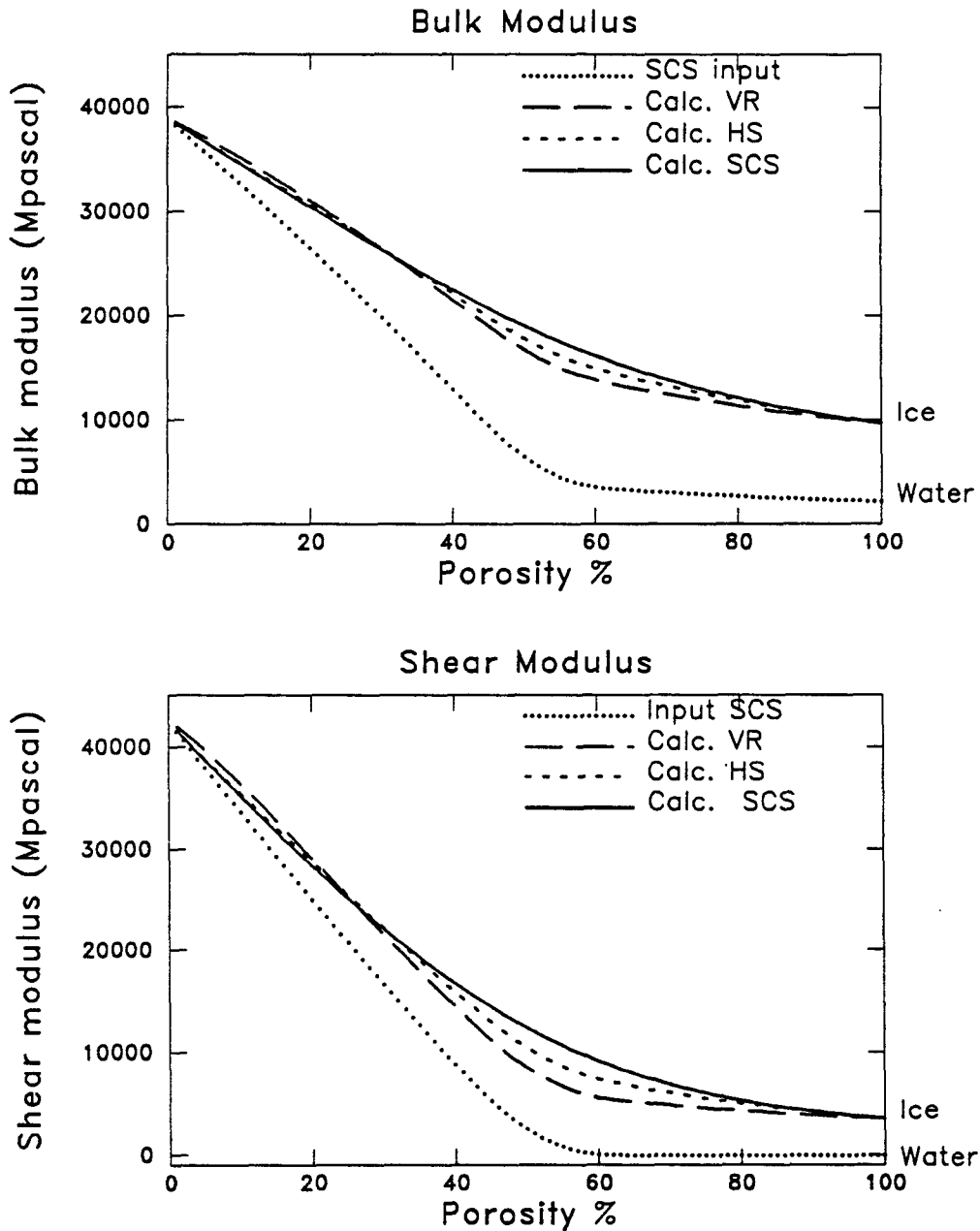


Figure 5.3: Sensitivity of BAM to type of bounds (VR or HS) and comparison between BAM and SCS for determination of elastic moduli of frozen rocks given elastic moduli of the water saturated rock (SCS input for a "water-quartz aggregate"). Best agreement between SCS and BAM for "ice-quartz aggregate" is obtained using HS bounds. However, for porosity less than 40 % BAM exhibits little sensitivity to the type of bound used in calculations.

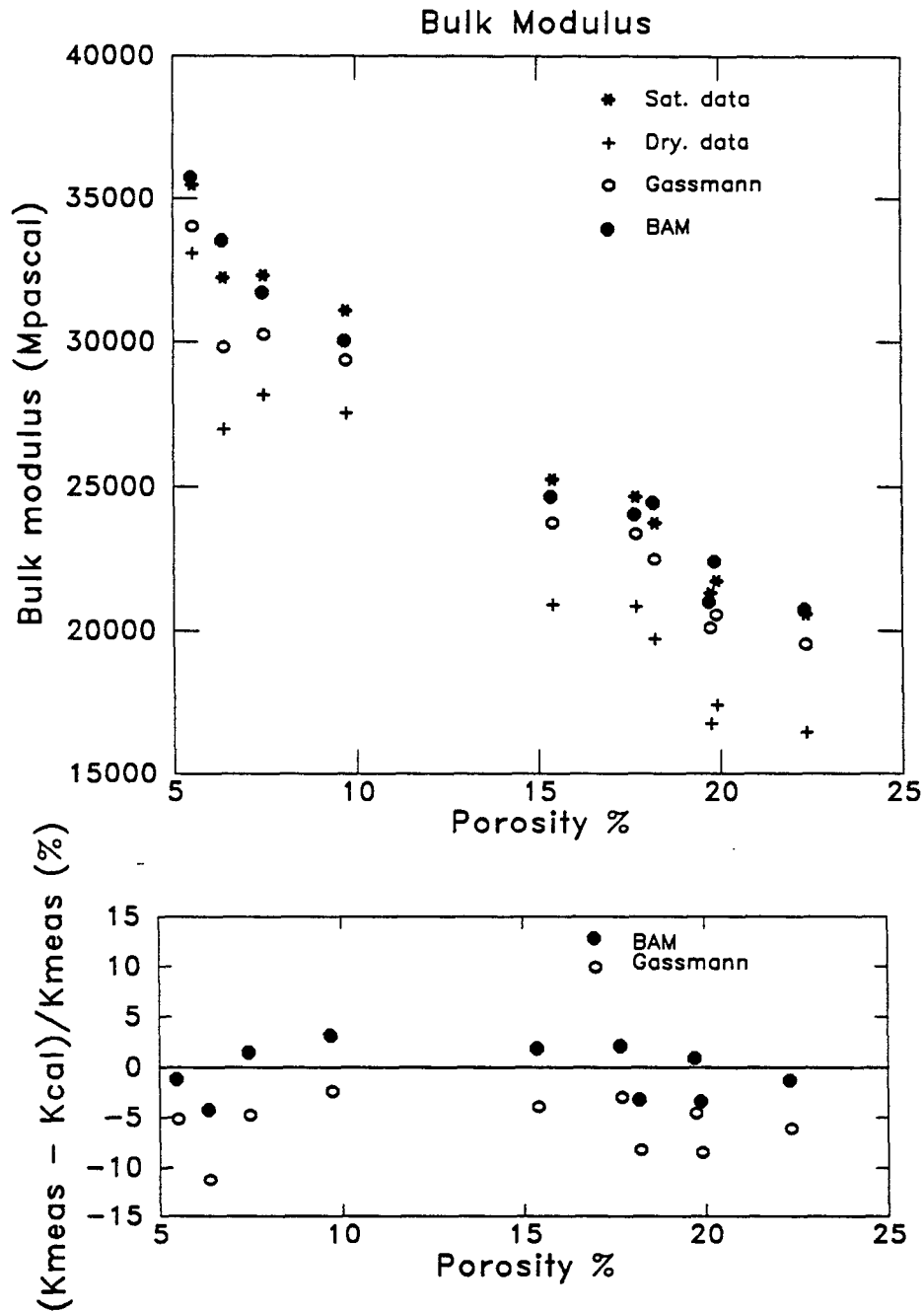


Figure 5.4: Prediction of water saturated bulk modulus in 10 different clay-free Sandstones from moduli measured in dry conditions (+). Comparison between experimental data (*), BAM predictions (●), and Gassmann's predictions (○). BAM gives an overall good estimate of saturated moduli from dry ones whereas Gassmann's predictions generally underestimates values of saturated moduli. (data from Han et al., 1986)

Using BAM, with VR bounds, the relationship between dry and saturated moduli can be written as follows:

$$K_{sat} = K_{dry} + \frac{\left(1 - \frac{M_{dry}}{M_m}\right) - \phi \frac{M_{dry}}{M_m} \left(1 - \frac{M_f}{M_m}\right)}{\frac{\phi}{M_f} + \frac{(1-\phi)}{M_m}} \quad (5.17)$$

$$G_{sat} = G_{dry} \quad (5.18)$$

Note that Gassmann's relationships and BAM require the exact same input parameters for calculation of saturated moduli from dry moduli, i.e., porosity, dry moduli, fluid moduli, and mineral moduli. In Figure 5.4a, dry (+) and saturated (*) data for bulk modulus are shown versus porosity for 12 different clay-free sandstones. Gassmann's predictions are marked as (o), and BAM predictions are marked as (•). In Figure 5.4b, the departure between measured and calculated moduli (in %) shows the good agreement between BAM predictions and data. Saturated modulus is predicted here within $\pm 5\%$ uncertainty, whereas Gassmann's relations generally underestimate bulk stiffness (from 2 to 12 %).

In Figure 5.5, BAM is applied to the calculation of water saturated velocity in Westerley granite (Data from Nur and Simmons, 1969) given dry velocity versus pressure. Very good agreement is obtained between experimental data and BAM predictions over the whole pressure range. At low stress, we find that velocity data lie in between the HS upper and lower bound. Low velocity values measured at low stress are attributed to the presence of compliant microcracks that represent 30 % of the overall porosity. Upon closure of these cracks, velocity increases asymptotically toward HS upper bound suggesting that most of the remaining porosity is in the form of very stiff pores.

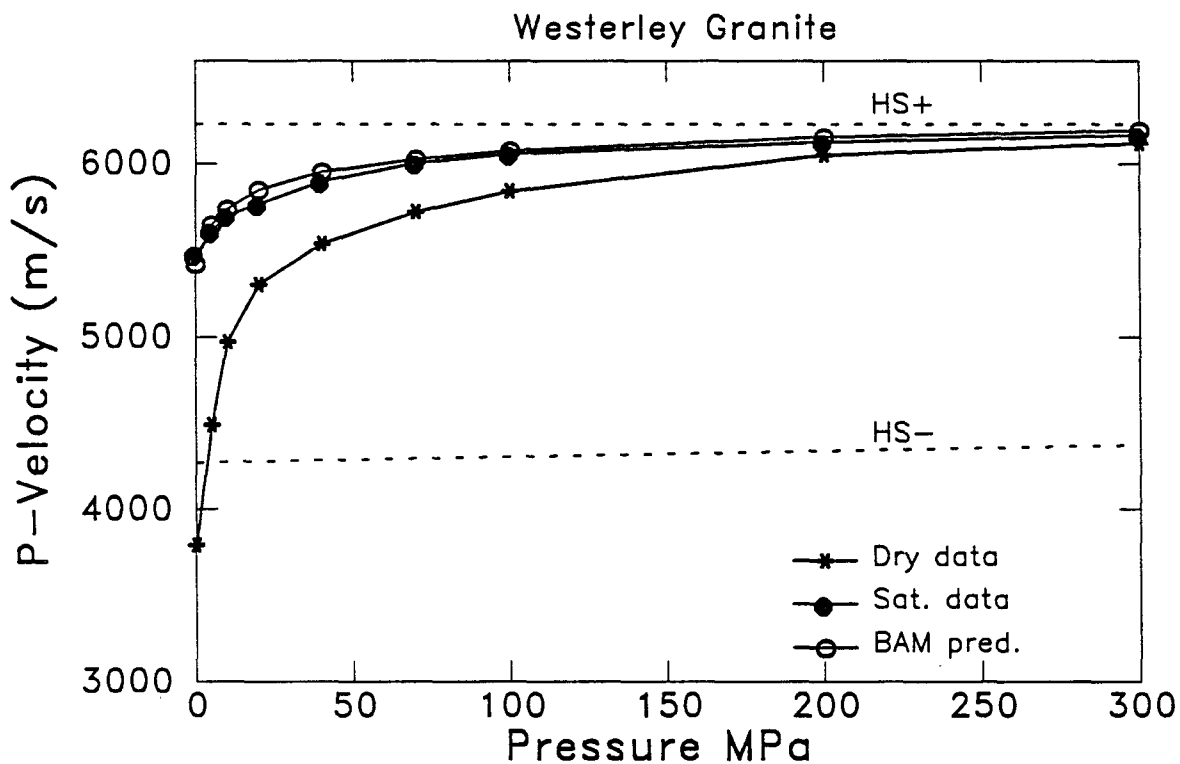


Figure 5.5: P-Velocity versus Pressure in Westerley granite in dry and saturated conditions (Data from Nur and Simmons, 1969). Velocity in saturated conditions is estimated from dry measurements using BAM (\ominus). At low stress saturated velocity is located in between HS upper and lower bounds due to presence of cracks. With increasing stress, cracks are closing and velocity approaches HS upper bound.

5.4 Velocity in water saturated rocks at permafrost temperatures

Another possible application of BAM is the prediction of temperature dependence of P and S velocities in rocks at permafrost temperature. When water undergoes a phase transition from solid to liquid, both P and S velocities exhibit a sharp drop in velocity (Bogorodskii, 1964; Bass et al., 1957). Shear modulus is found to decrease from 2.45 GPa at 0 °C to zero above 0 °C. Similarly, bulk modulus decreases from 7.3 GPa at 0°C to 2.2 GPa above 0°C (After Bogorodskii, 1964). In water saturated rocks, measurements of velocity vs. temperature show the same type of behavior, i.e., a rapid decrease in velocity when temperature increases above 0°C (Timur, 1968; King, 1983). We propose here to apply BAM to predict the temperature dependence of velocity in frozen rocks. We show in Figures 5.6, and 5.7, bulk and shear moduli data obtained from P and S velocity measurements in two water saturated rocks: Boise Sandstone, and Spergen limestone (after Toksoz et al., 1979). Velocities were measured at room temperature and at -40°C . We also show for comparison, bulk and shear moduli data in the water-ice system (data are from Bogorodskii, 1964) from room temperature to -15°C . Data were extrapolated to -40°C ., based on the linear increase of velocity with temperature observed in ice by Bogorodskii (1964) and Bass et al. (1957). Given the P and S velocity measurements at room temperature, and velocity of the water-ice system, we estimate the temperature dependence of bulk and shear moduli in these two rocks using input parameters listed in table 5.1. We find that the agreement between our predicted moduli and the measured moduli at -40°C is generally very good (within 4 %) for both bulk and shear moduli.

In Figure 5.8, BAM is used to estimate the bulk and shear moduli of a frozen diabase (data from Takeuchi and Simmons, 1973) versus pressure using velocity versus pressure measurements at room temperature. We find reasonable agreement between predicted and measured moduli for both bulk and shear moduli at high pressure.

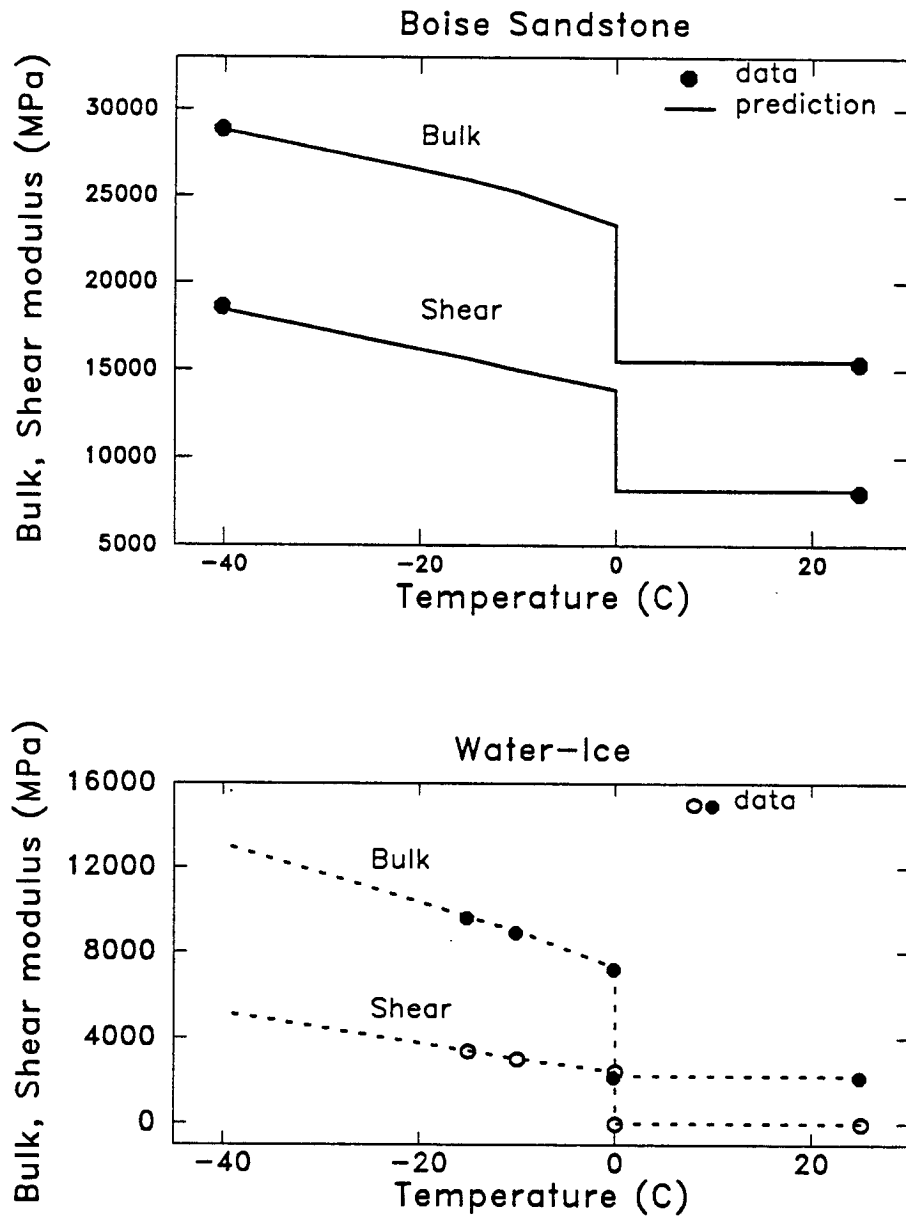


Figure 5.6: Bulk and Shear moduli in water saturated Boise Sandstone versus temperature. P and S velocity data (Toksoz et al., 1979) were measured on saturated samples at room temperature and -40°C . Temperature dependence of bulk and shear moduli is predicted from moduli measured at room temperature given the temperature dependence of elastic moduli in water-ice system. Data for Ice-Water system are from Bogorodskii (1964). Data at -40°C are well predicted using BAM.

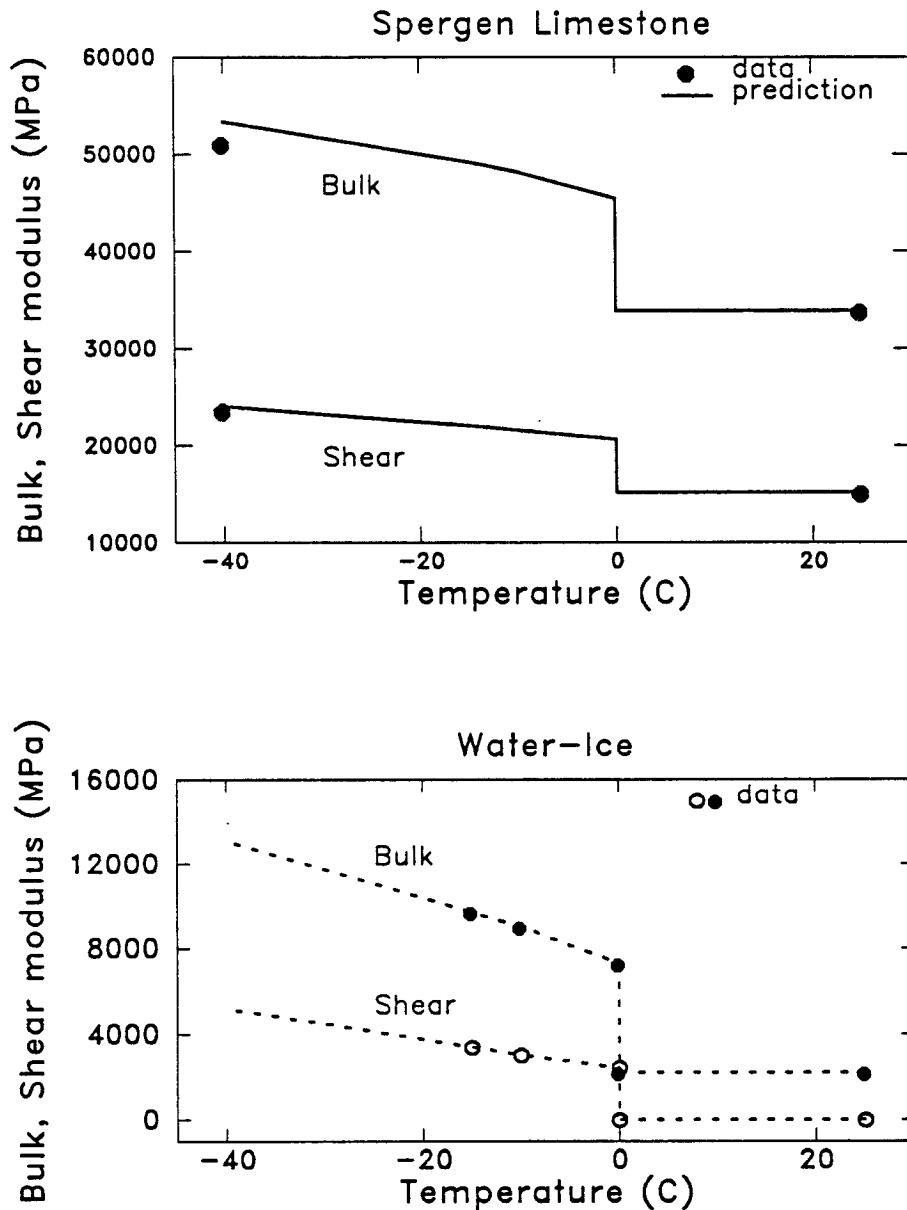


Figure 5.7: Bulk and Shear moduli in water saturated Spergen Limestone versus temperature. P and S velocity data (Toksoz et al., 1979) were measured on saturated samples at room temperature and -40°C . Temperature dependence of bulk and shear moduli is predicted from moduli measured at room temperature given the temperature dependence of elastic moduli in water-ice system. Data for Ice-Water system are from Bogorodskii (1964). Data at -40°C are well predicted using BAM.

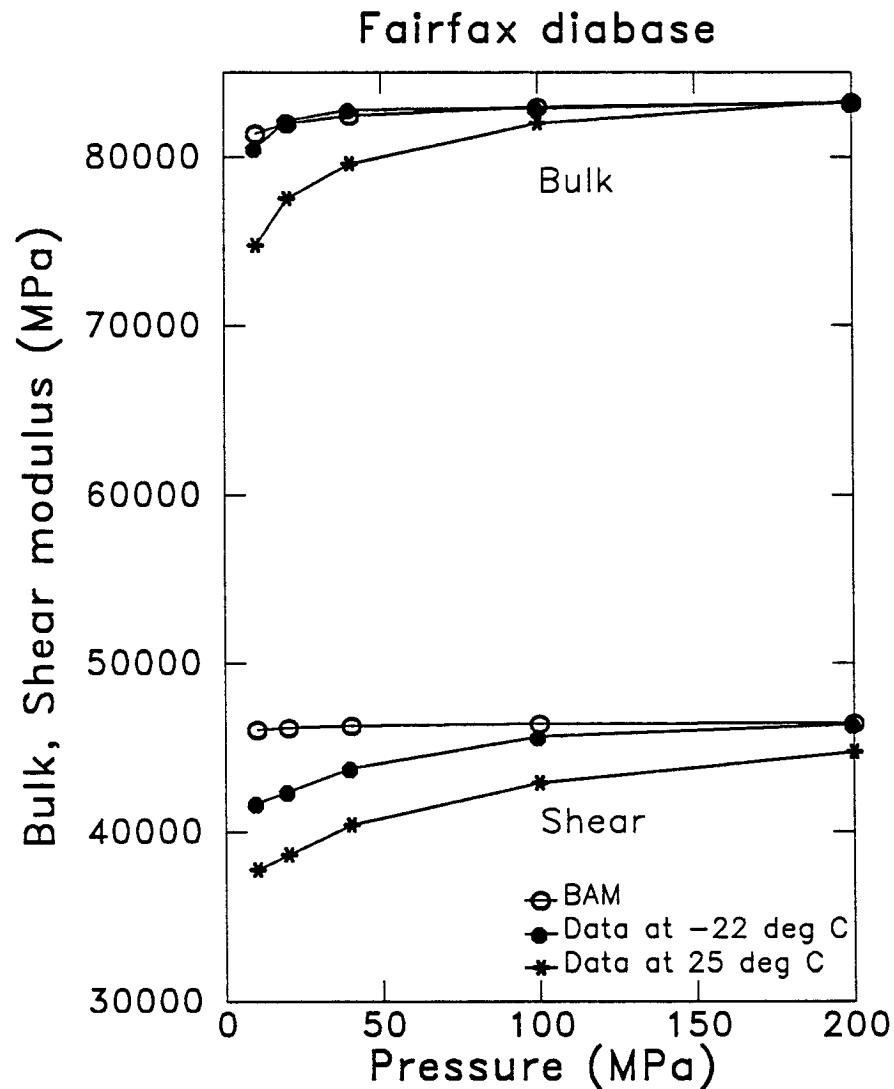


Figure 5.8: Bulk and Shear moduli of a low porosity diabase versus pressure at room temperature (*) and -22°C (●). Data are from Takeuchi and Simmons, 1973). The BAM predicted curve (○) for moduli vs. pressure at -22°C is calculated from moduli vs. pressure measured at room temperature. Good agreement between measured and predicted moduli is obtained at high stress. At low stress, the discrepancy which exists between predictions and measurements may be attributed to thermal expansion of ice and its weakening effect on the skeleton frame.

However, at lower pressure the lower shear modulus observed in experimental data is not reproduced with BAM. At this point it is important to recall the main assumption of BAM: The pore stiffness is unaffected by the type of pore filling fluid (i.e.; w remains unchanged). In the case of ice-water system, the coefficient of thermal expansion of ice may be responsible for crack opening upon freezing if: 1) the sample is undrained, or 2) cooling is not slow enough to let the fluid pressure equilibrate. This would decrease pore stiffness and consequently lower w upon freezing.

5.5 Velocity vs. temperature in Hydrocarbon saturated rocks

P and S velocities in hydrocarbon saturated rocks has been extensively studied in recent years (Tosaya et al, 1987; Wang and Nur; 1988, Wang, 1988). In heavy oils or tar, P and S velocities decrease drastically upon increase in temperature due to a transition of the hydrocarbon from a solid to liquid state and a decrease of hydrocarbon viscosity with temperature. In Figure 5.9, P-velocity data measured on a wax saturated sandstone (After Wang; 1988, Chapter 5) show a sharp decrease of velocity (20 %) at the vicinity of wax melting point (60°C). Using dry velocity measurements and mineral and hydrocarbon properties moduli we estimate a P-velocity vs. temperature curve for Massillon Light sandstone. Using BAM, we find a good qualitative agreement between measured and calculated velocity with a 16 % decrease in P-velocity near the wax melting point due to a decrease of both bulk and shear moduli at the phase transition from solid to liquid wax. The discrepancy between measured and calculated velocity could be attributed to 1) thermal expansion of wax and its effect on the stiffness of the rock skeleton frame and 2) high viscosity of wax below 30°C and its effect on effective shear modulus.

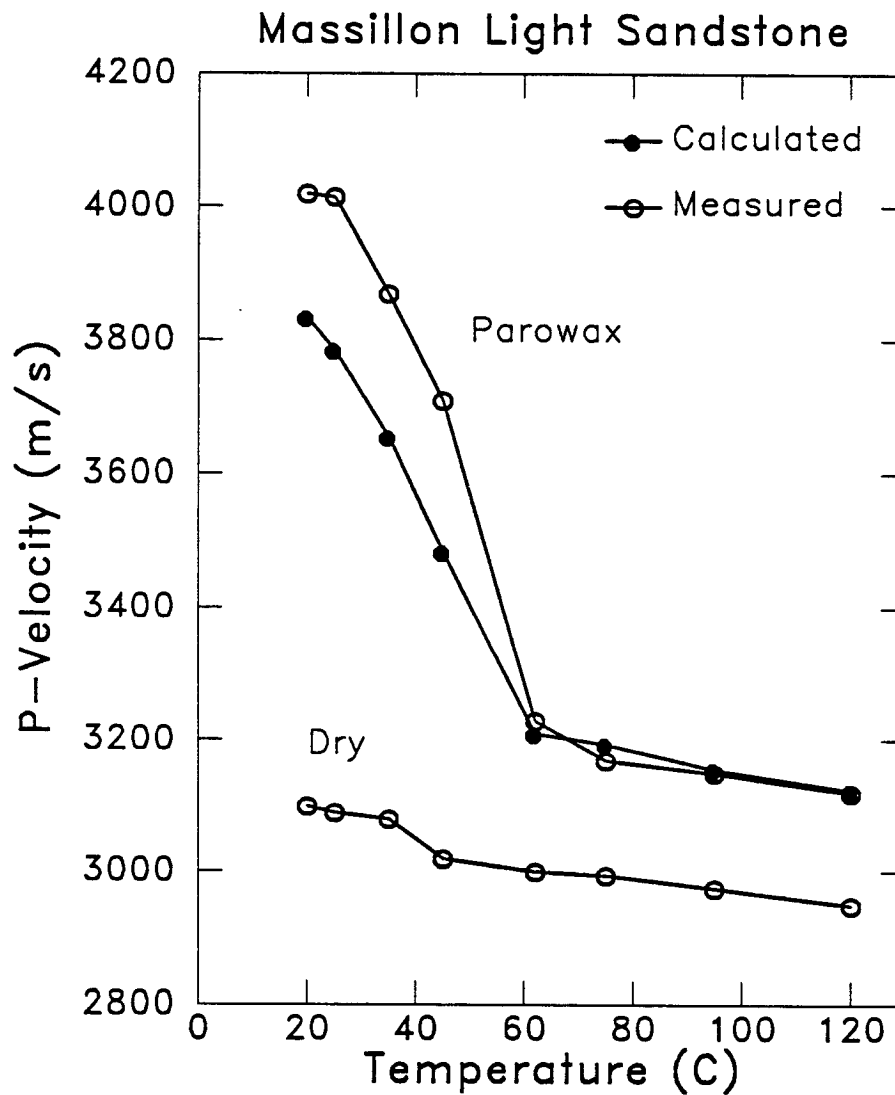


Figure 5.9: Compressional velocity in Massillon Light sandstone saturated with parowax versus temperature. Velocity measurements in dry and wax saturated (o) conditions are from Wang (1988). BAM prediction (●) for velocity versus temperature in a wax saturated rock is obtained from velocity measurements in dry conditions and temperature dependence of velocity in wax (see Wang, 1988). Discrepancy between BAM and measurements could be attributed to coefficient of thermal expansion of wax and effect of wax viscosity on shear modulus.

Table 5.1

<i>Rock type</i>	K_m (GPa)	G_m (GPa)	<i>Mineral Density</i> (g/cm ³)
Westerley Granite	59	34	2.65
Clay free Sandstone	38	44	2.65
Boise Sandstone	38	35	2.67
Spergen Limestone	78	35	2.70
Fairfax Diabase	83	46	3.00
Massillon Sandstone	38	42	2.65

5.6 Conclusion

We propose to describe the dependence of elastic properties of rocks on elastic moduli of their pore-filling material using a bound averaging method. In this method we assume as a first order approximation that the stiffness of the pores is unaffected by the type of fluid. This allows us to estimate elastic moduli of a rock saturated with a given pore-filling material (including materials with non zero shear stiffness) from the moduli measured on the same rock saturated with a different pore-filling material. The method is applied successfully to three systems: air-water, water-ice, and solid-liquid hydrocarbons. The method might also be used to estimate the effect of infilling material (clay, calcite..) on elastic moduli of porous rocks and sediments.

References

- Anderson, D. M., and Morgenstern, N. R., 1973, Physics, chemistry, and mechanics of frozen ground: A review, *in* Permafrost - the North American contribution to the 2nd Internat. Conf. Yakutsk: National Acad. Sci., 257-295.
- Bass R, D. Rossberg, and G. Ziegler, 1957, Die elastischen konstanten des eises, *Zeitschrift fur Physik* , **149**, 199-203.
- Biot , M.A., 1956, Theory of propagation of elastic waves in a fluid saturated porous solid, 1. Low-frequency range: *J. Acoust. Soc. Am.*, **28**, 168-178.
- Biot , M.A., 1956, Theory of propagation of elastic waves in a fluid saturated porous solid, 2. Higher frequency range: *J. Acoust. Soc. Am.* , **28**, 179-191.

- Bogorodskii, V. V., 1964, Elastic moduli of ice crystals, *Sov. Phys. Acoust.*, **10**, 124-126.
- Gassmann, F., 1951, Elastic waves through a packing of spheres: *Geophysics*, **16**, 673-685.
- Han, D., Nur, A., and Morgan, D., 1986, Effect of porosity and clay content on wave velocity in sandstones: *Geophysics*, **51**, 2093-2107.
- Hashin Z. and S. Shtrikman, 1963, A variational approach to the elastic behavior of multiphase materials, *J. Mech. Phys. Solid*, **11**, 127-140.
- King, M.S., 1984, The influence of clay-sized particles on seismic velocity for canadian arctic permafrost, *Can. J. Earth Sci.*, **21**, 19-24.
- Nur A., and G. Simmons, 1969, The effect of saturation on velocity in low porosity rocks, *Earth Planet. Sci. Lett*, **7**, 183-193.
- Reuss, A., 1929, Berechnung der fließgrenze von mischkristallen auf grund der plastizitätsbedingung für einkristalle: *Zeitschrift für Angewandte Mathematik and Mechanik*, **9**, 49-58.
- Takeuchi, S., and G. Simmons, 1973, Elasticity of water-saturated rocks as a function of temperature and pressure, *J. Geophys. Res.*, **78**, 3310-3320.
- Timur, A., 1968, Velocity of compressional waves of porous media at permafrost temperatures, *Geophysics*, **33**, 584-596.
- Toksoz, M.N., D.H. Johnston, and A. Timur, 1979, Attenuation of seismic waves in dry and saturated rocks: 1 Laboratory measurements, *Geophysics*, **44**, 681-690.
- Tosaya, C., A. Nur, D. Vo-Thanh, and G. Da Prat, 1987, Laboratory seismic method for remote monitoring of thermal EOR, *Soc. Pet. Eng. Res. Eng.*, **2**, 235-242.
- Voigt W. 1928, *Lehrbuch der Kristallphysik*, Teubner, Leipzig.
- Wang Z., 1988, Wave velocity in hydrocarbons and hydrocarbon saturated rocks with applications to EOR monitoring: Ph.D. thesis, Stanford University.
- Wang, Z., and A. Nur, 1988, Effect of temperature on wave velocities in sands and sandstones with heavy hydrocarbons, *Soc. Pet. Eng., Res. Eng.*, **3**, 158-164.
- Watt J.P., G.F. Davies, and R.J. O'Connell, 1976, The elastic properties of composite materials, *Rev. Geophys. Sp. Phys.*, **14**, 541-560.